SEEK AND DESTROY

Theranostics of hyperinsulinemic hypoglycemia using exendin-based tracers

Marti Boss

Department of Medical Imaging
Radboudumc

ISBN
978-94-6421-293-8

Cover
Annemie van der Haghen

Design/lay-out
Promotie In Zicht (www.promotie-inzicht.nl)

Print
Ipskamp Printing

SEEK AND DESTROY

Theranostics of hyperinsulinemic hypoglycemia using exendin-based tracers

Proefschrift

ter verkrijging van de graad van doctor
aan de Radboud Universiteit Nijmegen
op gezag van de rector magnificus prof. dr. J.H.J.M. van Krieken,
volgens besluit van het college van decanen
in het openbaar te verdedigen op woensdag 9 juni 2021
om 10.30 uur precies

door

Marti Boss
geboren op 19 januari 1985
te Arnhem

Promotor
Prof. dr. Martin Gotthardt

Copromotoren
Dr. Sanne van Lith
Dr. Maarten Brom

Manuscriptcommissie
Prof. dr. Henry Timmers
Dr. Annemarie Boleij
Prof. dr. Felix Mottaghy *(Universiteit Maastricht & Universitätsklinikum Aachen, Duitsland)*

Paranimfen
Annemarie Eek
Frauke Swieringa

It's not that what is past casts its light on what is present,
or what is present its light on what is past; rather,
image is that wherein what has been
comes together in a flash with the now to form
a constellation.

Walter Benjamin

Searching…… Seek and Destroy!

Metallica

Table of contents

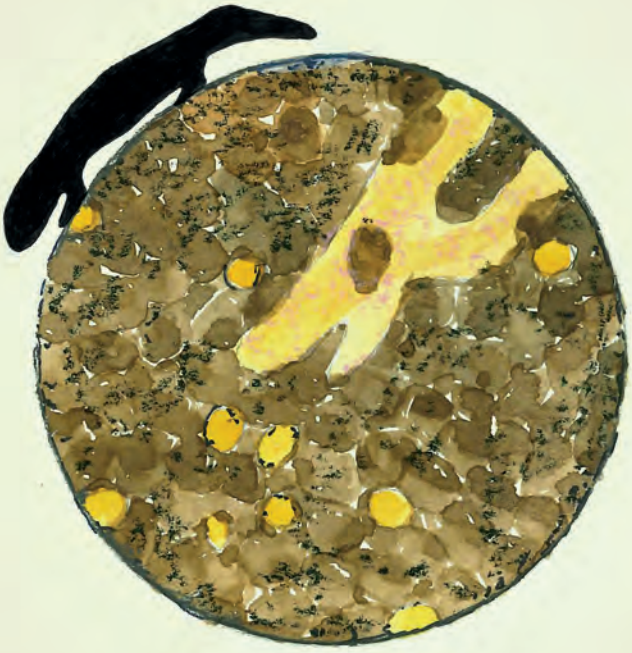

CHAPTER 1

General introduction

Rationale

The rationale of this thesis is to use targeted molecular imaging and photodynamic therapy to overcome the challenges in diagnosis and therapy of hyperinsulinemic hypoglycemia. For this purpose, we use exendin-based tracers targeting the glucagon-like peptide 1 receptor.

Molecular imaging

molecular imaging can provide information about biological processes associated with malignancies at the cellular or molecular level. Combined with the anatomical reference provided by conventional imaging modalities such as computed tomography (CT) and magnetic resonance imaging (MRI), this allows for highly sensitive localization of tumors. Molecular imaging can be applied for preoperative diagnostics and postoperative monitoring as well as during surgery to aid tumor detection and resection.

Localization of tumors with molecular imaging can be achieved by targeting specific tumor-associated antigens using various molecules. Monoclonal antibodies (mAbs) and peptides are widely used targeting molecules. mAbs are often very specific and have high target affinity. They also have relatively slow pharmacokinetics, which leads to slow clearance from the circulation and high uptake in target organs. Furthermore, mAbs contain an abundance of reactive amino-acid residues which can be used for conjugation of dyes (radionuclides, fluorescent tags etc.) The use of peptides as targeting molecules benefits from their small size, which leads to faster pharmacokinetics and target accumulation as well as rapid clearance from non-target tissue. The small size of peptides also poses a disadvantage, since conjugation of imaging agents could result in dramatic changes in their pharmacokinetic properties. In general, tumor uptake values of peptide-based agents are lower than uptake values of antibody-based agents. However, because of the fast pharmacokinetics of peptides, higher tumor-to-background values can be reached.

Radionuclide imaging

Radionuclide imaging is based on the detection of γ-photons. Because of the highly penetrating nature of these γ-photons, radionuclide imaging is not hindered by limitations in penetration depth in biological tissue. It is therefore a very suitable technique for non-invasive preoperative whole-body tumor detection. The nuclear imaging technique single photon emission computed tomography (SPECT) visualizes

gamma rays using a collimator and a detection crystal. Positron emission tomography (PET) detects gamma rays produced by positron-emitting radionuclides. These positrons will annihilate upon contact with an electron, resulting in the production of two 511 keV gamma rays traveling in opposite directions. With both SPECT and PET, 3-dimensional reconstructions of the images show the distribution of the tracer in the body. PET has certain advantages over SPECT including a superior sensitivity (approximately two to three times higher) and resolution, making it more suitable for detection of small lesions. Also, PET enables precise quantitative image analysis.

The most widely used type of radionuclide imaging is imaging of glucose metabolism with fluorine-18-fluorodeoxyglucose ([^{18}F]FDG) PET. However, PET and SPECT have also been successfully applied to image specific tumor associated targets such as the somatostatin-receptor (SSR) for neuroendocrine tumors (1, 2) or the prostate specific membrane antigen (PSMA) for prostate cancer (3, 4). When developing a targeted radiotracer, the choice of SPECT or PET radionuclide is important. The physical half-life of the radionuclide should correspond well with the biological half-life of the targeting molecule (5). For long-circulating targeting molecules like antibodies, radionuclides with a long physical half-life like ^{111}In (67 hours) for SPECT (6) and ^{89}Zr (78 hours) for PET (7) are convenient. For small molecules, like peptides, with faster pharmacokinetics, PET radionuclides with short half-lives like ^{68}Ga (68 minutes) (8) and ^{18}F (110 minutes) (9) would be suitable. SPECT and PET are used for pre-operative scanning, used to localize lesions and for planning of surgical treatment. However, the translation of these preoperative images into the operating room often proves challenging. During the operation, the position of structures can differ from the appearance on the preoperative scan, or the malignant tissue can be obscured by surrounding tissue. SPECT and PET do not offer real-time information for detailed tumor-delineation in the operating room (10). Radio-guidance, which makes use of a gamma probe to detect radiation intra-operatively, can provide such real-time information for tumor localization. However, this technique relies solely on an acoustic signal, without a real-time in situ image. Achieving accurate tumor delineation is therefore still challenging (11).

Fluorescence imaging

A molecular imaging technique that could provide real-time intra-operative information is fluorescence imaging. This technique uses fluorophores, which are molecules that can be excited by light of a specific wavelength. This subsequently leads to the emission of a photon of a slightly longer wavelength, which can be detected with a fluorescence camera. Fluorescence imaging is hindered by a limited penetration

depth, because of tissue absorption and scattering of the photons. However, the high sensitivity and spatial resolution of fluorescence imaging allows for precise delineation of tumors during surgery. The most widely used fluorescence imaging technique is a non-targeted approach using the fluorophore indocyanine green (ICG), which has many applications, such as lymph node detection (12), and visualization of liver metastases (13). Currently there is much attention for the development of fluorescent tracers targeting specific tumor antigens, like folate receptor-alpha (FRa) in ovarian cancer (14) or vascular endothelial growth factor-A (VEGF-A) in breast cancer (15).

In the choice of fluorophores, near infrared (NIR) dyes are preferable since photons in the NIR region (650-900 nm) have a higher tissue penetration depth than photons in the visible light region (400-600 nm) (16). Another important property in the choice of a fluorophore is a large Stokes shift (the difference in wavelength between the positions of the band maxima of the absorption and emission spectra), which results in minimal interference between the excitation and emission wavelengths. Furthermore, to acquire an adequate fluorescent signal, a sufficiently high molar absorption coefficient and quantum yield are crucial (17, 18). Dyes should also be water-soluble to avoid aggregation of the dye in aqueous solutions (18). A frequently used dye for fluorescence guided surgery is IRDye800CW, which has been conjugated to multiple targeting moieties and is increasingly used for clinical fluorescence guided surgery in various solid tumor types (19-21).

Photodynamic therapy

While precise detection of tumors using radionuclide imaging and fluorescence imaging can lead to major improvements in the surgical treatment of cancer, resection of tumors is in some cases hampered by the proximity of vital structures. In such cases, treatment could be further improved by photodynamic therapy (PDT). Photodynamic therapy (PDT) is a technique using photosensitizers (PSs), which are molecules that can be activated using light of a specific wavelength. The activated PS will be converted from the ground singlet state into the excited singlet state. Upon decay back to the ground state the PS can emit fluorescence or undergo intersystem crossing and switch into an excited triplet state (Figure 1). It can then react with a substrate, which reacts with oxygen to produce oxygenated products, or it can directly react with oxygen to form $^1O_2$. These reactive oxygen species cause cell killing by direct cellular damage, vascular shutdown or activation of an immune response against targeted cells (22, 23).

The use of PDT has a long history, with the first anti-tumor effects in mice already reported in 1972 (25) and the first clinical trial in patients with skin cancer

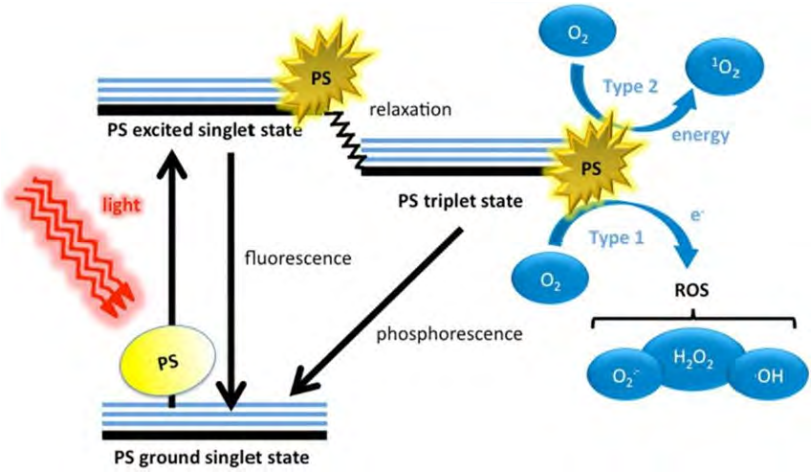

Figure 1 Schematic illustration of the principle of PDT. Figure from Dai et al. (24) under the Creative Commons Attribution license (CC-BY).

in 1978 (26). However, PDT is still not extensively used in the clinic. For a long time only non-targeted PDT approaches have been evaluated. The minimal efficiency in tumor targeting in these approaches resulted in inadequate tumor eradication. Also, high off-target accumulation, like in the skin, resulted in unwarranted side effects - especially since the first-generation PSs were activated by visible light (27). Currently, several targeted tracers for PDT are under development, for example targeting the epidermal growth factor receptor (EGFR) for tumor angiogenesis (28) and the human epidermal growth factor receptor 2 (HER2) for breast cancer (28, 29). PSs which are currently mostly used are chlorine-based PSs and phthalocyanines. Phthalocyanines absorb light at a higher wavelength than chlorine-based PSs, leading to a higher penetration depth. IRDye700DX is phthalocyanine which is frequently used and is already applied in a clinical trial for targeted PDT of head and neck cancer (30). In addition to the favorable excitation characteristics of IRDye700DX, this PS has a high quantum yield and hydrophilicity.

Hyperinsulinemic hypoglycemia

In healthy people, blood glucose levels are maintained within a narrow range with normal values between 4 and 6 mmol per liter. One of the hormones responsible for blood glucose homeostasis is insulin, which is produced by the beta cells in the pancreatic islets of Langerhans. Insulin acts to lower blood glucose levels by stimulating uptake of glucose into the liver, skeletal muscles and fat. Insulin production by pancreatic beta cells is usually a well-regulated process (Figure 2).

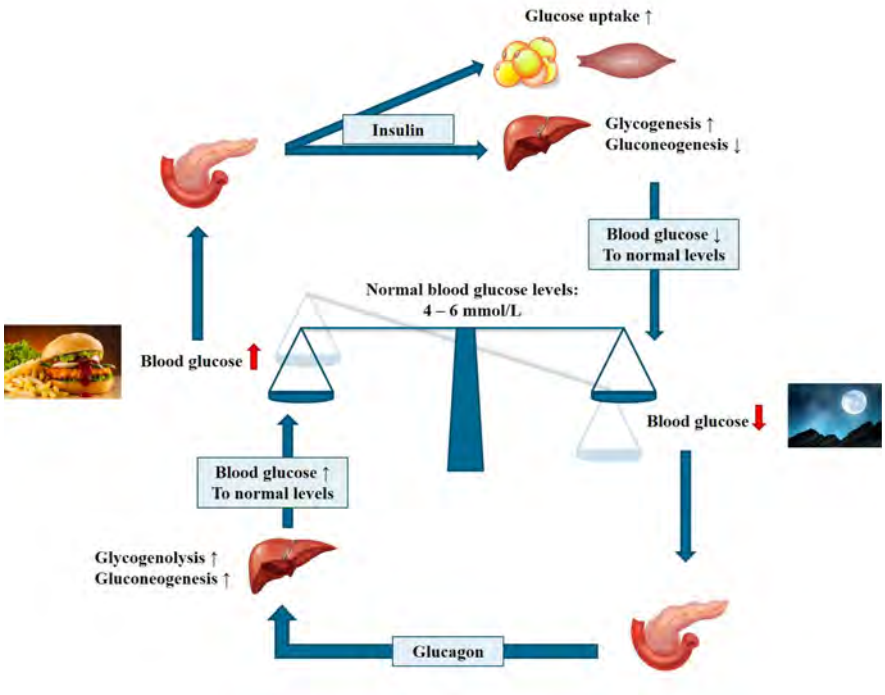

Figure 2 Schematic representation of maintenance of blood glucose levels by insulin and glucagon.

Its production is stimulated by high blood glucose levels as well as other substances like the incretin hormones glucagon-like peptide 1 (GLP-1) and glucose-dependent insulinotropic peptide (GIP), which are produced in the intestines upon food consumption. When blood glucose levels decrease, insulin production is slowed or stopped. If glucose levels drop below physiological values, the hormone glucagon is released from alpha cells in the islets of Langerhans. Glucagon promotes the

release of glucose into the blood from glycogen stores in the liver, thereby preventing hypoglycemia.

While insulin production is normally well-regulated, uncontrolled overproduction can arise, which can lead to hyperinsulinemic hypoglycemia. This is a dangerous disorder, since glucose is the most important energy substrate for the brain (31). Prolonged hypoglycemia can therefore lead to brain damage.

Adult endogenous hyperinsulinemic hypoglycemia

Potential causes of adult endogenous hyperinsulinemic hypoglycemia

Insulinomas

Adult endogenous hyperinsulinemic hypoglycemia (AHH) is most commonly caused by an insulinoma. An insulinoma is a subtype of pancreatic neuroendocrine tumor, which arises from the pancreatic beta cells. The insulinoma is the most common sporadic islet cell tumor of the pancreas and occurs with an incidence of 1-4 people per million per year. Insulinomas can occur at any age, but are most often found in people between 40 and 50 years of age, with a slightly higher incidence in women than men (60 : 40%). About 5 – 10% of insulinomas are part of hereditary disorders like multiple endocrine neoplasms type 1 (MEN-1). Insulinomas are benign in about 90% of cases and are mostly solitary and small (82% < 2 cm, 47% < 1 cm) (33, 34).

Nesidioblastosis

In about 0.5 to 5% of cases, AHH is caused by nesidioblastosis. Nesidioblastosis is characterized by a proliferation of abnormal beta cells throughout the pancreas. Histologic features of nesidioblastosis include enlarged islet size and number, increased periductular islets, enlarged beta cell nuclei and abundant clear cytoplasm. The cause of nesidioblastosis in adults is unknown. Genetic effects as well as reactive processes in response to metabolic and hormonal changes are suggested (35, 36).

Symptoms and diagnosis

Clinical symptoms of AHH are episodic, heterogeneous and not specific. Episodes of hypoglycemia occur in most cases after fasting or exercise, but can also occur postprandially (37). Hypoglycemia leads to neuroglycopenic symptoms such as diplopia, blurred vision, recurrent headaches, behavioral changes, confusion, agitation, dizziness, weakness and amnesia. Also autonomic symptoms such as palpitations, tremor, diaphoresis, hunger and paresthesia can occur. Because of recurrent and prolonged hypoglycemia, impaired awareness of hypoglycemia is often seen in patients with AHH (38). This is especially dangerous, since prolonged hypoglycemia can lead to seizures, loss of consciousness and even brain damage

or brain death. Since many patients use continuous eating to prevent or remedy hypoglycemia, weight gain often occurs (31, 34).

Because of the heterogeneity of the symptoms of AHH, a diagnosis is not always readily achieved. Symptoms can be misattributed to psychiatric, neurological or cardiac disorders, which can lead to a delay in diagnosis (39). Upon recognition of the symptoms, a definite diagnosis is achieved biochemically by the presence of low blood glucose levels with inappropriately high insulin levels during a 12- to 71-hour period of fasting (40).

Treatment

The only curative treatment for insulinomas is surgical resection. The type of surgery depends on the size and the location of the tumor and its relation to the pancreatic duct, major vessels and adjacent organs. In the case of sporadic insulinomas with a size smaller than 3 mm and a distance of more than 2-3 mm from the pancreatic duct, enucleation is possible. In other cases, depending on the location of the tumor, pancreaticoduodenectomy, partial pancreatectomy or distal pancreatectomy is performed (34).

Nesidioblastosis is primarily treated with medication. Diazoxide, which inhibits insulin secretion by opening ATP-sensitive potassium channels of beta cells, is used most often. Other medications include somatostatin analogs, glucocorticoids and calcium-channel blockers (35).

Diagnostic challenges

Since, in contrast to nesidioblastosis, insulinomas can be cured by surgical resection of the tumor, differentiating between these conditions is essential for treatment planning. Additionally, precise localization of insulinomas is important for planning of the surgical procedure. However, diagnosis and localization of insulinomas is hampered by the nature of the tumors. Detection of insulinomas with conventional imaging techniques such as CT and MRI is hindered by the small size of the tumors, resulting in a sensitivity of these techniques of only 44% and 53%, respectively (41). Besides conventional imaging, PET imaging of the somatostatin receptor (SSTR) subtypes 2 and 5, using [^{68}Ga]-DOTATOC and [^{68}Ga]-DOTATATE is also applied. This is the standard nuclear imaging technique for neuroendocrine tumors, which often express these SSTR subtypes. However, most insulinomas have a low density of the SSTR subtypes 2 and 5, leading to reported detection rates between 33% and 85% (42, 43). Since these currently available non-invasive methods for diagnosis and localization of insulinomas do not always provide a conclusive diagnosis, more invasive techniques like intra-arterial calcium stimulation and venous sampling (ASVS) and endoscopic ultrasound (EUS) are used. These techniques have sensitivities for detection of insulinomas

of 85% and 75%, respectively (41, 44-47). Because non-invasive detection of insulinomas is such a challenge, development of a more sensitive non-invasive imaging technique for the detection of insulinomas would be of great interest.

Treatment challenges

Even after detection of insulinomas, treatment is still challenging. The surgical procedures carry risks of complications such as pancreatic fistulas, abscesses, wound infections, pseudocyst formation and bleeding. Also certain medical complications can occur after insulinoma surgery, such as pancreatitis, pulmonary embolism and diabetes mellitus (48). Treatment of nesidioblastosis is a challenge as well, since diazoxide often leads to significant side effects like fluid retention, hypotension, hypertrichosis and bone marrow suppression. Other forms of medication have varying success. In nesidioblastosis patients with severe side effects or unresponsiveness to medicinal treatment, partial pancreatectomy is the only treatment option (31).

Congenital hyperinsulinism

The most common cause of persistent hypoglycemia in neonates is congenital hyperinsulinism (CHI). CHI is a very rare disorder which occurs in 1:35000 – 1:40000 live births (49). Mutations in 12 genes (*ABCC8, KCNJ11, GLUD1, GCK, HADH, SLC16A1, HNF1A, HK1, PGM1* and *PMM2*) have been found to be associated with CHI and novel genetic mechanisms are still being discovered. Histologically, there are three subforms of CHI; focal, diffuse and atypical. In focal CHI, accounting for 30-40% of cases, there are abnormal beta cells localized in a specific region (usually 2-10 mm in size) in the pancreas. Focal CHI is caused by paternal mutations in genes encoding beta cell ATP sensitive potassium channels (*ABCC8* or *KCNJ11*) and concurrent somatic loss of the maternal chromosome 11p15 region within the focal area. Diffuse CHI accounts for 60-70% of cases and affects all pancreatic beta cells. This subform is most commonly caused by homozygous recessive or compound heterozygous mutations in the beta cell ATP sensitive potassium channels. Atypical CHI involves rare cases in which the pancreatic histology does not fit the focal or diffuse disease pattern (50).

Symptoms and diagnosis

CHI most often presents in neonates, but can also present in infants, children and in rare cases in adulthood (51). Like AHH, CHI presents with a variety of symptoms, ranging from non-specific adrenergic symptoms like poor feeding, hunger, palpitations and sweating, to life-threatening neuroglycopenic symptoms like seizures, unconsciousness, lethargy, coma and even death (52). Early diagnosis of CHI is very important to minimize the risk of permanent brain damage as a result of an inadequate supply of glucose to the brain. CHI is suspected in patients

with recurrent and persistent hypoglycemia, upon which blood samples are collected during hypoglycemic episodes to confirm the diagnosis biochemically. This confirmation relies on inappropriate levels of insulin and c-peptide for the level of plasma glucose. In some cases serum insulin levels are low or undetectable and diagnosis has to be confirmed by other biochemical features like low β-hydroxy-butyrate and fatty acid concentration combined with clinical features (53).

Treatment

In addition to early diagnosis of the disease, starting treatment to prevent hypoglycemic episodes is crucial in CHI. Early treatment and emergency management include oral and/or intravenous glucose infusion, glucagon administration and frequent feeding. Focal CHI can be cured by surgical removal of the lesion. Depending on the location of the lesion, this can be achieved with enucleation or partial pancreatectomy. Diffuse CHI is primarily treated with medication. Like in adult nesidioblastosis, diazoxide is the primary medication used for treatment of CHI. In addition, somatostatin analogs and calcium channel blockers are used. In patients with diffuse CHI who are unresponsive to medicinal treatment, near-total pancreatectomy can be performed (49, 53).

Diagnostic challenges

After initial diagnosis of CHI, it is important for treatment planning to determine the subform of the disease. If mutational analysis is not conclusive, imaging is performed. Focal lesions cannot be detected by conventional imaging or SSTR PET imaging (54). Also, the invasive techniques ASVS and transhepatic portal venous insulin sampling (THPVS) are not always reliable for detection of focal CHI (55). The current imaging technique used to detect focal lesions in patients with CHI is ^{18}fluoro-L-dioxyphenylalanine ([^{18}F]F-DOPA) PET. This technique was reported to have a sensitivity of 85% for the diagnosis of focal CHI and was also successful for precise localization of the lesions, which is crucial for planning of the surgery. Despite the high sensitivity of [^{18}F]F-DOPA PET, focal lesions are still missed in some cases.

Treatment challenges

While focal CHI, if correctly diagnosed, can be cured by surgical treatment, treatment of diffuse CHI is much more challenging. Medicinal treatment, like mentioned above, is often associated with severe side effects and is not always effective. In patients unresponsive to medication, extensive surgery is required, which carries a high risk of developing pancreatic exocrine insufficiency and diabetes. Also, despite the extensiveness of the surgery, some patients continue to have hypoglycemic episodes (56).

Targeting the GLP-1 receptor

The glucagon-like peptide 1 receptor (GLP-1R) is a G-protein-coupled receptor expressed in several tissues, including the pancreatic beta cells. Benign insulinomas express high levels of the GLP-1R in nearly 100% of cases. Activation of the GLP-1R stimulates the adenylyl cyclase pathway, resulting in increased insulin synthesis and secretion. The GLP-1R is activated by binding of the hormone GLP-1. This peptide hormone is produced and secreted by intestinal enteroendocrine L-cells. Endogenous GLP-1 is rapidly degraded by the enzyme dipeptidyl peptidase-4 (DPP-4), neutral endopeptidase 24.11 and cleared by the kidneys. As a result, the physiological half-life of GLP-1 is only about 2 minutes, rendering it unsuitable as a targeting peptide for imaging purposes.

In this thesis we therefore target the GLP-1R with the GLP-1 analogue exendin-4. This peptide is derived from the saliva of the Gila Monster (Heloderma Suspectum), a lizard native to the southwestern United States and northwestern Mexican state of Sorona (57) (Figure 3). Exendin-4 shares 53% sequence homology with GLP-1 and binds the GLP-1R with high affinity. Since it is more resistant to degradation by DPP-4, it has a longer physiological half-life (58). Several exendin-based tracers for imaging of insulinomas have already been developed. The first exendin-based tracers that were developed were tracers for SPECT/CT. ^{111}In-labeled exendin ([Lys^{40}(Ahx-DTPA-[^{111}In]In)NH_2]-exendin-4 and [Lys^{40}(Ahx-DOTA-[^{111}In]In)NH_2]-exendin-4) showed high tumor uptake in the insulinoma Rip1Tag2 mouse model and also provided the first successful clinical results by detection of insulinomas with a higher sensitivity than conventional imaging (59-62). Also SPECT/CT with ^{99m}Tc-labeled-exendin ([Lys^{40}(Ahx-HYNIC-[^{99m}Tc]Tc/EDDA)NH_2]-exendin-4) was used for insulinoma detection. With this tracer, insulinomas could be localized in several patients in which conventional imaging was negative (63).

Figure 3 Gila Monster (Heloderma Suspectum).

Because of the better sensitivity and spatial resolution of PET compared to SPECT, there is recently a focus on the development of exendin-based tracers for PET imaging. ^{68}Ga-labeled exendin ([^{68}Ga]Ga-DOTA-exendin-4 and [^{68}Ga]Ga-NOTA-exendin-4) was shown to be more sensitive for insulinoma detection than ^{111}In-labeled exendin as well as conventional imaging techniques (64-66).

Thesis outline

In this thesis, the aim was to develop and investigate exendin-4 based tracers for targeted molecular imaging and photodynamic therapy of hyperinsulinemic hypoglycemia.

The **first part** of this thesis focusses on the use of radiolabeled exendin for diagnostic imaging in hyperinsulinemic hypoglycemia.

In **chapter 2**, we investigate the effectiveness of the radiotracer [^{68}Ga]Ga-NODAGA-exendin-4 for the localization of insulinomas by PET/CT. In a prospective multicenter trial in 42 patients, a direct comparison between this novel imaging method and the current standard non-invasive imaging procedures CT, MRI and somatostatin receptor PET is performed.

In **chapter 3**, we examine the effectiveness of [^{68}Ga]Ga-NODAGA-exendin-4 PET for the detection and localization of focal CHI. Based on prospective as well as retrospective data of CHI patients, the performance of [^{68}Ga]Ga-NODAGA-exendin-4 PET is compared to [^{18}F]F-DOPA PET.

The safety of the use of [^{68}Ga]Ga-NODAGA-exendin-4 for diagnostic and research purposes is investigated in **chapter 4**, in which human PET-based dosimetry is performed to estimate radiation doses from this radiotracer to adults as well as children.

The **second part** of this thesis focusses on the treatment of hyperinsulinemic hypoglycemia and the potential benefit of fluorescent exendin-based tracers.

In **chapter 5**, the potential of the near infrared fluorescent tracer exendin-4-IRDye-800CW for targeting of GLP-1R positive cells is assessed *in vitro* and *in vivo* as well as the feasibility and translatability of performing fluorescence imaging with this tracer.

The potential of the alternative treatment option photodynamic therapy is assessed in **chapter 6**, in which the efficacy and specificity of targeted photodynamic therapy of GLP-1R positive lesions using the tracer exendin-4-IRDye700DX is examined *in vitro* and *in vivo*.

A general discussion of the results and the implications for the future of diagnosis and therapy of hyperinsulinemic hypoglycemia are given in **chapter 7**.

References

1. Barrio M, Czernin J, Fanti S, Ambrosini V, Binse I, Du L, et al. The Impact of Somatostatin Receptor-Directed PET/CT on the Management of Patients with Neuroendocrine Tumor: A Systematic Review and Meta-Analysis. Journal of nuclear medicine : official publication, Society of Nuclear Medicine. 2017;58(5):756-61.
2. Bodei L, Ambrosini V, Herrmann K, Modlin I. Current Concepts in (68)Ga-DOTATATE Imaging of Neuroendocrine Neoplasms: Interpretation, Biodistribution, Dosimetry, and Molecular Strategies. Journal of nuclear medicine : official publication, Society of Nuclear Medicine. 2017;58(11):1718-26.
3. Hofman MS, Iravani A. Gallium-68 Prostate-Specific Membrane Antigen PET Imaging. PET clinics. 2017;12(2):219-34.
4. Schwarzenboeck SM, Rauscher I, Bluemel C, Fendler WP, Rowe SP, Pomper MG, et al. PSMA Ligands for PET Imaging of Prostate Cancer. Journal of nuclear medicine : official publication, Society of Nuclear Medicine. 2017;58(10):1545-52.
5. Azhdarinia A, Ghosh P, Ghosh S, Wilganowski N, Sevick-Muraca EM. Dual-labeling strategies for nuclear and fluorescence molecular imaging: a review and analysis. Molecular imaging and biology : MIB : the official publication of the Academy of Molecular Imaging. 2012;14(3):261-76.
6. Nagengast WB, Hooge MN, van Straten EM, Kruijff S, Brouwers AH, den Dunnen WF, et al. VEGF-SPECT with (1)(1)(1)In-bevacizumab in stage III/IV melanoma patients. European journal of cancer (Oxford, England : 1990). 2011;47(10):1595-602.
7. Heskamp S, Raave R, Boerman O, Rijpkema M, Goncalves V, Denat F. (89)Zr-Immuno-Positron Emission Tomography in Oncology: State-of-the-Art (89)Zr Radiochemistry. Bioconjugate chemistry. 2017;28(9):2211-23.
8. Kallur KG, Ramachandra PG, Rajkumar K, Swamy SS, Desai I, Rao RM, et al. Clinical Utility of Gallium-68 PSMA PET/CT Scan for Prostate Cancer. Indian journal of nuclear medicine : IJNM : the official journal of the Society of Nuclear Medicine, India. 2017;32(2):110-7.
9. Giesel F, Will L, Kesch C, Freitag M, Kremer C, Merkle J, et al. Biochemical recurrence of prostate cancer: initial results with (18)F-PSMA-1007 PET/CT. Journal of nuclear medicine : official publication, Society of Nuclear Medicine. 2018.
10. Kherlopian AR, Song T, Duan Q, Neimark MA, Po MJ, Gohagan JK, et al. A review of imaging techniques for systems biology. BMC systems biology. 2008;2:74.
11. Tsuchimochi M, Hayama K. Intraoperative gamma cameras for radioguided surgery: technical characteristics, performance parameters, and clinical applications. Physica medica : PM : an international journal devoted to the applications of physics to medicine and biology : official journal of the Italian Association of Biomedical Physics (AIFB). 2013;29(2):126-38.
12. Crane LM, Themelis G, Arts HJ, Buddingh KT, Brouwers AH, Ntziachristos V, et al. Intraoperative near-infrared fluorescence imaging for sentinel lymph node detection in vulvar cancer: first clinical results. Gynecologic oncology. 2011;120(2):291-5.
13. van der Vorst JR, Schaafsma BE, Hutteman M, Verbeek FP, Liefers GJ, Hartgrink HH, et al. Near-infrared fluorescence-guided resection of colorectal liver metastases. Cancer. 2013;119(18):3411-8.
14. van Dam GM, Themelis G, Crane LM, Harlaar NJ, Pleijhuis RG, Kelder W, et al. Intraoperative tumor-specific fluorescence imaging in ovarian cancer by folate receptor-alpha targeting: first in-human results. Nature medicine. 2011;17(10):1315-9.
15. Harlaar NJ, Koller M, de Jongh SJ, van Leeuwen BL, Hemmer PH, Kruijff S, et al. Molecular fluorescence-guided surgery of peritoneal carcinomatosis of colorectal origin: a single-centre feasibility study. The lancet Gastroenterology & hepatology. 2016;1(4):283-90.
16. Patterson MS, Chance B, Wilson BC. Time resolved reflectance and transmittance for the non-invasive measurement of tissue optical properties. Applied optics. 1989;28(12):2331-6.
17. Haque A, Faizi MS, Rather JA, Khan MS. Next generation NIR fluorophores for tumor imaging and fluorescence-guided surgery: A review. Bioorganic & medicinal chemistry. 2017;25(7):2017-34.
18. Luo S, Zhang E, Su Y, Cheng T, Shi C. A review of NIR dyes in cancer targeting and imaging. Biomaterials. 2011;32(29):7127-38.

19. Gao RW, Teraphongphom N, de Boer E, van den Berg NS, Divi V, Kaplan MJ, et al. Safety of panitumumab-IRDye800CW and cetuximab-IRDye800CW for fluorescence-guided surgical navigation in head and neck cancers. Theranostics. 2018;8(9):2488-95.
20. Li D, Zhang J, Chi C, Xiao X, Wang J, Lang L, et al. First-in-human study of PET and optical dual-modality image-guided surgery in glioblastoma using (68)Ga-IRDye800CW-BBN. Theranostics. 2018;8(9):2508-20.
21. Hekman MC, Rijpkema M, Muselaers CH, Oosterwijk E, Hulsbergen-Van de Kaa CA, Boerman OC, et al. Tumor-targeted Dual-modality Imaging to Improve Intraoperative Visualization of Clear Cell Renal Cell Carcinoma: A First in Man Study. Theranostics. 2018;8(8):2161-70.
22. Dolmans DE, Fukumura D, Jain RK. Photodynamic therapy for cancer. Nature reviews Cancer. 2003; 3(5):380-7.
23. Henderson BW, Dougherty TJ. How does photodynamic therapy work? Photochemistry and photobiology. 1992;55(1):145-57.
24. Dai T, Fuchs BB, Coleman JJ, Prates RA, Astrakas C, St Denis TG, et al. Concepts and principles of photodynamic therapy as an alternative antifungal discovery platform. Frontiers in microbiology. 2012;3:120.
25. Diamond I, Granelli SG, McDonagh AF, Nielsen S, Wilson CB, Jaenicke R. Photodynamic therapy of malignant tumours. Lancet (London, England). 1972;2(7788):1175-7.
26. Dougherty TJ, Kaufman JE, Goldfarb A, Weishaupt KR, Boyle D, Mittleman A. Photoradiation therapy for the treatment of malignant tumors. Cancer research. 1978;38(8):2628-35.
27. van Straten D, Mashayekhi V, de Bruijn HS, Oliveira S, Robinson DJ. Oncologic Photodynamic Therapy: Basic Principles, Current Clinical Status and Future Directions. Cancers. 2017;9(2).
28. Kameyama N, Matsuda S, Itano O, Ito A, Konno T, Arai T, et al. Photodynamic therapy using an anti-EGF receptor antibody complexed with verteporfin nanoparticles: a proof of concept study. Cancer biotherapy & radiopharmaceuticals. 2011;26(6):697-704.
29. Mitsunaga M, Ogawa M, Kosaka N, Rosenblum LT, Choyke PL, Kobayashi H. Cancer cell-selective in vivo near infrared photoimmunotherapy targeting specific membrane molecules. Nature medicine. 2011;17(12):1685-91.
30. Gillenwater AM, Cognetti D, Johnson JM, Curry J, Kochuparambil ST, McDonald D, et al. RM-1929 photo-immunotherapy in patients with recurrent head and neck cancer: Results of a multicenter phase 2a open-label clinical trial. Journal of Clinical Oncology. 2018;36(15_suppl):6039-.
31. Davi MV, Pia A, Guarnotta V, Pizza G, Colao A, Faggiano A. The treatment of hyperinsulinemic hypoglycaemia in adults: an update. Journal of endocrinological investigation. 2017;40(1):9-20.
32. Roder PV, Wu B, Liu Y, Han W. Pancreatic regulation of glucose homeostasis. Experimental & molecular medicine. 2016;48:e219.
33. de Herder WW, Niederle B, Scoazec JY, Pauwels S, Kloppel G, Falconi M, et al. Well-differentiated pancreatic tumor/carcinoma: insulinoma. Neuroendocrinology. 2006;84(3):183-8.
34. Kinova MK. Diagnostics and treatment of insulinoma. Neoplasma. 2015;62(5):692-704.
35. Dravecka I, Lazurova I. Nesidioblastosis in adults. Neoplasma. 2014;61(3):252-6.
36. Witteles RM, Straus IF, Sugg SL, Koka MR, Costa EA, Kaplan EL. Adult-onset nesidioblastosis causing hypoglycemia: an important clinical entity and continuing treatment dilemma. Archives of surgery (Chicago, Ill : 1960). 2001;136(6):656-63.
37. Placzkowski KA, Vella A, Thompson GB, Grant CS, Reading CC, Charboneau JW, et al. Secular trends in the presentation and management of functioning insulinoma at the Mayo Clinic, 1987-2007. The Journal of clinical endocrinology and metabolism. 2009;94(4):1069-73.
38. Cryer PE. Symptoms of hypoglycemia, thresholds for their occurrence, and hypoglycemia unawareness. Endocrinology and metabolism clinics of North America. 1999;28(3):495-500, v-vi.
39. Suzuki K, Miyamoto M, Miyamoto T, Hirata K. Insulinoma with early-morning abnormal behavior. Internal medicine (Tokyo, Japan). 2007;46(7):405-8.
40. Service FJ, Natt N. The prolonged fast. The Journal of clinical endocrinology and metabolism. 2000;85(11):3973-4.

41. Mehrabi A, Fischer L, Hafezi M, Dirlewanger A, Grenacher L, Diener MK, et al. A systematic review of localization, surgical treatment options, and outcome of insulinoma. Pancreas. 2014;43(5):675-86.
42. Antwi K, Fani M, Heye T, Nicolas G, Rottenburger C, Kaul F, et al. Comparison of glucagon-like peptide-1 receptor (GLP-1R) PET/CT, SPECT/CT and 3T MRI for the localisation of occult insulinomas: evaluation of diagnostic accuracy in a prospective crossover imaging study. European journal of nuclear medicine and molecular imaging. 2018;45(13):2318-27.
43. Prasad V, Sainz-Esteban A, Arsenic R, Plockinger U, Denecke T, Pape UF, et al. Role of (68)Ga somatostatin receptor PET/CT in the detection of endogenous hyperinsulinaemic focus: an explorative study. European journal of nuclear medicine and molecular imaging. 2016;43(9):1593-600.
44. Guettier JM, Kam A, Chang R, Skarulis MC, Cochran C, Alexander HR, et al. Localization of insulinomas to regions of the pancreas by intraarterial calcium stimulation: the NIH experience. The Journal of clinical endocrinology and metabolism. 2009;94(4):1074-80.
45. Druce MR, Muthuppalaniappan VM, O'Leary B, Chew SL, Drake WM, Monson JP, et al. Diagnosis and localisation of insulinoma: the value of modern magnetic resonance imaging in conjunction with calcium stimulation catheterisation. Eur J Endocrinol. 2010;162(5):971-8.
46. Mossman AK, Pattison DA, Hicks RJ, Hamblin PS, Yates CJ. Localisation of occult extra-pancreatic insulinoma using glucagon-like peptide-1 receptor molecular imaging. Intern Med J. 2018;48(1):97-8.
47. Rayamajhi SJ, Lee J, Mittal BR, Jessop AC, Chasen B, Bhosale P. Cross sectional and nuclear medicine imaging of pancreatic insulinomas. Abdom Radiol (NY). 2017;42(2):531-43.
48. Richards ML, Gauger PG, Thompson NW, Kloos RG, Giordano TJ. Pitfalls in the surgical treatment of insulinoma. Surgery. 2002;132(6):1040-9; discussion 9.
49. Senniappan S, Shanti B, James C, Hussain K. Hyperinsulinaemic hypoglycaemia: genetic mechanisms, diagnosis and management. Journal of inherited metabolic disease. 2012;35(4):589-601.
50. Demirbilek H, Hussain K. Congenital Hyperinsulinism: Diagnosis and Treatment Update. Journal of clinical research in pediatric endocrinology. 2017;9(Suppl 2):69-87.
51. Gutgold A, Gross DJ, Glaser B, Szalat A. Diagnosis of ABCC8 Congenital Hyperinsulinism of Infancy in a 20-Year-Old Man Evaluated for Factitious Hypoglycemia. The Journal of clinical endocrinology and metabolism. 2017;102(2):345-9.
52. Iglesias P, Diez JJ. Management of endocrine disease: a clinical update on tumor-induced hypoglycemia. European journal of endocrinology / European Federation of Endocrine Societies. 2014;170(4):R147-57.
53. Galcheva S, Al-Khawaga S, Hussain K. Diagnosis and management of hyperinsulinaemic hypoglycaemia. Best practice & research Clinical endocrinology & metabolism. 2018;32(4):551-73.
54. Adzick NS, Thornton PS, Stanley CA, Kaye RD, Ruchelli E. A multidisciplinary approach to the focal form of congenital hyperinsulinism leads to successful treatment by partial pancreatectomy. Journal of pediatric surgery. 2004;39(3):270-5.
55. Stanley CA, Thornton PS, Ganguly A, MacMullen C, Underwood P, Bhatia P, et al. Preoperative evaluation of infants with focal or diffuse congenital hyperinsulinism by intravenous acute insulin response tests and selective pancreatic arterial calcium stimulation. The Journal of clinical endocrinology and metabolism. 2004;89(1):288-96.
56. Arya VB, Senniappan S, Demirbilek H, Alam S, Flanagan SE, Ellard S, et al. Pancreatic endocrine and exocrine function in children following near-total pancreatectomy for diffuse congenital hyperinsulinism. PloS one. 2014;9(5):e98054.
57. Raufman JP. Bioactive peptides from lizard venoms. Regulatory peptides. 1996;61(1):1-18.
58. Goke R, Fehmann HC, Linn T, Schmidt H, Krause M, Eng J, et al. Exendin-4 is a high potency agonist and truncated exendin-(9-39)-amide an antagonist at the glucagon-like peptide 1-(7-36)-amide receptor of insulin-secreting beta-cells. The Journal of biological chemistry. 1993;268(26):19650-5.
59. Christ E, Wild D, Ederer S, Behe M, Nicolas G, Caplin ME, et al. Glucagon-like peptide-1 receptor imaging for the localisation of insulinomas: a prospective multicentre imaging study. The lancet Diabetes & endocrinology. 2013;1(2):115-22.
60. Gotthardt M, Lalyko G, van Eerd-Vismale J, Keil B, Schurrat T, Hower M, et al. A new technique for in vivo imaging of specific GLP-1 binding sites: first results in small rodents. Regulatory peptides. 2006;137(3):162-7.

61. Wild D, Behe M, Wicki A, Storch D, Waser B, Gotthardt M, et al. [Lys40(Ahx-DTPA-111In)NH2] exendin-4, a very promising ligand for glucagon-like peptide-1 (GLP-1) receptor targeting. Journal of nuclear medicine : official publication, Society of Nuclear Medicine. 2006;47(12):2025-33.
62. Wild D, Macke H, Christ E, Gloor B, Reubi JC. Glucagon-like peptide 1-receptor scans to localize occult insulinomas. N Engl J Med. 2008;359(7):766-8.
63. Sowa-Staszczak A, Trofimiuk-Muldner M, Stefanska A, Tomaszuk M, Buziak-Bereza M, Gilis-Januszewska A, et al. 99mTc Labeled Glucagon-Like Peptide-1-Analogue (99mTc-GLP1) Scintigraphy in the Management of Patients with Occult Insulinoma. PLoS One. 2016;11(8):e0160714.
64. Antwi K, Fani M, Heye T, Nicolas G, Rottenburger C, Kaul F, et al. Comparison of glucagon-like peptide-1 receptor (GLP-1R) PET/CT, SPECT/CT and 3T MRI for the localisation of occult insulinomas: evaluation of diagnostic accuracy in a prospective crossover imaging study. Eur J Nucl Med Mol Imaging. 2018.
65. Antwi K, Fani M, Nicolas G, Rottenburger C, Heye T, Reubi JC, et al. Localization of Hidden Insulinomas with (6)(8)Ga-DOTA-Exendin-4 PET/CT: A Pilot Study. J Nucl Med. 2015;56(7):1075-8.
66. Luo Y, Pan Q, Yao S, Yu M, Wu W, Xue H, et al. Glucagon-Like Peptide-1 Receptor PET/CT with 68Ga-NOTA-Exendin-4 for Detecting Localized Insulinoma: A Prospective Cohort Study. J Nucl Med. 2016;57(5):715-20.

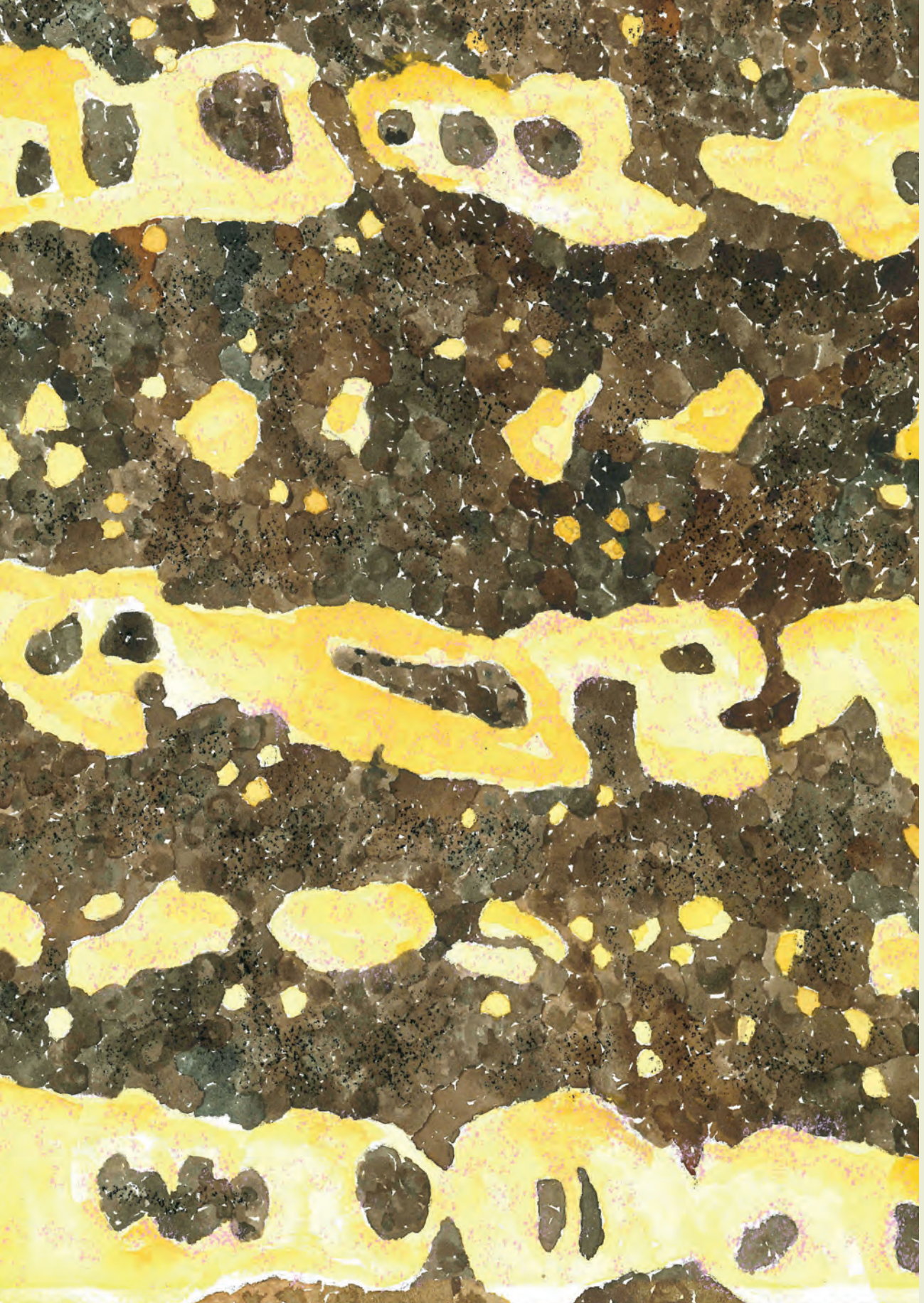

PART 1

Diagnostics

Non-invasive imaging of hyperinsulinemic hypoglycemia using [^{68}Ga]Ga-NODAGA-exendin-4

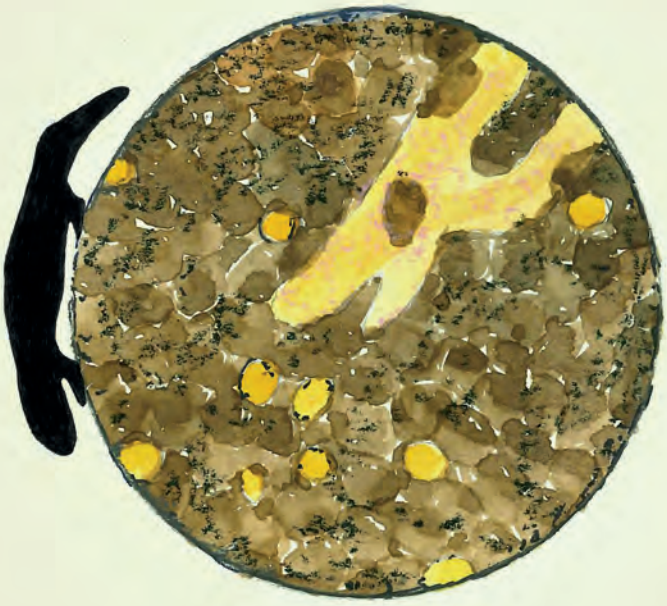

CHAPTER 2

[^{68}Ga]Ga-NODAGA-exendin-4 PET/CT for the localization of insulinomas

Marti Boss[1], Kirsi Mikkola[2], Maarten Brom[1], Annemarie Eek[1], Mijke Buitinga[1], Olof Eriksson[3], Damian Wild[4], Vikas Prasad[5,6], Adrienne Brouwers[7], Francois Pattou[8], Hans Hofland[9], Pirjo Nuutila[2,10], John Hermans[1], Martin Gotthardt[1]

In preparation

1 Department of Medical Imaging, Radboud University Medical Center Nijmegen, The Netherlands
2 Turku PET Center, University of Turku, Turku, Finland
3 Department of Medicinal Chemistry, Uppsala University, Uppsala, Sweden
4 Department of Nuclear Medicine, University of Basel Hospital, Basel, Switzerland
5 Department of Nuclear Medicine, Charité University Hospital of Berlin, Berlin, Germany
6 Department of Nuclear Medicine, University Hospital of Ulm, Ulm, Germany
7 Department of Surgery, University Medical Center Groningen, The Netherlands
8 Department of General and Endocrine Surgery, University Hospital, Lille, France
9 Department of Internal Medicine, Erasmus Medical Center Rotterdam, The Netherlands
10 Department of Endocrinology, Turku University Hospital, Turku, Finland

Abstract

Introduction
Insulinomas are usually small, benign pancreatic neuroendocrine tumors. Precise anatomical localization is crucial for surgical treatment. The current standard imaging techniques CT, MRI and somatostatin receptor (SSTR) PET have limited sensitivity. The glucagon-like peptide 1 (GLP-1) analog exendin specifically binds to the GLP-1 receptor, which is overexpressed in most insulinomas. We have performed a prospective multicenter imaging study to compare the effectiveness of [^{68}Ga]Ga-NODAGA-exendin-4 PET/CT (GLP-1R PET) with all current standard non-invasive imaging procedures for the localization of insulinomas.

Methods
42 adults aged 24-62 with biochemically proven hyperinsulinemic hypoglycemia were included. PET/CT images were obtained one and two hours after injection of 95-105 MBq [^{68}Ga]Ga-NODAGA-exendin-4 (5-7 μg). Current standard imaging, consisting of CT or MRI and SSTR PET, was performed within 8 weeks of GLP-1R PET in all patients. A patient-based analysis was performed with histopathology as a reference standard. Tumor-to-background ratios and contrast-to-noise ratios were determined by quantitative analysis of GLP-1R and SSTR PET images by a blinded observer.

Results
Lesions were identified in 33 patients. 31 patients underwent surgery and presence of an insulinoma was confirmed histopathologically. Analysis showed that GLP-1R PET localized insulinomas with a higher accuracy and sensitivity (90.6% and 93.5% respectively) than conventional imaging (78.1% and 80.6% respectively) and SSTR PET (59.4% and 61.3% respectively). In 12.5% of patients, a correct diagnosis and decision to perform surgery was only reached after GLP-1R PET. Mean tumor-to-background ratios were 12.2 ± 3.4 for GLP-1R PET compared to 4.0 ± 3.0 for SSTR PET ($p=0.0017$) and mean contrast-to-noise ratios were 24.1 ± 20.8 for GLP-1R PET compared to 5.3 ± 4.4 for SSTR PET ($p=0.022$). The lower peptide dose used in this study compared to previous studies with [^{68}Ga]Ga-DOTA-exendin-4 (4-7 μg vs. 12-24 μg respectively) resulted in fewer occurrences of nausea (5% vs. 27% of patients).

Conclusion
This study demonstrates the superior performance of GLP-1R PET/CT compared to current standard non-invasive imaging modalities for pre-operative localization of benign insulinomas. GLP-1R PET significantly influenced the clinical management of the patients in this population. Because of its high sensitivity and excellent imaging quality, GLP-1R PET/CT could have the potential to be used as the primary diagnostic imaging modality in patients with AHH.

Introduction

In this prospective trial, we have examined the effectiveness of a novel radiotracer for the non-invasive localization of insulinomas. Insulinomas are neuroendocrine tumors arising from the pancreatic beta cells. Insulinomas occur with an incidence of 1-4 people per million per year and are the most common cause of adult endogenous hyperinsulinemic hypoglycemia (AHH). In patients with an insulinoma, episodic hypoglycemia results in symptoms such as confusion, diplopia, dizziness and, in cases of prolonged hypoglycemia, even seizures, loss of consciousness or death (1, 2).

Insulinomas are benign in about 90% of cases and can only be completely cured by surgical removal. Preferred surgical procedures are pancreas-preserving, such as limited resection or enucleation (3). In order to plan such a surgical procedure and improve the clinical outcome of the patients, precise pre-operative localization of the tumor is essential. However, this is challenging because of the usually small size of insulinomas (82% < 2 cm, 47% < 1 cm). The non-invasive imaging methods triple phase CT, MRI and ultrasound are currently used, but these techniques have sensitivities of only about 44%, 53% and 33% respectively (4). Next to these non-invasive imaging techniques, angiography with intra-arterial calcium stimulation and venous sampling (ASVS) and endoscopic ultrasound (EUS) are used in cases of occult insulinomas, with a sensitivity of about 85% and 74.8% respectively (4, 5). These techniques have the disadvantage of being invasive and carrying risks of complications.

Imaging of the somatostatin receptor (SSTR) is the current standard nuclear imaging technique for the localization of neuroendocrine tumors. Sensitivities of this technique between 33% and 85% for the detection of insulinomas have been reported, probably dependent on the number and nature of the cases assessed (6, 7). While the SSTR subtypes 2 an 5 are expressed in high levels in the majority of neuroendocrine tumors, a mostly low receptor density is found in benign insulinomas (8). In contrast to the low expression of the SSTR, benign insulinomas express high levels of the glucagon-like peptide 1 receptor (GLP-1R) in 92% of cases (8). The GLP-1R is therefore an attractive alternative target for insulinoma detection with nuclear imaging.

In this study, we target the GLP-1R using the peptide exendin-4, a stable analogue of the hormone GLP-1, which specifically binds the GLP-1R with high affinity. Previous clinical studies have shown the potential of ^{111}In-labelled exendin for detection of insulinomas with single photon computed tomography (SPECT) (9-11). Subsequently, position emission tomography (PET) using ^{68}Ga-labelled exendin ([^{68}Ga]Ga-DOTA-exendin-4), which has the combined benefit of the higher sensitivity of PET as compared to SPECT and the lower radiation burden to the patient, was shown to perform better then ^{111}In-labelled exendin in a small

cross-over trial (12). Recently, the benefit of [^{68}Ga]Ga-DOTA-exendin-4 PET for detection of insulinomas over SPECT and magnetic resonance imaging (MRI) was shown in a large prospective trial (6).

Here, we report data from a clinical trial with an exendin-based radiotracer in which we used the chelator NODAGA, instead of DOTA, for radiolabelling with Gallium-68. This enables labeling with a higher specific activity (13), allowing the use of lower, sub-pharmacological, peptide doses for PET imaging, potentially leading to improved image quality, by more efficient targeting with lower background signals, and a prevention of adverse effects like hypoglycemia and nausea in patients. We performed a multicenter prospective trial in which we compared the effectiveness of [^{68}Ga]Ga-NODAGA-exendin-4 with current standard non-invasive imaging procedures (CT and/or MRI and SSTR PET/CT ([^{68}Ga]Ga-Dotatoc or [^{68}Ga]Ga-Dotatate)) for the localization of insulinomas.

Materials and methods

Study design and patients

In this prospective, multicenter imaging study (NCT03189953), patients were included at the Radboud University Medical Center Nijmegen and the University Medical Center Groningen in The Netherlands, the University of Turku in Finland and Uppsala University in Sweden. Recruitment of patients was performed both directly in these participating centers as well as by referral from several tertiary centers across Europe. Patients with biochemically proven AHH with neuroglycopenic symptoms in the fasting state with low plasma glucose levels and inappropriately high serum insulin and C-peptide levels were enrolled. Exclusion criteria were evidence of other malignancies than insulin-producing tumors in conventional imaging, renal insufficiency (creatinine clearance < 40 ml/min), pregnancy and breast feeding. The study was approved by the local institutional review board of each of the participating institutes. All included patients provided written informed consent in accordance with provisions of the Declaration of Helsinki.

Radiopharmaceutical preparation

Hydrochloric acid (HCl) was purchased from Rotem Industries. All other components were purchased as one disposable kit (reagent and hardware kit for synthesis of ^{68}Ga peptides using cationic purification, ABX, Germany). [^{68}Ga]Ga-NODAGA-exendin-4 was manufactured using a synthesizer module (GRP synthesizer, Scintomics, Germany). Gallium-68-chloride was obtained from a ^{68}Ge/^{68}Ga generator (Galliapharm, Eckert and Ziegler, Germany). The generator was eluted with 10 ml of 0.1 M HCl and gallium-68 was trapped on a polystyrene-H+

cartridge. The cartridge was eluted with 1.5 ml 5M NaCl in 0.1 M HCl into the reaction vial, containing 200 μl exendin-NODAGA (10 μg of peptide in water for injection), 475 μl 2.5 M 4-(2-hydroxyethyl)-1-piperazineethanesulfonic acid (HEPES) buffer and 50 μl ascorbic acid 100 mg/ml in water for injection. After 15 minutes incubation at 100°C, the vessel is cooled and 2 ml ethylenediaminetetraacetic acid (EDTA) 50 mM/ polysorbate 80 0.15% is added. [^{68}Ga]Ga-NODAGA-exendin-4 was purified on a HLB cartridge and sterilized by passing through a 0.2 μm filter (millex GV).

Imaging procedures

Standard imaging was performed according to local guidelines for insulinoma detection following standardized imaging protocols according to the study protocol of this trial. In each patient this at least included SSTR PET/CT (^{68}Ga-Dotatoc or ^{68}Ga-Dotatate), performed according to the EANM guidelines (14) and triple phase CT and/or MRI. For triple phase CT nonionic contrast agent was administered at a flow rate of 3,5 mL/s followed by a saline flush. Triple phase CT (automatic tube current modulation with maximum tube current, 230 mAs; tube voltage 120 kV; gantry rotation 0.5s) was performed using bolus tracking. The early arterial phase (scan initiation 5s after reaching the 100-Hounsfield-unit threshold in the abdominal aorta, resulting in a delay of 25s) and the portal-venous inflow phase (20s delay from the beginning of the arterial phase) covering the upper abdomen. The venous phase (50s delay from the arterial phase) was performed as a whole-body CT. Detector collimation was 16 x 0.75mm for arterial CT and 16 x 1.5mm for venous CT. Primary image reconstruction was performed at a 0.75- and 4mm slice thickness for arterial CT and a 2- and 5 mm thickness for venous CT (increment 0.5mm) (15). MRI was performed with a 1.5 or 3 Tesla system using multichannel body surface coils. Sequences incorporated contained the standard for abdominal imaging including precontrast T1 weighted, fat saturated T2 weighted, diffusion weighted and post contrast fat saturated T1 weighted sequences.

For GLP-1R imaging, patients were injected intravenously with [^{68}Ga]Ga-NODAGA-exendin-4 (105.6 ± 2.3 MBq) as a slow bolus over one minute. Patients fasted for 4 hours before injection of the tracer to prevent competition for binding to GLP-1Rs between endogenous GLP-1 and [^{68}Ga]Ga-NODAGA-exendin-4. Blood glucose levels were monitored before, and 15, 30, 60 and 120 minutes after injection of the tracer. Infusion with 5% glucose for 2 hours was started 15 minutes before or just after tracer injection, depending on blood glucose levels of the patients. Two consecutive PET scans were obtained at 60 and 120 minutes after injection of [^{68}Ga] Ga-NODAGA-exendin-4. Images of the abdomen were acquired with 2 bed positions at 10 minutes per bed position. A low-dose CT scan without contrast (40 mAs and 130 kV) was acquired for anatomical localization and attenuation

correction. The size of the CT transaxial matrix was 512 x 512 (0.98 × 0.98 mm), and the CT slice width was 3 mm. High definition reconstruction of the images was performed with 3 iterations, 21 subsets and a post reconstruction Gaussian filter of 3 mm in full width at half maximum. The transaxial PET matrix size was 200 x 200 and pixel size was 4 x 4 x 3 mm.

Evaluation

The reference standard was histologic evaluation and clinical outcome (normalization of blood glucose levels after surgery). Clinical reports of all standard imaging procedures were provided by radiologists or nuclear medicine physicians at the referring centers. Clinical reporting of GLP-1R PET/CT scans was performed by nuclear medicine physicians at the site of inclusion of the patient.

Quantitative analysis of SSTR and GLP-1R PET/CT scans of patients in which these were both positive, was performed by a non-blinded observer. Volumes of interest were drawn to determine uptake in the tumors (SUV_{mean}(tum)) using a fixed threshold set to 70 % of the maximum standardized uptake value (SUV_{max}) in the lesions in PET/CT images obtained 1 hour post injection. Volumes to measure uptake in the direct background of the lesions (SUV_{mean}(BG)) were drawn within the pancreas on all sides 16 mm around the tumor-volumes (with a gap of 8 mm (2 voxels) to account for spill-over of signal from the tumor). Also, volumes of interest were drawn manually around the whole pancreas excluding the tumor (SUV_{mean}(panc)). Tumor-to-background ratios were determined by: (SUV_{mean}(tum)) / (SUV_{mean}(BG)). Contrast-to-noise ratios, as a measure of image quality, were determined by: (SUV_{mean}(tum)) - (SUV_{mean}(panc)) / SD(panc).

Statistical analysis

Positive imaging tests supported by histopathology and normalization of blood glucose levels in the patient after surgery were regarded as true positives. A patient-based analysis was performed, meaning that in patients with multiple lesions, an imaging result was regarded as a true positive if at least one lesion was localized correctly in relation to histopathology. Numbers of correct assessments (conclusion of scan in correspondence with histopathology) and incorrect assessments (conclusion of scan not corresponding with histopathology) of the different imaging modalities were represented in 2 x 2 contingency tables and compared using a McNemar test for comparison of paired nominal data. Tumor-to-background ratios and contrast-to-noise ratios of GLP-1R PET and SSTR PET were compared using paired sample T-tests. All statistical analyses were performed using SPSS (version 22; SPSS, Chicago, IL).

Results

Imaging

We included 42 patients with biochemically confirmed AHH. Baseline characteristics of the patients are given in Table 1. All patients underwent imaging with SSTR PET/CT and 3-phase contrast enhanced CT and/or MRI. Twelve patients had undergone only triple phase CT, 17 patients only MRI and 13 patients had undergone both, CT and MRI. EUS was only performed in 17 patients. GLP-1R PET/CT and SSTR PET/CT was performed in all patients. Median time between SSTR PET/CT and GLP-1R PET/CT was 1.9 (0.1 – 4.1) weeks. Median time between CT/MRI and GLP-1R PET/CT was 4.7 (0.3 – 11.1) weeks. Disease was expected to remain stable within these timeframes ensuring reliable comparison of the scans. CT/MRI, SSTR PET/CT and GLP-1R PET/CT revealed suspicious lesions in 64%, 50% and 74% of patients respectively (Table 1). The highest radiotracer uptake was present in the tumors and kidneys (Fig 3).

Table 1 Characteristics of study participants.

Participants (n=42)	
Age	55 (41 - 62)
Sex	
Female	28/42 (67%)
Male	14/42 (33%)
Duration of symptoms (months)	14 (3 – 42)
Fasting test	
Duration (hours)	20 (10 – 44)
Plasma glucose (mmol/L)	2.0 (1.8 – 2.4)
C-peptide (nmol/L)	0.8 (0.5 – 1.0)
Insulin (mU/L)	14.0 (6.5 – 24.5)
Detection of suspicious lesions	
CT	14/25 (56%)
MRI	18/30 (60%)
Conventional (CT & MRI)	27/42 (64%)
SSTR PET/CT	21/42 (50%)
EUS	12/17 (71%)
GLP-1R PET/CT	31/42 (74%)

Data are given as number/total or median and interquartile range.

Two patients (5%) experienced nausea and 1 patient (2%) experienced vomiting following injection of [^{68}Ga]Ga-NODAGA-exendin-4. No other adverse effects were observed. In all patients, exogenous glucose infusion (5%, 250ml/h) for 2 hours was started 15 minutes before or just after injection of the tracer. As a result, no severe hypoglycemic episodes occurred in any of the patients.

Surgery and histopathology

Results of all imaging modalities were used for surgical planning. Median time between GLP-1R PET/CT and surgery was 49 (18 – 69) days. Combined results of all imaging modalities revealed the presence of a suspicious lesion in 33 patients. Of these patients, 2 patients declined surgery because symptoms could be sufficiently managed with diet (patient 16) or medication (patient 27). In the other 31 patients, successful surgery was performed and histological evaluation showed the presence of 1 or multiple insulinomas with a size of 7 – 35 mm. Plasma glucose values normalized after the procedure in all these patients with no further episodes of hypoglycemia.

Of the 11 patients in which none of the imaging procedures revealed a suspicious focal lesion, only 1 patient (patient 24) underwent surgery (body/tail resection). Surgery confirmed diffuse beta cell hyperplasia and blood glucose values normalized after the procedure.

Since histopathology and clinical follow-up were the reference standard, patients who did not undergo surgery were excluded from analysis. An overview of the performed procedures is shown in Figure 1 and results of imaging as well as surgical outcomes of all patients are summarized in Table 2.

Outcomes

Results of SSTR PET/CT, 3-fase CT, MRI, conventional imaging (combined results of 3-fase CT and MRI) and GLP-1R PET/CT, for all 32 patients with histopathological confirmation, are summarized in Table 3. GLP-1R PET/CT has higher accuracy and sensitivity (90.6% and 93.5% resp.) than the other imaging modalities (78.1% and 80.6% for anatomical imaging resp. and 59.4% and 61.3% for SSTR PET/CT resp.). Since in this patient population, there were no false positive results with any of the imaging modalities, positive predictive values are 100% for all modalities.

Crosstabs directly comparing GLP-1R PET/CT with the standard imaging modalities, based on the number of correct (corresponding with histopathology) and incorrect outcomes (not corresponding with histopathology) of the scans, are depicted in Figure 2. Results of the GLP-1R PET/CT were correct in 30 of 32 cases, compared to 20 correct results of SSTR PET/CT. In only one of the two cases in which the result of GLP-1R PET/CT showed no lesion, while an insulinoma proved to be present, the lesion was discovered with SSTR PET/CT. In the other case only

EUS correctly identified the presence of a lesion. Importantly, GLP-1R PET/CT provided correct results for 11 out of 12 cases in which SSTR PET/CT was incorrect, showing that GLP-1R PET/CT outperformed SSTR PET/CT ($p<0.05$).

Conventional imaging provided correct result in 26 cases, compared to 30 with GLP-1R PET/CT. Also, conventional imaging was able to provide a correct result in one of the 2 cases in which GLP-1R PET/CT was incorrect. GLP-1R PET/CT was correct in 5 out of 6 cases in which conventional imaging was incorrect. While this result does not reach statistical significance ($p = 0.22$), GLP-1R imaging did have an added value over conventional imaging in this patient population. Especially since in 4 of the 32 patients (12.5%), a lesion was only correctly identified using GLP-1R PET/CT while all standard imaging modalities were negative. The decision to perform surgery in these patients was therefore based solely on the results of the GLP-1R PET/CT.

Image quality

GLP-1R PET/CT and SSTR PET/CT images of 2 patients are shown in Figure 3. Results of image quantification are shown in Figure 4. Mean tumor-to-background ratios were (12.2 ± 3.4) for GLP-1R PET compared to (4.0 ± 3.0) for SSTR PET ($p=0.0017$) and mean contrast-to-noise ratios were (24.1 ± 20.8) for GLP-1R PET compared to (5.3 ± 4.4) for SSTR PET ($p=0.022$), indicating the superior image quality of the GLP-1R PET, allowing to better distinguish the lesion from the surrounding pancreatic tissue.

Table 2 Overview of imaging results and surgical outcome of all included patients.

	Imaging							Outcome	
Patient nr	CT	MRI	SSTR PET/CT	GLP-1R PET/CT	EUS	Total positive procedures	Localization	Surgery type	Tumor size
1	neg	x	neg	neg	x	0	No lesion	No surgery	NA
2	x	TP	TP	TP	x	3	Tail	Tail resection	17
3	x	TP	TP	TP	x	3	Tail	Tail resection	12
4	x	TP	TP	TP	x	3	Body	Body/tail resection	18
5	TP	TP	FN	TP	TP	4	Tail	Tail resection	7
6	x	neg	neg	neg	x	0	No lesion	No surgery	NA
7	x	FN	TP	TP	TP	3	Uncinate process	Enucleation	8/12 (2 lesions)
8	x	FN	FN	TP	x	1	Tail	Tail resection	9
9	FN	FN	FN	TP	FN	1	Tail	Body/tail resection	10
10	TP	TP	TP	TP	x	4	Tail	Tail resection	10
11	neg	neg	neg	neg	x	0	No lesion	No surgery	NA
12	x	TP	TP	TP	x	3	Body	Body/tail resection	11
13	neg	neg	neg	neg	neg	0	No lesion	No surgery	NA
14	x	TP	TP	TP	TP	4	Head/body	Pancreatico-duodenectomy	27-32 (multiple lesions)
15	x	TP	TP	TP	x	3	Tail	Tail resection	unknown
16	x	pos	pos	pos	x	3	Head	No surgery, patient stable with diet	NA
17	neg	x	neg	neg	neg	0	No lesion	No surgery	NA
18	x	TP	TP	TP	x	3	Tail	Tail resection	20
19	TP	x	TP	TP	x	3	Tail	Tail resection	18
20	TP	TP	TP	TP	x	4	Tail	Tail resection	17
21	x	TP	TP	TP	x	3	Head	Pancreatico-duodenectomy	12

22	TP	TP	FN	TP	TP	4	Tail	Tail resection	12
23	x	TP	FN	TP	x	2	Body	Enucleation	12
24	x	TN	TN	TN	TN	0	No lesion	Body / tail resection	No lesion
25	FN	FN	FN	FN	TP	1	Tail	Tail resection	20
26	x	neg	neg	neg	x	0	No lesion	No surgery	NA
27	x	pos	pos	pos	x	3	Head	No surgery, patient stable on diazoxide	NA
28	TP	x	TP	TP	TP	4	Tail	Tail resection	21
29	FN	x	FN	TP	x	1	Body	Pancreatico-duodenectomy	11
30	TP	x	TP	FN	x	2	Head	Pancreatico-duodenectomy	35
31	FN	FN	FN	TP	TP	2	Body	Body / tail resection	9
32	TP	x	TP	TP	TP	4	Body	Body / tail resection	10
33	neg	x	neg	neg	neg	0	No lesion	No surgery	NA
34	TP	FN	FN	TP	TP	3	Tail	Tail resection	3/10 (two-part lesion)
35	TP	x	TP	TP	x	3	Body	Body / tail resection	9
36	TP	TP	TP	TP	x	4	Body	Enucleation	20
37	TP	FN	FN	TP	x	2	Body	Body / tail resection	13
38	neg	x	neg	neg	x	0	No lesion	No surgery	NA
39	TP	x	TP	TP	x	3	Head	Pancreatico-duodenectomy	12
40	FN	TP	FN	TP	TP	3	Head	Pancreatico-duodenectomy	15
41	FN	TP	FN	TP	TP	3	Tail	Tail resection	13
42	TP	x	TP	TP	TP	4	Head	Pancreatico-duodenectomy	12

Imaging results with histopathological confirmation are given as TP (true positive), FN (false negative) or TN (true negative) and imaging results without histopathological confirmation are given as pos (positive) or neg (negative).

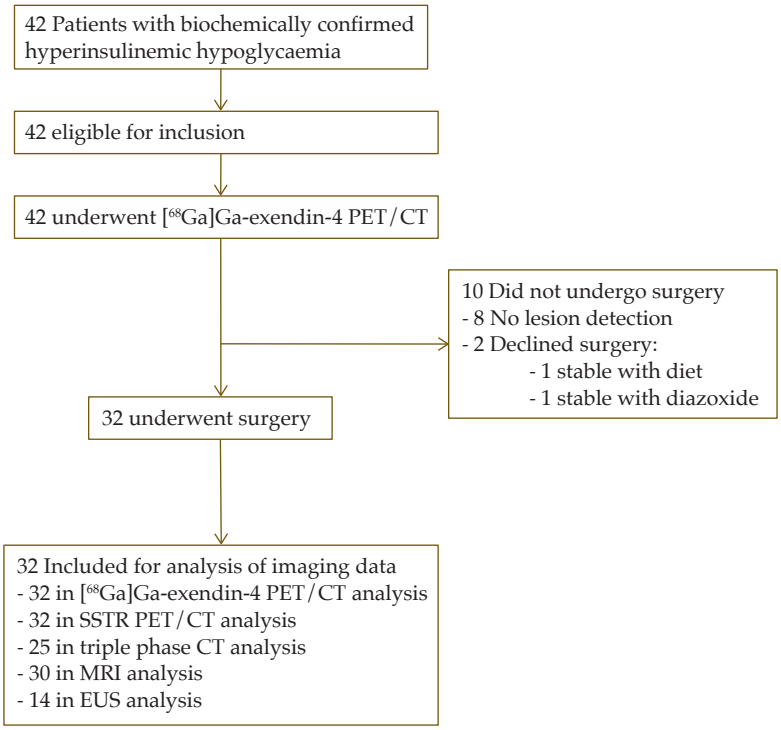

Figure 1 Flow chart of patient inclusion and analysis

Table 3 Overview of imaging results in participants who have undergone surgery resulting in conclusive histopathological analysis.

Imaging procedures	**Accuracy**	**Sensitivity**
Standard imaging		
3-phase CT (n=20)	70.0%	70.0%
MRI (n=23)	69.6%	72.7%
Conventional (CT & MRI) (n=32)	78.1%	80.6%
SSTR PET/CT (n=32)	59.4%	61.3%
GLP-1R PET/CT (n=32)	**90.6%**	**93.5%**

Accuracy and sensitivity are given in percentages. Tumor-to-background ratios and contrast-to-noise ratios of tracer uptake are given as mean ± SD.

A

	GLP-1R PET/CT	
SSTR PET/CT	Correct	Incorrect
Correct	19	1
Incorrect	**11**	1

B

	GLP-1R PET	
Conventional	Correct	Incorrect
Correct	25	1
Incorrect	**5**	2

C

	GLP-1R PET	
Standard	Correct	Incorrect
Correct	26	1
Incorrect	**4**	1

Figure 2 Crosstabs comparing the number of correct (correctly corresponding to histopathology) and incorrect (not corresponding with histopathology) assessments of GLP-1R PET/CT and SSTR PET/CT (A), Conventional imaging (B) and the combination of all standard imaging modalities (C).

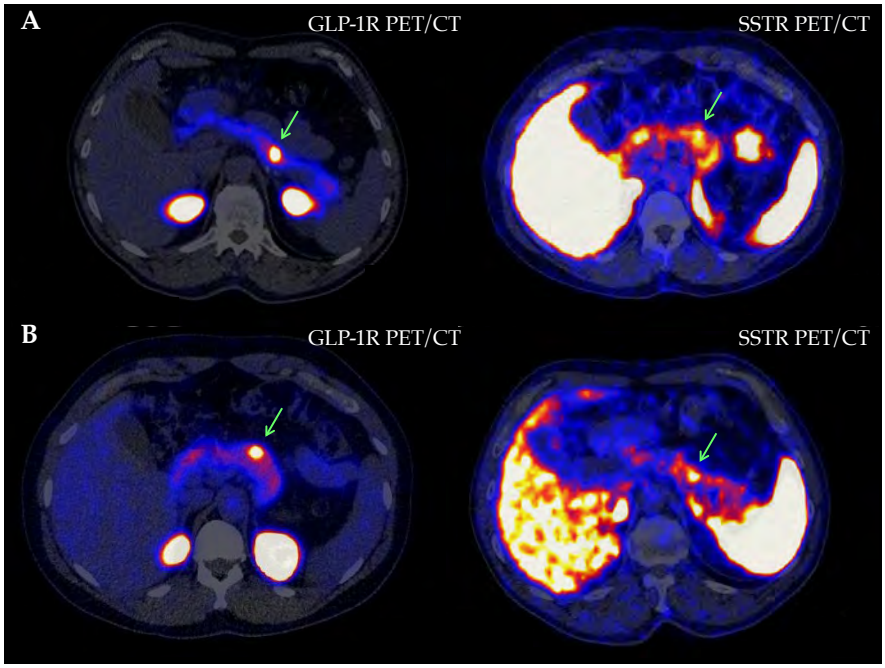

Figure 3 GLP-1R PET/CT and SSTR PET/CT images of patient 4 (A) and patient 9 (B). Location of tumors is indicated with green arrows.

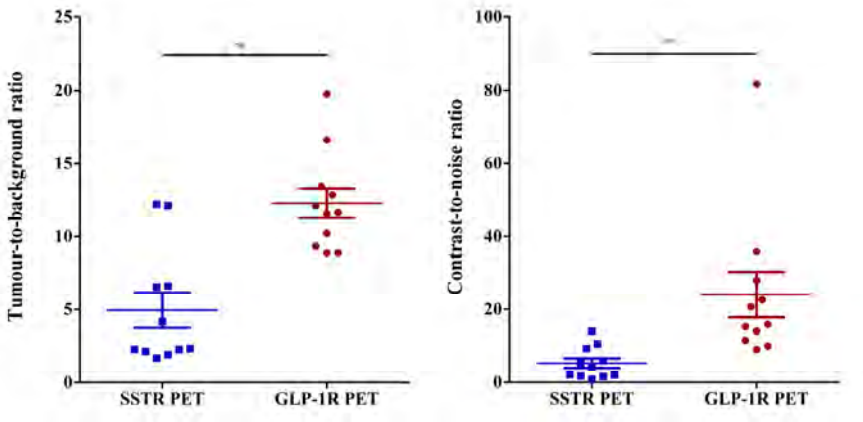

Figure 4 Tumor-to-background and contrast-to-noise ratios of GLP-1R PET and SSTR-PET images, * indicates P<0.05.

Discussion

The results of this prospective multicenter imaging trial show a superior accuracy (90.6%) and sensitivity (93.5%) of GLP-1R PET/CT for the localization of insulinomas compared to current standard imaging modalities. With GLP-1R PET/CT alone, 30 out of 32 patients (94%) were correctly diagnosed. In 4 out of 32 patients (12.5%), correct diagnosis and decision to perform surgery was only reached with GLP-1R PET/CT. GLP-1R PET/CT therefore significantly influenced the clinical management of the patients in this population.

SSTR PET/CT had an accuracy and sensitivity of only 59.4% and 61.3% respectively. While a detection rate of 85% was reported for SSTR PET/CT in a previous study (7), the levels of accuracy and sensitivity of SSTR PET/CT found in this study correspond well with expression levels of SSTR subtype 2 (69%) reported previously in insulinoma samples, using in vitro autoradiography (8). In addition to the superior detection rate of GLP-1R PET/CT, the image quality, quantified as tumor-to-background ratios and contrast-to-noise ratios, was clearly superior to SSTR PET.

A previous prospective imaging study by Antwi *et al*., comparing GLP-1R PET/CT using [^{68}Ga]Ga-DOTA-exendin-4 with conventional imaging, reported levels of accuracy (93.9%) and sensitivity (94.6%) of GLP-1R PET/CT for detection of insulinomas, which are comparable to this study. In this previous study, an accuracy of 67.6% and sensitivity of 69.4% was reported for the study MRI (6), which is also comparable to the accuracy and sensitivity (69.6% and 72.7% resp.)

found for MRI in the current trial. In the current trial however, GLP-1R PET was compared to the combination of conventional imaging modalities performed by the referring centers in the included patients, thereby better reflecting the current standard of care of patients with confirmed AHH in these centers and thus reflecting current best clinical practice. This combination of conventional imaging modalities resulted in an accuracy of 78.1% and sensitivity of 80.6%. While insulinomas can be difficult to discriminate from surrounding pancreatic tissue using conventional imaging, GLP-1R imaging provides more straightforward detection, because of the high tumor-to-background ratios. An interesting case which demonstrates this is patient 8. Both MRI as well as SSTR PET/CT were assessed as showing no suspicious lesions. However, after GLP-1R PET/CT revealed a very clear hotspot in the pancreatic body, the MRI was re-assessed and correlated with the GLP-1R PET after which a hypo-intense lesion was found at the same site (Figure 5).

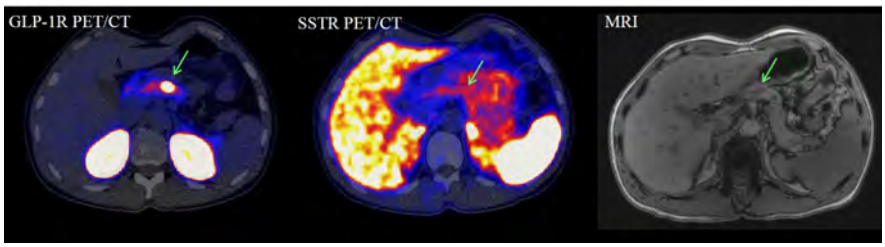

Figure 5 Images of GLP-1R PET/CT, SSTR PET/CT and MRI (T1) of patient 8. Location of the tumor is indicated with green arrows.

In our patient population, the median size of the lesions identified by GLP-1R PET/CT was 12 (10 – 18) mm, including 5 lesions smaller than 10 mm, showing the excellent sensitivity of the technique. The nature of the cases included in our trial thereby matches with the cases included in the trial by Antwi *et al.*, in which a median tumor size of 12 mm was reported as well. The 2 false negative GLP-1R PET/CT findings in the current trial were identified in patients with tumors of 20 mm (patient 25) and 35 mm (patient 30). These are therefore probably unrelated to the size of the tumors, but related to the lack of GLP-1R expression, which is in agreement with to the GLP-1R expression rate of 92% found by Reubi *et al*.

Without invasive procedures such as EUS and AVSV, GLP-1R PET correctly diagnosed 30 out of 32 patients in our study population. Performance of EUS identified a lesion in only 1 additional patient. In addition to the multiple non-invasive imaging procedures which were performed in all patients, 13 patients

underwent an EUS before being referred for GLP-1R PET/CT. Performing GLP-1R PET as the primary diagnostic imaging procedure, potentially combined with contrast enhanced CT for optimal anatomical correlation and surgical planning, could thus grossly reduce the burden for AHH patients, eliminating the need for additional diagnostic procedures in most patients.

The first studies on GLP-1R imaging for detection of insulinoma have focused on SPECT/CT using ^{111}In-labeled exendin (9, 16). The use of an exendin-based PET tracer has the advantage of the higher sensitivity and spatial resolution of the scanner and has therefore been shown to perform better than GLP-1R SPECT/CT (6, 12). In contrast to previous studies on GLP-1R PET/CT in patients with AHH (6, 12, 17), we used the chelator NODAGA instead of DOTA. Because of the higher specific activity achieved through the use of this chelator and optimized labeling protocols, we injected a peptide dose of 4-7 μg in contrast to 12-24 μg used with [^{68}Ga]Ga-DOTA-exendin. This lower peptide dose reduces the pharmacological effects of the peptide, resulting in the occurrence of nausea in only 5% of patients in this study compared to 27% of patients injected with [^{68}Ga]Ga-DOTA-exendin. The ability to perform GLP-1R PET/CT imaging using such a low peptide dose with [^{68}Ga]Ga-NODAGA-exendin is also favorable for the use of this tracer in children, in whom this technique could benefit diagnostic imaging of congenital hyperinsulinism, as is currently being assessed in a prospective trial (NCT03768518).

A limitation of this study is the comparison of GLP-1R PET/CT to standard procedures performed according to the protocols of the referring centers. This could entail certain variation in the execution of these imaging procedures. Also, GLP-1R PET/CT was compared to all current standard imaging modalities except ^{18}F-DOPA PET/CT. While ^{18}F-DOPA PET/CT is performed for diagnostic imaging of patients with AHH in certain centers, we did not include it in this trial, since it was not used as a standard diagnostic procedure in the majority of the referring centers. Previous studies assessing ^{18}F-DOPA PET/CT included no more than 11 patients and showed detection rates of 90% (18), 73% (19) and 50% (20). Antwi *et al*. Could not detect any insulinoma using ^{18}F-DOPA in 5 patients in which GLP-1R PET/CT had a detection rate of 93% (6). These inconsistent results for ^{18}F-DOPA compared to the consistently high reported sensitivity of GLP-1R PET/CT probably point towards a better performance of GLP-1R PET/CT.

The study is furthermore limited by the fact that biochemically proven AHH is no confirmation of the presence of an insulinoma. Histopathological confirmation and clinical outcome was chosen as a reference standard and only patients undergoing surgery could therefore be included in the analysis. A considerable number of patients in this study (19%) did not undergo surgery because no lesion was detected with any of the imaging techniques, including GLP-1R PET. Therefore, it is not possible to accurately assess the number of false and true negative results.

While insulinomas are the most common cause of AHH and in the general population only 0.5% to 5% of cases are instead caused by diffuse beta cell hyperplasia, the percentage of patients with diffuse beta cell hyperplasia in this study is probably higher because of an inclusion bias because of referral of difficult cases with negative imaging results.

Conclusion

This study demonstrates the superior performance of [^{68}Ga]Ga-NODAGA-exendin-4 PET/CT compared to current standard non-invasive imaging modalities for pre-operative localization of benign insulinomas. Because of its high sensitivity and excellent imaging quality, [^{68}Ga]Ga-NODAGA-exendin-4 PET/CT has the potential to be the primary diagnostic imaging modality in patients with AHH. [^{68}Ga]Ga-NODAGA-exendin-4 PET combined with contrast enhanced CT could provide a one stop shop procedure for insulinoma diagnostics, which would eliminate the need for any further diagnostics in most patients. Since currently multiple different imaging procedures are performed, sometimes repeatedly, in most patients to reach a definite diagnosis, such a one stop shop procedure would benefit the patients considerably and could additionally improve cost-effectiveness of the diagnostic process for AHH.

References

1. Kinova MK. Diagnostics and treatment of insulinoma. Neoplasma. 2015;62(5):692-704.
2. Senniappan S, Shanti B, James C, Hussain K. Hyperinsulinaemic hypoglycaemia: genetic mechanisms, diagnosis and management. Journal of inherited metabolic disease. 2012;35(4):589-601.
3. Richards ML, Gauger PG, Thompson NW, Kloos RG, Giordano TJ. Pitfalls in the surgical treatment of insulinoma. Surgery. 2002;132(6):1040-9; discussion 9.
4. Mehrabi A, Fischer L, Hafezi M, Dirlewanger A, Grenacher L, Diener MK, et al. A systematic review of localization, surgical treatment options, and outcome of insulinoma. Pancreas. 2014;43(5):675-86.
5. Guettier JM, Kam A, Chang R, Skarulis MC, Cochran C, Alexander HR, et al. Localization of insulinomas to regions of the pancreas by intraarterial calcium stimulation: the NIH experience. The Journal of clinical endocrinology and metabolism. 2009;94(4):1074-80.
6. Antwi K, Fani M, Heye T, Nicolas G, Rottenburger C, Kaul F, et al. Comparison of glucagon-like peptide-1 receptor (GLP-1R) PET/CT, SPECT/CT and 3T MRI for the localisation of occult insulinomas: evaluation of diagnostic accuracy in a prospective crossover imaging study. European journal of nuclear medicine and molecular imaging. 2018;45(13):2318-27.
7. Prasad V, Sainz-Esteban A, Arsenic R, Plockinger U, Denecke T, Pape UF, et al. Role of (68)Ga somatostatin receptor PET/CT in the detection of endogenous hyperinsulinaemic focus: an explorative study. European journal of nuclear medicine and molecular imaging. 2016;43(9):1593-600.
8. Reubi JC, Waser B. Concomitant expression of several peptide receptors in neuroendocrine tumours: molecular basis for in vivo multireceptor tumour targeting. European journal of nuclear medicine and molecular imaging. 2003;30(5):781-93.
9. Christ E, Wild D, Ederer S, Behe M, Nicolas G, Caplin ME, et al. Glucagon-like peptide-1 receptor imaging for the localisation of insulinomas: a prospective multicentre imaging study. The lancet Diabetes & endocrinology. 2013;1(2):115-22.
10. Wild D, Macke H, Christ E, Gloor B, Reubi JC. Glucagon-like peptide 1-receptor scans to localize occult insulinomas. The New England journal of medicine. 2008;359(7):766-8.
11. Christ E, Wild D, Forrer F, Brandle M, Sahli R, Clerici T, et al. Glucagon-like peptide-1 receptor imaging for localization of insulinomas. The Journal of clinical endocrinology and metabolism. 2009;94(11):4398-405.
12. Antwi K, Fani M, Nicolas G, Rottenburger C, Heye T, Reubi JC, et al. Localization of Hidden Insulinomas with (6)(8)Ga-DOTA-Exendin-4 PET/CT: A Pilot Study. Journal of nuclear medicine : official publication, Society of Nuclear Medicine. 2015;56(7):1075-8.
13. Fani M, Del Pozzo L, Abiraj K, Mansi R, Tamma ML, Cescato R, et al. PET of somatostatin receptor-positive tumors using 64Cu- and 68Ga-somatostatin antagonists: the chelate makes the difference. Journal of nuclear medicine : official publication, Society of Nuclear Medicine. 2011;52(7):1110-8.
14. Virgolini I, Ambrosini V, Bomanji JB, Baum RP, Fanti S, Gabriel M, et al. Procedure guidelines for PET/CT tumour imaging with 68Ga-DOTA-conjugated peptides: 68Ga-DOTA-TOC, 68Ga-DOTA-NOC, 68Ga-DOTA-TATE. European journal of nuclear medicine and molecular imaging. 2010;37(10):2004-10.
15. Denecke T, Grieser C, Froling V, Steffen IG, Rudolph B, Stelter L, et al. Multislice computed tomography using a triple-phase contrast protocol for preoperative assessment of hepatic tumor load in patients with hepatocellular carcinoma before liver transplantation. Transplant international : official journal of the European Society for Organ Transplantation. 2009;22(4):395-402.
16. Christ E, Wild D, Antwi K, Waser B, Fani M, Schwanda S, et al. Preoperative localization of adult nesidioblastosis using (6)(8)Ga-DOTA-exendin-4-PET/CT. Endocrine. 2015;50(3):821-3.
17. Cuthbertson DJ, Banks M, Khoo B, Antwi K, Christ E, Campbell F, et al. Application of Ga(68) -DOTA-exendin-4 PET/CT to localize an occult insulinoma. Clinical endocrinology. 2016;84(5):789-91.
18. Kauhanen S, Seppanen M, Minn H, Gullichsen R, Salonen A, Alanen K, et al. Fluorine-18-L-dihydroxyphenylalanine (18F-DOPA) positron emission tomography as a tool to localize an insulinoma or beta-cell hyperplasia in adult patients. The Journal of clinical endocrinology and metabolism. 2007;92(4):1237-44.

19. Imperiale A, Sebag F, Vix M, Castinetti F, Kessler L, Moreau F, et al. 18F-FDOPA PET/CT imaging of insulinoma revisited. European journal of nuclear medicine and molecular imaging. 2015;42(3):409-18.
20. Nakuz TS, Berger E, El-Rabadi K, Wadsak W, Haug A, Hacker M, et al. Clinical Value of (18)F-FDOPA PET/CT With Contrast Enhancement and Without Carbidopa Premedication in Patients with Insulinoma. Anticancer research. 2018;38(1):353-8.

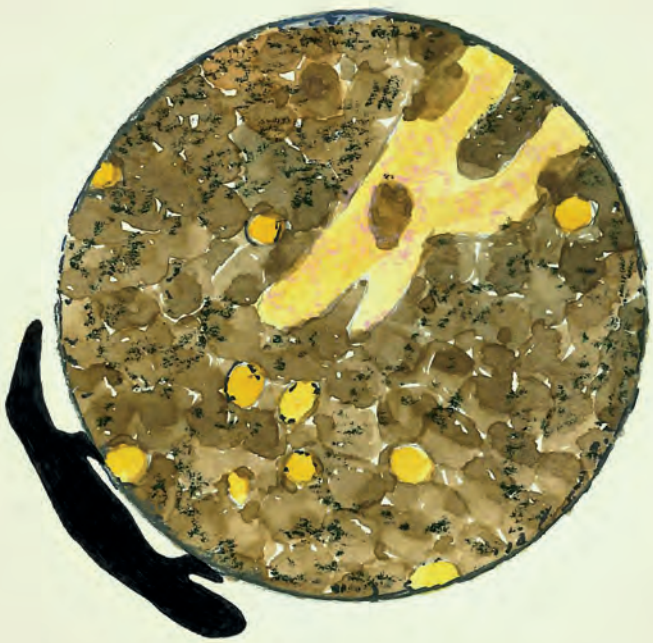

CHAPTER 3

[^{68}Ga]Ga-NODAGA-exendin-4 PET improves the diagnostic accuracy of focal congenital hyperinsulinism

Marti Boss[1], Christof Rottenburger[2,3], Winfried Brenner[4], Oliver Blankenstein[5], Vikas Prasad[4,6], Sonal Prasad[4,7], Paolo de Coppi[8], Mijke Buitinga[1], Pirjo Nuutila[9,10], Timo Otonkoski[11,12], Khalid Hussain[13], Maarten Brom[1], Annemarie Eek[1], Jamshed Bomanji[3], Pratik Shah[14,15], Martin Gotthardt[1]

Submitted

1 Department of Medical Imaging, Radboud University Medical Centre Nijmegen, Nijmegen, The Netherlands
2 Division of Nuclear Medicine, University Hospital Basel, Basel, Switzerland
3 Institute of Nuclear Medicine, University College London, London, United Kingdom
4 Department of Nuclear Medicine, Charité-Universitätsmedizin Berlin, Berlin, Germany
5 Department of Pediatric endocrinology, Charité University Hospital of Berlin, Berlin, Germany
6 Department of Nuclear Medicine, University Hospital of Ulm, Ulm, Germany
7 Berlin Experimental Radionuclide Imaging Center (BERIC), Charité-Universitätsmedizin Berlin, Berlin, Germany
8 Department of Pediatric Surgery, Great Ormond Street Hospital for Children NHS Foundation Trust, London, United Kingdom
9 Department of Endocrinology, Turku University Hospital, Turku, Finland
10 Turku PET Center, University of Turku, Turku, Finland
11 Stem cells and Metabolism Research Program, Faculty of Medicine, University of Helsinki, Helsinki, Finland
12 Children's Hospital, University of Helsinki and Helsinki University Hospital, Helsinki, Finland
13 Department of Pediatric Medicine, Division of Endocrinology, Sidra Medical and Research Centre, Doha, Qatar
14 Pediatric Endocrinology Department, Great Ormond Street Hospital for Children NHS Foundation Trust, London, United Kingdom
15 Department of Pediatric Endocrinology, The Royal London Children's Hospital, Bart's Health NHS Trust, London, United Kingdom

Abstract

Background

Surgery with curative intent can be offered to congenital hyperinsulinism (CHI) patients, provided that the lesion is focal. Radiolabeled exendin-4 specifically binds the glucagon-like peptide 1 (GLP-1) receptor (GLP-1R) on pancreatic beta cells. In this study we compared the performance of [^{18}F]F-DOPA PET (DOPA PET) and PET with the new tracer [^{68}Ga]Ga-NODAGA-exendin-4 (Exendin PET) in the preoperative diagnostics of focal CHI

Methods

Nineteen CHI patients underwent both DOPA PET and Exendin PET prior to surgery. The images were evaluated in three settings a) standard clinical reading b) blinded expert reading and c) joined reading. Target (lesion) / non target (normal pancreas) ratio were determined using maximum standard uptake value (SUV_{max}). Image quality was rated by pediatric surgeons in a questionnaire.

Findings

Fourteen/nineteen patients having focal lesions underwent surgery. Based on clinical readings, the sensitivity of Exendin PET (100% (CI 77-100%)) was higher than DOPA PET (71% (CI 42-92%)). Interobserver agreement between readings was higher for Exendin than DOPA PET (Fleiss' kappa 0.91 vs. 0.56). Exendin PET provided significantly ($p=0.021$) higher target / non target ratios (2.02 ± 0.65) than DOPA PET (1.40 ± 0.40). On a five point scale, Pediatric surgeons rated Exendin PET superior to DOPA PET.

Interpretation

Exendin PET has higher clinical sensitivity and better interobserver correlation than DOPA PET for the detection of focal CHI. Better contrast and image quality makes Exendin PET superior to DOPA in surgeons' intra-operative quest for lesion localization.

Introduction

CHI is the most common cause of persistent and recurrent hypoglycemia in neonates. It occurs with an incidence of one in 35000-40000 births (*1*). CHI often presents in neonates with poor feeding, seizures, jitteriness, hypotonia, apnea, cyanosis, hypothermia or a hypoglycemia-induced life-threatening event (*2*). CHI can also present in infancy or childhood and in rare cases even in adolescents or young adults (*3*). To avoid brain injury by hypoglycemia, an early diagnosis and proper treatment of CHI are of crucial importance. The diagnosis of CHI is based on clinical findings as well as hypoglycemic events combined with inappropriately high insulin levels (*4*). In diffuse CHI, which accounts for 60-70% of all cases, there is diffuse involvement of the pancreatic beta cells with enlarged hyperfunctioning cells with abnormally large nuclei and abundant cytoplasm (*5,6*). This subform is caused by recessive or dominant mutations in the *ABCC8* or *KCNJ11* genes, encoding for the beta cell ATP-sensitive potassium channels. Diffuse CHI is primarily treated with medication for the suppression of insulin secretion, such as diazoxide. However, many patients with recessive mutations in the *ABCC8* and *KCNJ11* genes are unresponsive to this therapy and near-total pancreatectomy may then be the only option to avoid devastating hypoglycemia. Even after such an invasive procedure, which carries a risk of developing insulin-dependent diabetes and exocrine pancreatic insufficiency, some children present with recurring hypoglycemia requiring further treatment with medication or even re-operation (*7*).

Focal CHI accounts for 30-40% of all CHI cases associated with the K_{ATP} channel genes. This form is characterized by focal adenomatous islet cell hyperplasia caused by the concurrence of a paternal mutation in the *ABCC8* or *KCNJ11* gene and somatic loss of heterozygocity of the maternal chromosome 11p15 region within a limited region in the pancreas (*8,9*). Because there is only involvement of a specific area in the pancreas in focal CHI, this subform can be treated successfully by partial pancreatectomy or limited lesionectomy, which can cure the disease in case of complete removal of the lesion (*6*). Since focal CHI can be treated with much less invasive surgery than diffuse CHI, correct differentiation between these subforms is of great importance. Also, precise pre-surgical localization of the focal lesion is important for correct surgical planning and optimization of surgical outcome. If the lesion resides in the body or tail of the pancreas, even a minimally invasive, laparoscopic procedure may be performed (*10*).

The current standard imaging technique used for non-invasive detection of focal CHI is ^{18}fluoro-L-dioxyphenylalanine ([^{18}F]F-DOPA) PET (DOPA PET) (*11*). This technique was shown to have a sensitivity of 85%-89% for the diagnosis of focal CHI (*12*), so in some cases focal lesions are still missed. In this study, we use a new radiotracer based on the peptide exendin-4, which specifically binds to the

GLP-1R expressed on pancreatic beta cells with high affinity (*13*). ^{68}Ga-labeled exendin has already been shown to detect insulinomas with high sensitivity (*14,15*), and the specific tracer used in the current study, [^{68}Ga]Ga-NODAGA-exendin-4, is currently being assessed in a large prospective trial for insulinoma imaging (NCT03189953). We have now analyzed data of patients with CHI who underwent both DOPA PET and [^{68}Ga]Ga-NODAGA-exendin-4 PET (Exendin PET) to compare the effectiveness of these two imaging techniques for the diagnosis and localization of focal CHI.

Materials and methods

Study design and patients

In this multicenter imaging study (NCT03768518), patients were included at the Great Ormond Street Hospital London in the United Kingdom and the Radboud University Medical Center Nijmegen in The Netherlands. Recruitment of patients was performed directly in these centers as well as by referral from several tertiary centers across Europe.

Patients were enrolled with biochemically proven endogenous CHI who were unresponsive to medical treatment and qualified for DOPA PET based on mutation analysis (no genetically proven diffuse CHI based on a homozygous or compound heterozygous *ABCC8/KCNJ11* mutation). Exclusion criteria were renal insufficiency (creatinine clearance < 40 ml/min) and evidence of other malignancies than insulin producing lesions in imaging studies. The study was approved by the local institutional review board of each of the participating institutes. Parents of all included patients provided written informed consent in accordance with provisions of the Declaration of Helsinki.

In addition, data from subsequent CHI patients diagnosed and treated at the Charité University Hospital Berlin in Germany were analyzed in accordance with national drug regulations. Parents of these patients provided written informed consent for the use of the new radiotracer as well.

Radiopharmaceutical preparation of [^{68}Ga]Ga-NODAGA-exendin-4

GRP synthesizer module was purchased from Scintomics GmbH, Germany and Modular Lab PharmTracer synthesis module from Eckert & Ziegler GmbH, Germany. Hydrochloric acid (HCl) was supplied by Rotem Industries Ltd. ^{68}GaCl3 was obtained from 1850 MBq ^{68}Ge/^{68}Ga generator (Galliapharm®, Eckert & Ziegler GmbH, Germany), SEPPAK C8 Plus Light Cartridges (C8) were purchased from Waters, UK and Chromafix® PS-H+ (small) from Macherey NagelTM, Germany. All other components were acquired as one disposable kit (Reagent and hardware

kit for synthesis of ^{68}Ga peptides using cationic purification) from ABX GmbH, Germany.

GRP Synthesizer Module (RadboudUMC Nijmegen)

The generator was eluted with 10 ml of 0.1 N HCl and ^{68}Ga was trapped on a polystyrene-H+ (PS-H+) cartridge. The cartridge was then eluted with 1.5 ml of 5M NaCl in 0.1 M HCl (eluent) into the reaction vial, containing 200 μl of exendin-NODAGA (10 μg of peptide in water for injection (WFI)), 475 μl of 2.5 M 4-(2-hydroxyethyl)-1-piperazineethanesulfonic acid (HEPES) buffer and 50 μl ascorbic acid (100 mg/ml in WFI). After 15 minutes incubation at 100°C, the vessel is cooled and 2 ml ethylenediaminetetraacetic acid (EDTA), 50 mM/polysorbate 80 0.15% is added. [^{68}Ga]Ga-NODAGA-exendin-4 was purified on a HLB cartridge, sterilized by passing through a 0.2 μm filter (millex GV) and diluted with saline.

Modular Lab PharmTracer Module (Charité Berlin and UCLH London)

The C18 cartridge of the cassette (C4-GA68-AFPP) was replaced by a C8 cartridge and the STRATA X cartridge was replaced by a PS-H+ cartridge (s) after pre-conditioning with 2ml of eluent followed by 5 ml of WFI. The generator was then eluted with 10 ml of 0.1 N HCl and ^{68}Ga was trapped on the PS-H+(s) cartridge. The cartridge was eluted with 1.7 ml of eluent into the reaction vial, containing 200 μl exendin-NODAGA (10 μg of peptide in WFI), 475 μl of 2.5 M HEPES buffer and 50 μl ascorbic acid (100 mg/ml in WFI). After 10 minutes incubation at 85 °C, the reactor was allowed to cool down to 70° C before adding 2 ml of EDTA, 50 mM/ polysorbate 80 0.15%. [^{68}Ga]Ga-NODAGA-exendin-4 was purified on a C8 cartridge, sterilized by passing through a 0.2 μm filter (millex GV) and diluted with saline.

Quality controls were performed on Radio-HPLC and Radio-TLC systems with a radiochemical purity of ≥ 95%. The pH of the tracer was around 6, the radiochemical yield and the molar specific activity were determined to be 50-60% and 175-200 MBq/nmol, respectively.

Procedures

In all patients, [^{18}F]F-DOPA (3 MBq/kg with a lower limit of 40 MBq) was injected as a slow bolus over one minute. Patients were not fasted and no pre-treatment with carbidopa was performed. A PET acquisition of one bed position and ten minutes per bed position was started 20 minutes after injection of the tracer. Depending on assessment of the first scan, additional PET acquisitions were performed at 40 and/or 60 minutes after injection of the tracer.

For Exendin PET, [^{68}Ga]Ga-NODAGA-exendin-4 (1.6 MBq/kg with a lower limit of 20 MBq, corresponding to a peptide dose of maximally 0.12 μg/kg and a lower limit of 1.4 μg) was injected intravenously as a slow bolus over five minutes

in all patients. Patients were fasted for one hour prior to injection of the tracer aiming to reduce endogenous GLP-1 production. Blood glucose levels were monitored before, and at least at 5, 10, 15, 30, 60, 90 and 120 minutes after injection of the tracer. Since blood glucose levels may decrease as a result of exendin injection, close monitoring was performed. Intravenous glucose injection was given to all patients as required to manage glucose levels during the procedure.

PET acquisition methods varied because of differences in institutional standard of care for CHI patients. Details on Exendin PET/CT and PET/MRI acquisition procedures for all centers as well as reconstruction parameters are given in Table 1. At the Great Ormond Street Hospital London, a protocol has been developed over the last eight years for DOPA PET/CT to be carried out under oral sedation with chloral hydrate in children with CHI to avoid general anesthesia (manuscript in submission). The same protocol was adopted to undertake the Exendin PET in London.

At the Radboudumc in Nijmegen, one patient was included. Scans in Nijmegen were performed without anesthesia with the use of a vacuum mattress.

Real world evidence from an institutional database of 11 CHI patients who underwent an Exendin PET for diagnostic purposes at the Charité University Hospital Berlin were included. In Berlin, patients are imaged under inhalation anesthesia with isoflurane under the supervision of an anesthesiologist unless older children are able to undergo the procedure without sedation.

Evaluation

Histological evaluation and clinical outcome (normalization of blood glucose levels after surgery) were used as a reference standard. Clinical reading of DOPA PET and Exendin PET scans was performed at the site of patient inclusion. The clinical reading was performed by a pediatric endocrinologist (hyperinsulinism expert) together with a nuclear medicine physician and a pediatric surgeon at the site of the PET scan. In addition, all DOPA and Exendin PET images were re-evaluated by one (MG) blinded Exendin-experienced nuclear medicine physician (expert reading). Additionally, a joint re-evaluation of all images was performed by this Exendin-experienced nuclear medicine physician together with a pediatric endocrinologist highly experienced in DOPA PET reading. For the expert and joint readings all images were evaluated in terms of the subform of the disease (focal vs. diffuse) and, if detected, the size and location of the focal lesion. For exact localization of the focal lesion, the pancreas was divided into six areas based on anatomical relation to the pancreatic duct and portal vein (Figure 1). In all image evaluations, images from all timepoints were used for interpretation.

Quantitative analysis of all DOPA PET and Exendin PET/CT or PET/MR scans was performed by a non-blinded expert. Volumes of interest were drawn to

Table 1 Imaging and reconstruction parameters.

GOSH London	
Scanner	PET/CT: Discovery PET/CT 710 slice scanner (GE Healthcare)
PET acquisition	List mode, start with tracer injection, 50 min duration
PET reconstruction	2 iterations, 24 subsets, standard Z filter 5 mm, 256x256 matrix
CT parameters	Low-dose CT scan without contrast, 100 kV, modulated between 10 and 210 mA, slice thickness 5 mm, 50 cm field of view
RadboudUMC Nijmegen	
Scanner	PET/CT: Biograph mCT-40 time-of-flight (Siemens)
PET acquisition	Static, started 45 minutes after tracer injection, 10 min duration
PET reconstruction	3 iterations, 21 subsets, post-reconstruction Gaussian filter of 3 mm in full width at half maximum, 200x200 matrix
CT parameters	Low-dose CT scan without contrast, 120 kV, 50mA, slice thickness 5 mm, 780 mm field of view
Charité Berlin	
Scanner	PET/CT: Philips Gemini TF16 ASTONISH PET/MRI: Siemens Biograph mMR
PET acquisition	PET/CT: dynamic, started with tracer injection, 40 min duration PET/MRI: List mode, started with tracer injection, 1 hour duration
PET reconstruction	PET/CT + PET/MRI: 8 frames à 5 min; 20 min p.i. 1 frame à 10 min; 30 min p.i. 1 frame à 10 min PET/CT: BLOB-OS-TF, reconstruction filter "smooth", 144x144, 4.0x4.0x4.0 mm PET/MR: 3 iterations, 21 subsets, post-reconstruction Gaussian filter of 4 mm, 172x172 matrix, pixel spacing 4.2x4.2x2.0 mm
CT parameters	Low-dose CT without contrast, 100 kV, modulated between 10 and 210 mA, slice thickness 5 mm, 50 cm field of view
MRI parameters	Attenuation: STARVIBE, TR 3.9 ms, TE 1.2 ms, Alpha 10.6° Additional sequences: axial HASTE, axial STARVIBE, coronal T2-STIR / TIRM

determine tracer uptake expressed as maximum standardized uptake value (SUV_{max}) in different parts of the pancreas as well as in visible focal lesions. SUV_{max} ratios of the areas with the highest tracer uptake and of the area with the next highest tracer uptake were determined. VOIs were drawn over the head, body and tail of the pancreas. Within these VOIs, isocontour VOIs were created consisting of the voxels with the 30% highest intensity (example of resulting VOIs are depicted in Figure 2). For quantification of the dynamic PET scans, reconstructed images of

the timeframe 30 to 40 minutes (Berlin) or 40 to 45 minutes (London) after injection were used.

To estimate the optimal imaging time point for Exendin PET, SUV_{max} ratios in reconstructed images of five-minute intervals over the imaging period from 0 to 45 minutes after tracer injection were determined in four patients with focal disease at the Great Ormond Street Hospital in London.

To evaluate image quality and correlation of imaging results with the intra-operative findings, DOPA PET and Exendin PET images of 13 patients with a detected focal lesion were rated by the involved pediatric surgeon using a questionnaire based on the Leiden-surgical rating scale (Figure 3).

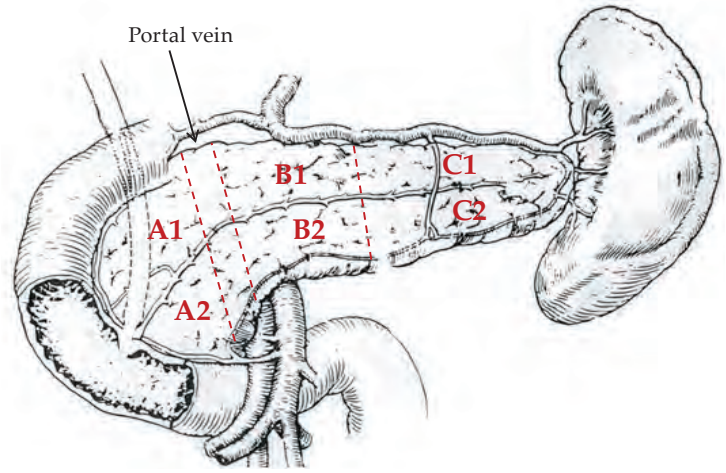

A = Head
B = Body
C = Tail
1 = Above the pancreatic duct
2 = Below the pancreatic duct

Figure 1 Image used for annotation of location of focus within the pancreas.

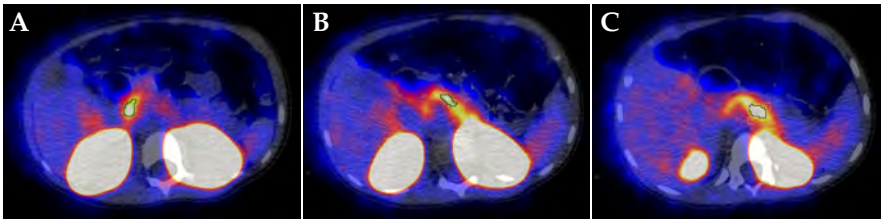

Figure 2 VOIs created of the voxels with the 30% highest intensity in the head (A), body (B) and tail (C) of the pancreas, used to calculate SUVmax ratios.

Surgeon questionnaire

The questionnaire for the pediatric surgeons, used to assess image quality and correlation of imaging results with intra-operative findings, contained the following questions:

1) How many CHI surgeries have you performed during your career?
   1. > 10
   2. < 10

2) How many CHI surgeries have you performed during the last 3 years
   1. > 5
   2. < 5

3) How do you rate the preoperative image quality for your decision on performing surgery? lesion? Please rate according to the following scale:
   1. Image quality extremely poor for decision making
   2. Image quality poor for decision making
   3. Image quality acceptable for decision making
   4. Image quality good for decision making
   5. Image quality optimal for decision making

1) How well did the imaging results correlate with the intraoperative findings? Please rate according to the following scale:
   1. Extremely poor correlation with intra-operative findings
   2. Poor correlation with intra-operative findings
   3. Acceptable correlation with intra-operative findings
   4. Good correlation with intra-operative findings
   5. Optimal correlation with intra-operative findings

2) Which imaging modality would you prefer for future CHI patients?

Figure 3 Surgeon questionnaire.

Statistical analysis

Positive imaging results confirmed by histopathology and the clinical outcome in terms of normalization of blood glucose levels in the patient after surgery were regarded as true positives. 59% confidence intervals for sensitivity were calculated using the Clopper-Pearson method. Interobserver variation was calculated using Fleiss' kappa. SUV_{max} ratios in DOPA PET and Exendin PET scans were compared using paired sample T-tests. Surgeon scores of image quality were compared using Wilcoxon signed rank tests. Statistical analyses were performed using SPSS (version 22; SPSS, Chicago, IL).

Results

Patients

We included data of 19 CHI patients. Baseline characteristics of the patients are given in Table 2 and clinical details of the patients are given in Table 3. All patients underwent DOPA PET and Exendin PET, with a median time of 13 (4 – 72) days between the procedures. Upon clinical reading of the scans, DOPA PET revealed focal areas of high tracer uptake suspicious for focal lesions in ten patients (53%) and Exendin PET revealed suspicious focal lesions in 14 patients (74%) (Table 4). The study profile is depicted in Figure 4.

Table 2 Patient characteristics.

Participants (n=19)	
Age (months)	8.3 (4.0 – 22.0)
Age at diagnosis (days)	7 (1.5 – 12)
Sex	
Female	8/19 (42%)
Male	11/19 (58%)
Genetic mutation	
Paternal ABCC8 mutation	16/19 (84%)
No or unknown mutation	3/19 (16%)
Response to medication	
Full	5/19 (26%)
Partial	14/19 (74%)

Data are given as median and interquartile range or number/total and percentage

Table 3 Pre-operative clinical patient data

Patient nr	Age (months)	Results of mutation analysis	Treatment	Treatment response
1	18	Paternal ABCC8 mutation	Lanreotide + gastrostomy feeds	Partial
2	22	Paternal ABCC8 mutation	Octreotide + Diazoxide + gastrostomy feeds	Partial
3	125	Paternal ABCC8 mutation	Octreotide, switched to Lanreotide	Full response to Lanreotide
4	50	Paternal ABCC8 mutation	Octreotide + gastrostomy feeds	Partial
5	61	Paternal ABCC8 mutation	Octreotide + Sirolimus + gastrostomy feeds	Partial
6	12	Paternal ABCC8 mutation	Octreotide	Full
7	8	Paternal ABCC8 mutation	Octreotide + gastrostomy feeds	Partial
8	8	Paternal ABCC8 mutation	Octreotide	Partial
9	4	Paternal ABCC8 mutation	Octreotide	Full
10	5	Paternal ABCC8 mutation	Octreotide + Diazoxide	Partial (limited)
11	2	Paternal ABCC8 mutation	Octreotide	Partial
12	2	Paternal ABCC8 mutation	Octreotide (continuous)	Partial
13	9	Paternal ABCC8 mutation	Octreotide	Partial
14	10	Unknown (no mutation in ATP-sensitive potassium channel)	Octreotide + Diazoxide + gastrostomy feeds	Partial
15	68	No mutation in known CHI-genes	Diazoxide	Partial/full
16	4	No mutation in known CHI-genes	Octreotide	Full
17	4	Paternal ABCC8 mutation	Octreotide	Partial
18	6	Paternal ABCC8 mutation	Octreotide	Full
19	3	Paternal ABCC8 mutation	Octreotide	Partial

Table 4 Sensitivity of DOPA PET and Exendin PET based on clinical and study readings.

	DOPA PET	Exendin PET
Focal lesions detected (clinical reading)	10/19 (53%)	14/19 (74%)
Sensitivity		
Based on clinical reading	71% (42 – 92%)	100% (77 – 100%)
Based on expert reading	86% (57 – 98%)	93% (66 – 100%)
Based on joint reading	100% (77 – 100%)	100% (77 – 100%)

Data given as value and 95% confidence interval, and percentages of agreement between readings. Sensitivity is calculated for cases with focal lesions only.

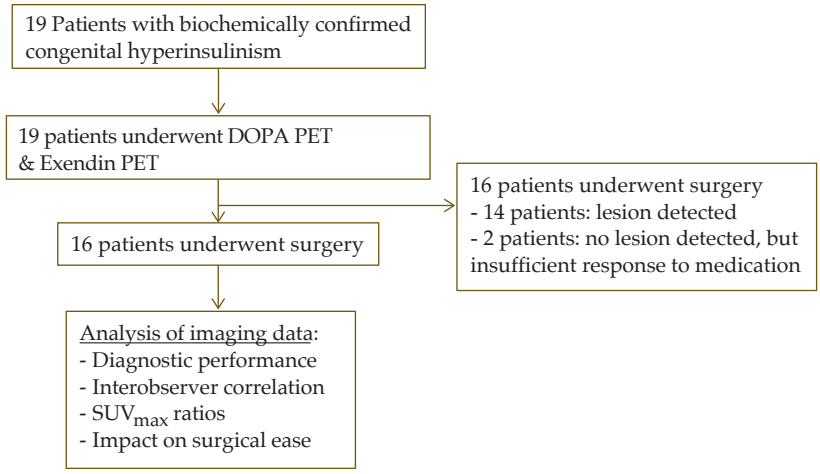

Figure 4 Study profile.

Tolerability

One patient (5%) experienced vomiting following injection of [^{68}Ga]Ga-exendin. In two patients (11%), episodes of mild hypoglycemia occurred following injection of [^{68}Ga]Ga-exendin, requiring intervention. In the other patients, glucose levels were stable (> 3.5 mmol/L) under regular monitoring and intravenous glucose infusion. No other adverse events occurred in any of the patients.

Surgery

Results of both imaging procedures were used for surgical planning. Suspicious lesions were detected by clinical reading of the PET images in 14 patients. These patients underwent surgery and presence of a focal lesion was confirmed by histopathological evaluation in all of these. All surgically treated patients with focal lesions were cured after surgery (normalization of blood glucose levels in long-term follow-up).

Of the remaining five patients, in which no focal lesion was detected by clinical reading (diffuse tracer uptake on both DOPA and Exendin PET), two underwent near-total pancreatectomy because of insufficient response to medication. In line with the imaging results, histopathology indicated focal disease in these patients.

Diagnostic performance

Results of the DOPA PET and Exendin PET are summarized in Table 4. In this patient population, Exendin PET has a sensitivity of 100% (CI 77-100%) for detection of focal lesions compared to a sensitivity of 71% (CI 42-92%) for DOPA PET, based on clinical readings of the images. In four out of 19 patients (21%), focal lesions were only identified using Exendin PET in the clinical reading. In these patients, the surgery planning was based solely on the results of the Exendin PET. DOPA PET and Exendin PET images of these four cases are shown in figure 5. Based on the clinical readings, Exendin PET performed better for detection of focal lesions in CHI.

Interobserver correlation

Upon re-evaluation of the DOPA PET images by an expert nuclear medicine physician, two additional focal lesions were identified, increasing the sensitivity to 86% (57-98%). In the expert readings of the Exendin PET images, one focal lesion was missed, decreasing the sensitivity to 93% (66-100%). By joint reading of the images by an expert nuclear medicine physician and pediatric endocrinologist, all focal lesions were detected on both Exendin PET and DOPA PET. While the sensitivity of both techniques reached 100%, the interobserver agreement between the readings is higher for Exendin PET than DOPA PET (Fleiss' kappa 0.91 vs. 0.56). For Exendin PET there is almost perfect agreement while for DOPA PET, the level of agreement between the readings is only moderate. The increased sensitivity of DOPA PET only upon re-evaluation of the images, together with the higher interobserver agreement in evaluation of the Exendin PET images, clearly indicates a facilitated and more reliable interpretation of the Exendin PET images compared to the DOPA PET images leading to more unequivocal results.

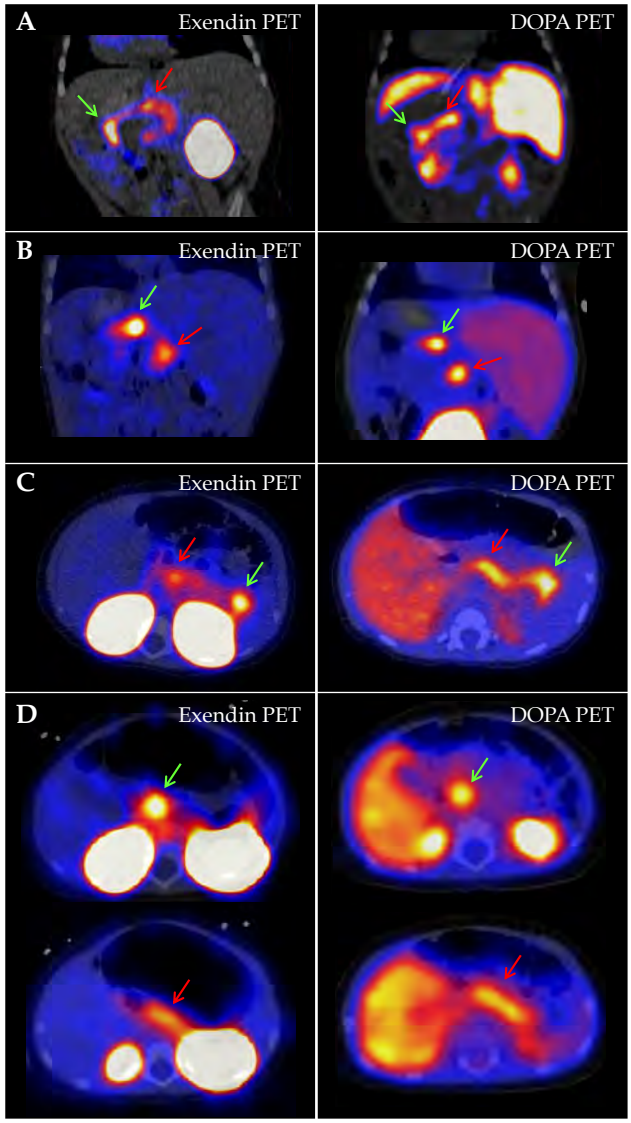

Figure 5 Exendin PET and DOPA PET images of patient 2 (A), patient 4 (B), patient 6 (C) and patient 9 (D), in which Exendin PET scans were reported as focal while DOPA PET scans were reported as diffuse in clinical readings. Locations of the focal lesions (for F-DOPA PET detected during joined readings) are indicated with green arrows. In D, the focal lesion in the head is indicated with green arrows and for comparison tracer uptake in the tail is indicated with red arrows. Presence of focal lesions was confirmed by histopathology in all four patients.

Semiquantitative analysis

In patients with histopathologically proven focal CHI, SUV_{max} ratios between the focal lesion and the area of the pancreas with the next highest tracer uptake are significantly higher in Exendin PET than DOPA PET (2.02 ± 0.65 and 1.40 ± 0.40, respectively, p=0.021), while SUV_{max} ratios in patients with diffuse disease (between the two pancreatic regions with the highest tracer uptake) were comparably low (1.08 ± 0.06 for Exendin PET and 1.15 ± 0.13 for DOPA PET) (Figure 6). These quantitative data show that Exendin PET provides better contrast to discriminate between focal and diffuse disease, and thus explains the different findings for interobserver agreement levels of the two tracers.

Quantification of reconstructed images of five-minute intervals over the imaging period shows some variability between patients in the timepoint which shows the highest SUV_{max} ratio. SUV_{max} ratios over time of these patients are depicted in Figure 7. For all four patients, the highest SUV_{max} ratio is between 30 and 45 minutes after tracer injection. This therefore seems to be the best timeframe for Exendin PET imaging.

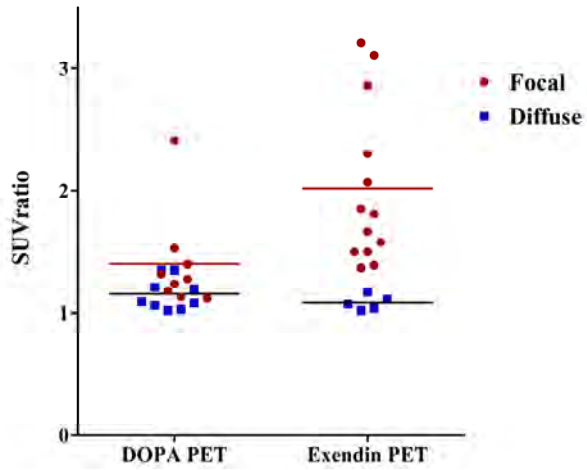

Figure 6 SUV_{max} ratios between the area with the highest tracer uptake and the area with the next highest tracer uptake. Scans with identified focal lesions during clinical reading are depicted in red. Scans reported to show diffuse disease are depicted in blue.

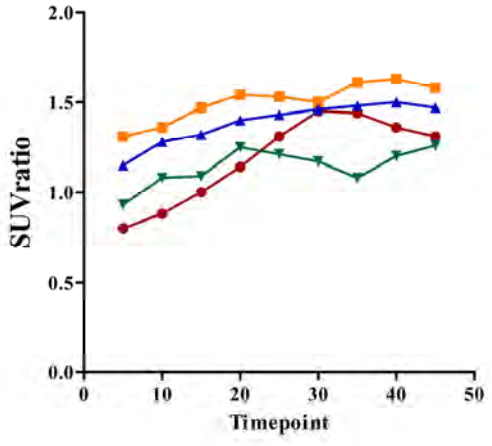

Figure 7 SUV_{max} ratios in Exendin PET images at different imaging timepoints of 4 patients with detected focal lesions.

Surgical ease

The influence of the PET image quality on the surgical ease was measured by rating of the DOPA and Exendin PET images by the involved pediatric surgeons. These surgeons were all experienced surgeons who have performed more than ten CHI surgeries during their career and more than five CHI operations during the last three years. Rating of the PET image quality by the surgeons showed significantly higher scores for Exendin PET than for DOPA PET for the decision to perform surgery (4.5 vs. 3.8 resp., p=0.025, figure 8A) as well as correlation of the imaging results with intra-operative findings (4.4 vs. 3.7 resp., p=0.0083, figure 8B). Out of 13 cases, surgeons reported to prefer Exendin PET imaging for future CHI patients in nine cases, versus DOPA PET in only one case and no preference in three cases, indicating a better image quality of Exendin PET compared to DOPA PET and the possible benefit for the surgical treatment of CHI patients.

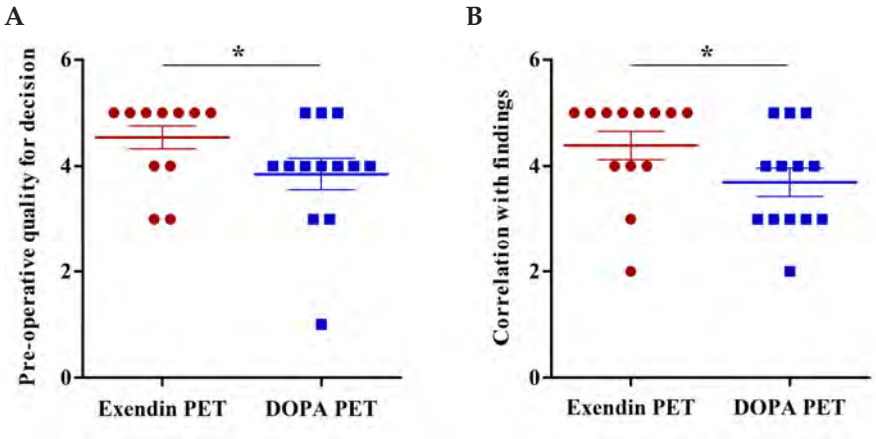

Figure 8 Rating scores of Exendin PET and DOPA PET images by pediatric surgeons. Scores on preoperative image quality for the decision to perform surgery (A) and correlation of imaging results with intraoperative findings (B). * Indicates $p<0.05$.

Discussion

The results of the present study indicate that Exendin PET is a promising tool for detection and localization of focal CHI. Standard clinical reading of the images provided a correct diagnosis of focal CHI in all 14 histologically proven cases based on Exendin PET (sensitivity: 100%, CI: 77-100%), while in four of the 14 cases diffuse disease was incorrectly diagnosed based on DOPA PET (sensitivity 71%, CI: 42-92%). While sensitivity of both techniques reached 100% upon joint reading by an expert nuclear medicine physician and a pediatric endocrinologist, the higher sensitivity of Exendin PET in clinical readings indicates easier reading and superior performance providing more unequivocal results. The more reliable performance of Exendin PET is also indicated by the higher interrater agreement between clinicians and experienced readers. Previously, a large prospective study with 50 cases and retrospective reviews of 105 and 195 cases reported sensitivities of 88%, 85%, and 89% respectively, for diagnosis of focal CHI using DOPA PET (*12,16,17*). The fact that in our small population of 19 patients, four cases of focal CHI were clinically not identified using DOPA PET, is suggestive of a high complexity of the cases. An overrepresentation of such difficult cases in our study population could result from an increased incentive to refer patients with complex and equivocal imaging results for a new investigative diagnostic procedure. In this population, Exendin PET outperformed DOPA PET in the clinical non-expert setting,

facilitating curative surgery without the need for further medicinal treatment or near-total pancreatectomy in four additional patients. Exendin PET therefore had a major positive impact on the clinical management of these patients.

All focal lesions identified by Exendin PET were confirmed by histopathology. Four patients in which both, DOPA PET and Exendin PET indicated diffuse disease did not undergo surgery, but received continued medical treatment. Therefore, we cannot exclude the possibility that a focal lesion was missed in these patients by both imaging procedures.

Quantitative analysis of scans of patients with histopathologically confirmed focal CHI showed significantly higher SUV_{max} ratios in Exendin PET compared to DOPA PET (2.04 ± 0.56 vs. 1.23 ± 0.19 resp., $p=0.02$). The higher contrast between uptake in the focal lesion and the remainder of the pancreas in the Exendin PET scans enables easier detection of focal lesions, explaining the higher sensitivity of Exendin PET based on the initial clinical reading, and the higher rate of agreement in readings of Exendin PET images between clinical and expert readers, compared to DOPA PET images. This is of importance, especially in cases with a heterogeneous pattern of tracer uptake in the pancreas, which are usually difficult to diagnose (*12*).

The superior image quality of Exendin PET is important for both the scan reading and the surgical procedure, since successful surgery depends on precise pre-surgical diagnosis of focal CHI and subsequently finding and completely removing the focal lesion intraoperatively. This is reflected in the rating of the images by pediatric surgeons. Exendin PET could benefit the surgical treatment of CHI patients by facilitating the decision to perform surgery as well as the intra-operative localization of the focal lesion.

Image quantification of dynamic Exendin PET scans of four patients showed the highest SUV_{max} ratios, indicating that the best timeframe for imaging is between 30 and 45 minutes after tracer injection. Focal lesions in the tail of the pancreas, which overlap with the contour of the left kidney pose a diagnostic challenge with DOPA PET, which has been described previously (*12*). Because of the high renal accumulation of Exendin, this issue also occurs with Exendin PET. In such cases, performing additional scans at later time points could be beneficial, since uptake of Exendin in the kidneys was shown to decrease over time in adult patients (*18*).

The introduction of DOPA PET to discriminate between focal and diffuse CHI has had a major impact on the clinical approach for CHI patients by eliminating the need for more invasive diagnostic procedures like selective arterial calcium stimulation and simultaneous venous sampling (ASVS) or transhepatic portal venous insulin sampling (THPVS), and by optimizing surgical treatment because of increased diagnostic accuracy. In addition to the better image quality of Exendin PET compared to DOPA PET, another important advantage of Exendin PET is the

production of ^{68}Ga with a generator system, enabling on site production of the radiotracer even at PET centers without a cyclotron facility. Since [^{18}F]F-DOPA is often difficult to obtain, this could transform the care for focal CHI patients in such centers. An additional important advantage of [^{68}Ga]Ga-exendin-4 is the very low radiation dose to the patients, which we previously calculated to be about four-fold lower for newborn patients than the radiation dose from [^{18}F]F-DOPA (*18*).

Conclusion

In this study we provide the first clinical evidence for detection and localization of focal CHI using Exendin PET. These first results demonstrate a better image quality of Exendin PET compared to the standard DOPA PET, resulting in a higher sensitivity in clinical reading which changed the surgical management in four out of 19 patients. Exendin PET therefore has the potential to improve treatment of patients with focal CHI by improving the diagnostic accuracy and certainty. This could enable the performance of curative surgery in more patients and benefit surgical planning by providing more precise and reliable pre-operative images. While the performance of Exendin PET needs to be further assessed in a larger patient population, we believe that Exendin PET has the potential to replace DOPA PET as the primary diagnostic tool for focal CHI in the future.

References

1. Senniappan S, Shanti B, James C, Hussain K. Hyperinsulinaemic hypoglycaemia: genetic mechanisms, diagnosis and management. *J Inherit Metab Dis.* 2012;35:589-601.
2. Iglesias P, Diez JJ. Management of endocrine disease: a clinical update on tumor-induced hypoglycemia. *Eur J Endocrinol.* 2014;170:R147-157.
3. Gutgold A, Gross DJ, Glaser B, Szalat A. Diagnosis of ABCC8 Congenital Hyperinsulinism of Infancy in a 20-Year-Old Man Evaluated for Factitious Hypoglycemia. *J Clin Endocrinol Metab.* 2017;102:345-349.
4. Galcheva S, Al-Khawaga S, Hussain K. Diagnosis and management of hyperinsulinaemic hypoglycaemia. *Best Pract Res Clin Endocrinol Metab.* 2018;32:551-573.
5. Han B, Newbould M, Batra G, et al. Enhanced Islet Cell Nucleomegaly Defines Diffuse Congenital Hyperinsulinism in Infancy but Not Other Forms of the Disease. *Am J Clin Pathol.* 2016;145:757-768.
6. Lord K, Dzata E, Snider KE, Gallagher PR, De Leon DD. Clinical presentation and management of children with diffuse and focal hyperinsulinism: a review of 223 cases. *J Clin Endocrinol Metab.* 2013;98:E1786-1789.
7. Beltrand J, Caquard M, Arnoux JB, et al. Glucose metabolism in 105 children and adolescents after pancreatectomy for congenital hyperinsulinism. *Diabetes Care.* 2012;35:198-203.
8. Fournet JC, Mayaud C, de Lonlay P, et al. Unbalanced expression of 11p15 imprinted genes in focal forms of congenital hyperinsulinism: association with a reduction to homozygosity of a mutation in ABCC8 or KCNJ11. *Am J Pathol.* 2001;158:2177-2184.
9. Verkarre V, Fournet JC, de Lonlay P, et al. Paternal mutation of the sulfonylurea receptor (SUR1) gene and maternal loss of 11p15 imprinted genes lead to persistent hyperinsulinism in focal adenomatous hyperplasia. *J Clin Invest.* 1998;102:1286-1291.
10. Bax KN, van der Zee DC. The laparoscopic approach toward hyperinsulinism in children. *Semin Pediatr Surg.* 2007;16:245-251.
11. Otonkoski T, Nanto-Salonen K, Seppanen M, et al. Noninvasive diagnosis of focal hyperinsulinism of infancy with [18F]-DOPA positron emission tomography. *Diabetes.* 2006;55:13-18.
12. Laje P, States LJ, Zhuang H, et al. Accuracy of PET/CT Scan in the diagnosis of the focal form of congenital hyperinsulinism. *J Pediatr Surg.* 2013;48:388-393.
13. Brom M, Oyen WJ, Joosten L, Gotthardt M, Boerman OC. 68Ga-labelled exendin-3, a new agent for the detection of insulinomas with PET. *Eur J Nucl Med Mol Imaging.* 2010;37:1345-1355.
14. Antwi K, Fani M, Heye T, et al. Comparison of glucagon-like peptide-1 receptor (GLP-1R) PET/CT, SPECT/CT and 3T MRI for the localisation of occult insulinomas: evaluation of diagnostic accuracy in a prospective crossover imaging study. *Eur J Nucl Med Mol Imaging.* 2018;45:2318-2327.
15. Antwi K, Fani M, Nicolas G, et al. Localization of Hidden Insulinomas with (6)(8)Ga-DOTA-Exendin-4 PET/CT: A Pilot Study. *J Nucl Med.* 2015;56:1075-1078.
16. Hardy OT, Hernandez-Pampaloni M, Saffer JR, et al. Diagnosis and localization of focal congenital hyperinsulinism by 18F-fluorodopa PET scan. *J Pediatr.* 2007;150:140-145.
17. Treglia G, Mirk P, Giordano A, Rufini V. Diagnostic performance of fluorine-18-dihydroxyphenylalanine positron emission tomography in diagnosing and localizing the focal form of congenital hyperinsulinism: a meta-analysis. *Pediatr Radiol.* 2012;42:1372-1379.
18. Boss M, Buitinga M, Jansen TJP, Brom M, Visser EP, Gotthardt M. PET-Based Human Dosimetry of (68) Ga-NODAGA-Exendin-4, a Tracer for beta-Cell Imaging. *J Nucl Med.* 2020;61:112-116.

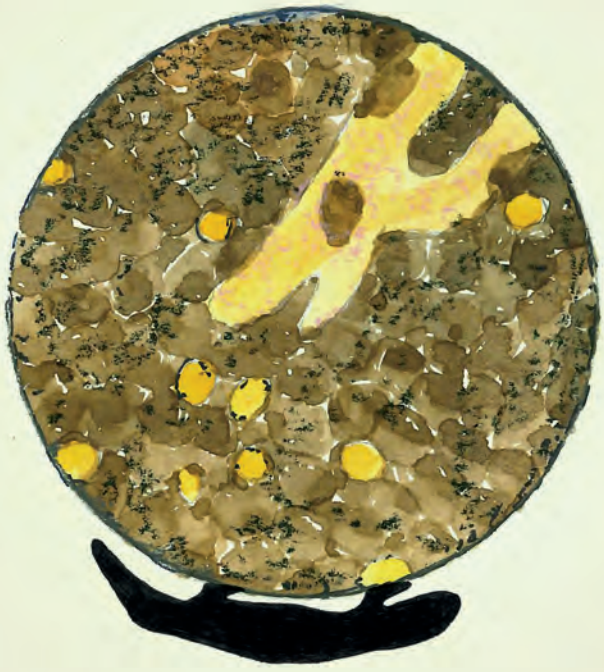

CHAPTER 4

PET-based dosimetry of [^{68}Ga]Ga-NODAGA-exendin-4 in humans, a tracer for beta cell imaging.

Marti Boss, Mijke Buitinga, Tom JP Jansen, Maarten Brom,
Eric P Visser, Martin Gotthardt

Journal of Nuclear Medicine, 2020 Jan;61(1):112-116. doi: 10.2967/jnumed.119.228627

Department of Medical Imaging, Radboud University Medical Center Nijmegen, The Netherlands

Abstract

Introduction

[^{68}Ga]Ga-NODAGA-exendin-4 is a promising tracer for beta cell imaging using PET/CT. Possible applications include pre-operative visualization of insulinomas as well as discrimination between focal and diffuse forms of congenital hyperinsulinism. There is also a significant role for this tracer in extending our knowledge on the role of beta cell mass in the pathophysiology of type 1 and type 2 diabetes by enabling non-invasive quantification of tracer uptake as a measure for beta cell mass. Calculating radiation doses from this tracer is important to assess its safety for use in patients (including young children) with benign diseases and healthy individuals.

Methods

Six patients with hyperinsulinemic hypoglycemia were included. After intravenous injection of 100 MBq of the tracer, 4 successive PET/CT scans were obtained at 30, 60, 120 and 240 minutes post injection. Tracer activity in the pancreas, kidneys, duodenum and remainder of the body were determined and time-integrated activity coefficients for the measured organs were calculated. OLINDA/EXM version 1.1 software was used to calculate radiation doses using the reference adult male and female models and to estimate radiation doses to children.

Results

The mean total effective dose for adults is very low (0.71 ± 0.07 mSv) for a standard injected dose of 100 MBq. The organs with the highest absorbed dose are the kidneys (47.3 ± 10.2 mGy/ 100 MBq). The estimated total effective dose is 2.32 ± 0.32 mSv for an injected dose of 20 MBq in newborns. This dose decreases to 0.77 ± 0.11 / 20 MBq for children of 1 year old and 0.59 ± 0.05 mSv for an injected dose of 30 MBq in 5 year old children.

Conclusion

Our human PET/CT based dosimetric calculations show that the effective radiation doses from the novel tracer [^{68}Ga]Ga-NODAGA-exendin-4 for adults as well as children are very low. The doses are lower than reported for other polypeptide tracers such as somatostatin analogs (2.1-2.6 mSv/ 100 MBq) and are beneficial for its application as a research tool, especially in case of repeated examinations.

Introduction

For new radiopharmaceuticals, estimating effective radiation doses is important to determine their safety for patients. The radiopharmaceutical [^{68}Ga]Ga-NODAGA-exendin-4 binds specifically to the glucagon-like peptide 1 (GLP-1) receptor (GLP-1R), which is expressed on pancreatic beta cells (1). It is a promising tracer for *in vivo* targeting of beta cells using positron emission tomography/ computed tomography (PET/CT) with several possible applications in clinical diagnostics of insulin-producing lesions as well as diabetes research. Since these applications entail the use of this radiopharmaceutical in patients with a generally normal life expectancy (i.e. patients with benign tumors or diabetes mellitus) and even in completely healthy individuals in control groups for research, performing dosimetric calculations is of substantial importance.

A promising application of this new tracer is pre-operative visualization of insulin-producing neuroendocrine tumors (insulinomas), for which current standard imaging methods have limited sensitivity (2-4). Clinical studies have shown the potential of ^{111}In-labelled exendin for detection of such tumors with single-photon emission computed tomography (SPECT)/CT (5-7). [^{68}Ga]Ga-exendin PET/CT has been demonstrated to be superior to ^{111}In-exendin SPECT/CT in a small cross-over clinical trial (8) and its superiority over conventional imaging was shown in a large prospective trial (9). Currently, a multicenter prospective trial is ongoing comparing the sensitivity of [^{68}Ga]Ga-NODAGA-exendin-4 PET/CT for detection of insulinomas with all current standard non-invasive imaging modalities (Somatostatin receptor PET/CT, triple phase CT and magnetic resonance imaging (MRI)) (NCT03189953). Next to this, [^{68}Ga]Ga-NODAGA-exendin-4 PET/CT is being investigated as a potential new imaging method to distinguish between diffuse and focal forms of congenital hyperinsulinism (NCT03768518) (10, 11).

In addition to these clinical applications, [^{68}Ga]Ga-NODAGA-exendin-4 has great potential as a research tool to determine beta cell mass *in vivo*. Changes in beta cell mass over time in type 1 diabetes as well as type 2 diabetes are not well characterized, since previous studies had to rely on data obtained after autopsy or pancreatectomy, which only provided data at a single point in time and did not always provide information from the complete pancreas (12, 13). By using [^{68}Ga]Ga-NODAGA-exendin-4 PET/CT, it would be possible to investigate the dynamics of beta cell mass during onset and progression of the disease. Hereby, this technique can contribute to the knowledge regarding the role of beta cell mass in the pathophysiology of diabetes.

For these applications of [^{68}Ga]Ga-NODAGA-exendin-4, a low effective radiation dose is important, especially for the possibility of performing repeated imaging. Moreover, low effective doses are essential since an important application

involves the use in often very young children with congenital hyperinsulinism. In this study we therefore performed human PET-based dosimetry in adult patients with a suspicion of insulinoma to determine effective radiation doses as well as organ absorbed doses and extrapolated these data to estimate radiation doses to children.

Materials and methods

Radiopharmaceutical preparation

Hydrochloric acid was purchased from Rotem Industries (Mishor Yamin: Israel**)**. All other components were purchased as one disposable kit (reagent and hardware kit for synthesis of ^{68}Ga peptides using cationic purification, ABX, Germany). [^{68}Ga]Ga-NODAGA-exendin-4 was manufactured using a synthesizer module (GRP synthesizer, Scintomics, Germany). Gallium-68-chloride was obtained from a ^{68}Ge/^{68}Ga generator (Galliapharm, Eckert and Ziegler, Germany). The generator was eluted with 10 ml of 0.1 M hydrochloric acid and gallium-68 was trapped on a polystyrene-H+ cartridge. The cartridge was eluted with 1.5 ml 5 M NaCl in 0.1 M hydrochloric acid into the reaction vial, containing 200 μl exendin-NODAGA (10 μg of peptide in water for injection), 475 μl 2.5 M 4-(2-hydroxyethyl)-1-piperazineethanesulfonic acid (HEPES) buffer and 50 μl ascorbic acid 100 mg/ml in water for injection. After 15 minutes incubation at 100°C, the vessel was cooled and 2 ml ethylenediaminetetraacetic acid (EDTA) 50 mM/ polysorbate 80 0.15% was added. [^{68}Ga]Ga-NODAGA-exendin-4 was purified on a HLB cartridge and sterilized by passing through a 0.2 μm filter (millex GV).

Human subjects

Six adult patients with a suspicion of insulinoma based on biochemically confirmed hyperinsulinemic hypoglycemia were included. Patients were diagnosed by a positive fasting test with the occurrence of neuroglycopenic symptoms in the fasting state combined with inappropriately low plasma glucose levels and high insulin and C-peptide levels. Characteristics of the patients are shown in table 1. Subjects were included as part of an ongoing prospective clinical trial for evaluation of [^{68}Ga]Ga-NODAGA-exendin-4 for diagnosis of insulinoma (ClinicalTrials.gov number: NCT03189953). Lesions were detected in three of the included patients (Figure 1). These patients underwent surgery, which confirmed presence of lesions at the indicated sites, which were histopathologically confirmed to be insulinomas. In the other three patients, nesidioblastosis was suspected, but no definite diagnosis could be reached. The study was approved by the Radboud University Medical Center institutional review board and all participants provided written consent.

Table 1 Patient characteristics, injected activities and time after injection of performed PET/CT scans.

Patient number	Sex	Age (y)	Weight (kg)	Injected activity (MBq)	Time after injection (min)			
					Scan 1	Scan 2	Scan 3	Scan 4
1	F	24	72.0	106.1	32	66	121	239
2	F	53	58.0	107.5	32	62	120	238
3	F	55	75.6	108.0	30	83	119	235
4	M	65	83.6	105.0	30	61	120	234
5	F	64	88.8	105.1	30	56	115	235
6	M	63	84.5	101.6	30	62	118	236

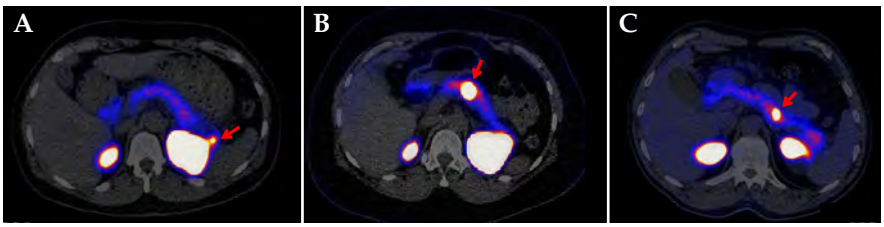

Figure 1 Transversal fused PET/CT images of the abdomen showing the detected insulinomas in patient 2 (A), patient 3 (B) and patient 4 (C). Lesions are indicated with red arrows.

PET/CT acquisition

Imaging was performed on a Siemens Biograph mCT-40 time-of-flight PET/CT scanner. Patients were injected intravenously with [68Ga]Ga-NODAGA-exendin-4 (105.6 ± 2.3 MBq, peptide dose 4-7 μg). Four consecutive PET scans were obtained at 30, 60, 120 and 240 minutes after injection. Images were acquired with 2 bed positions including the liver, pancreas and kidneys at 10 minutes per bed position. A low-dose CT scan without contrast (40 mAs and 130 kV) was acquired for anatomical localization and attenuation correction. The size of the CT transaxial matrix was 512 x 512 (0.98 × 0.98 mm), and the CT slice width was 3 mm. High definition reconstruction of the images was performed with 3 iterations, 21 subsets and a post-reconstruction Gaussian filter of 3 mm in full width at half maximum. The transaxial PET matrix size was 256 x 256 and pixel size was 3.18 x 3.18 x 3 mm.

Image analysis

The PET/CT images were analyzed using Inveon Research Workplace software (version 4.1; Siemens Healthcare). Volumes of interest (VOIs) were drawn over the kidneys, pancreas and duodenum, which showed visually identifiable tracer uptake on the PET/CT images. The total activity in each organ at each timepoint was determined by multiplying the mean activity concentration (Bq/ml) by the CT-derived VOI. Since the uptake in the kidneys is high compared to the pancreas, there is spillover of activity in the left kidney to the pancreatic tail, which could lead to an overestimation of tracer uptake in the pancreatic tail. To correct for this, the VOI of the left kidney was dilated by 9 mm and subtracted from the VOI of the pancreas. The tracer uptake in this part of the pancreas was then assumed to be equal to the mean uptake in the rest of the pancreas. Organ time-activity curves were plotted and cumulated activity was calculated as the area under the curves by the trapezoid rule. Only physical decay was assumed after the last measurement. The time-integrated activity coefficient was determined by dividing the cumulated activity by the total injected activity. The activity in the remainder of the body was determined by multiplying the total activity in the scanned area, minus the source organs, by the total body volume, based on length and body weight of the patient. With this, a homogenous tracer distribution over the remainder of the body was assumed.

Radiation dose estimates

The calculated time-activity coefficients of the source organs and the remainder of the body were used as input in OLINDA/EXM version 1.1 software. Organ absorbed doses and total effective doses for each patient were obtained using the reference adult male and female models. To estimate radiation doses in children, a comparable biodistribution of the tracer between adults and children was assumed. Organ absorbed doses and effective doses were determined using the newborn, 1-year old and 5-year old models.

Results

Figure 2 shows typical axial slices of [^{68}Ga]Ga-NODAGA-exendin-4 PET/CT images at various time points after injection. The highest tracer uptake is observed in the kidneys, which is a result of renal clearance of the tracer. Furthermore, highest specific tracer uptake is present in the pancreas and proximal duodenum. Retention of the tracer in these organs over time is high (Figure 2B). As a result, physical decay is the main cause of reduction in activity concentration in the organs over time (Figure 2A). Mean time-activity curves of these organs and the

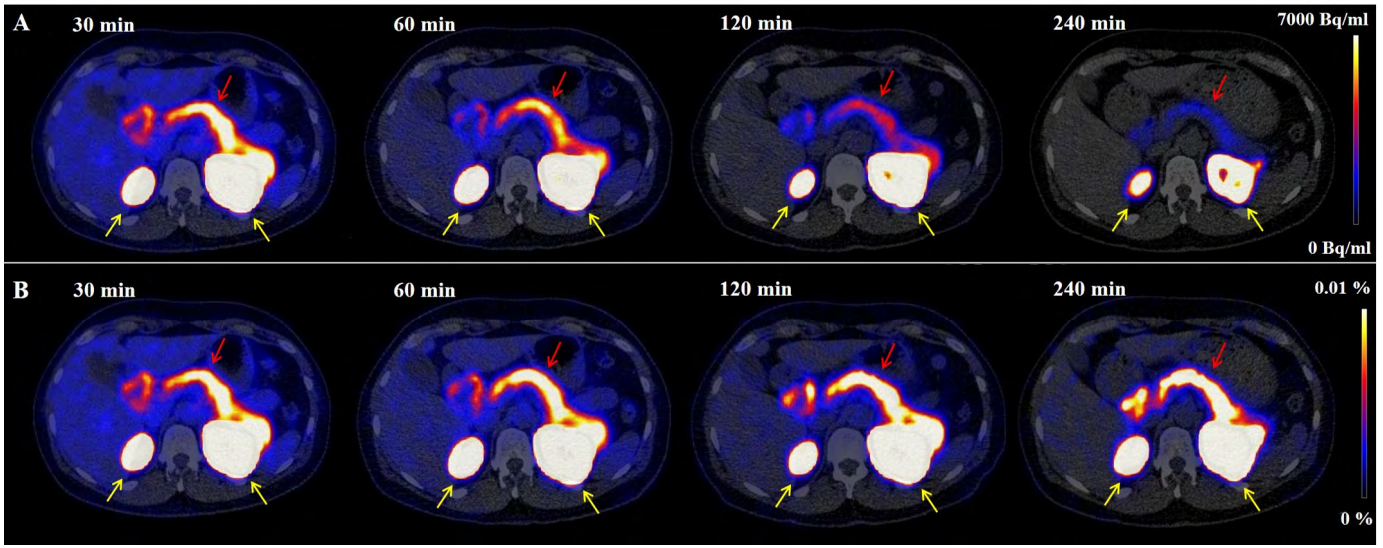

Figure 2 Transversal fused PET/CT images of the abdomen showing the biodistribution of [^{68}Ga]Ga-NODAGA-exendin-4 at 30, 60, 120 and 240 minutes after injection. (A) Tracer accumulation in Bq/ml showing washout as well as physical decay. (B) Tracer accumulation in % ID/g showing only washout of the tracer. Kidneys are indicated by yellow arrows and pancreas by red arrows.

remainder of the body of the patients are depicted in figure 3. Table 2 lists the mean organ absorbed doses and the effective dose acquired using the reference adult male and female models in OLINDA/EXM. The organs with the highest absorbed dose are the kidneys (0.47 ± 0.10 mGy/MBq), followed by the pancreas (0.023 ± 0.008 mGy/MBq), the adrenals (0.012 ± 0.002 mGy/MBq), the spleen (0.011 ± 0.001 mGy/MBq) and the small intestine (0.008 ± 0.001 mGy/MBq). Doses to the pancreas and small intestine partly consist of the organ self-dose, but will mostly originate from the kidneys. The mean total effective dose is very low (0.007 ± 0.0007 mSv/MBq).

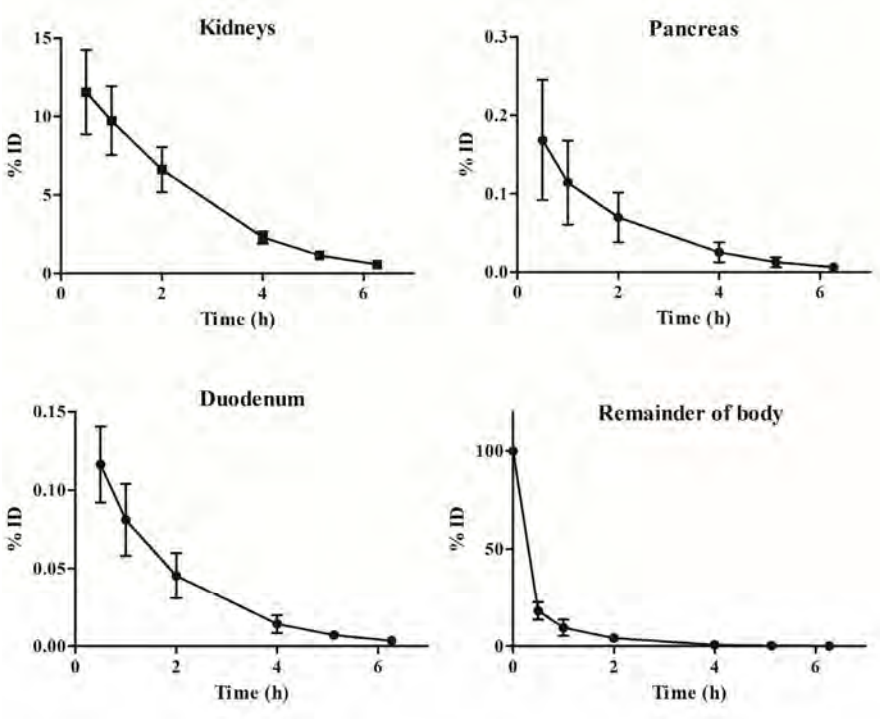

Figure 3 Time-activity curves of kidneys, pancreas, duodenum and remainder of body (n=6). Data are presented as the mean ± SD.

Estimated doses for newborn children and children of 1 year and 5 years old are depicted in table 3. The kidneys are the dose-limiting organs, receiving a dose of 5.4 ±1.1 mGy/MBq in newborns. This dose decreases with age to 2.0 ± 0.4 mGy/MBq in 1 year old children and 1.1 ± 0.2 mGy/MBq in 5-year old children. The estimated effective dose for newborns is 0.12 ± 0.02 mSv/MBq. This low dose decreases further to 0.019 ± 0.003 mSv/MBq for 5-year old children.

Table 2 Organ absorbed doses (mGγ/MBq) and effective doses (mSv/MBq) acquired using the reference adult models in Olinda/ EXM 1.1.

Site (n=6)	Mean	SD
Adrenals	0.012	0.002
Brain	0.005	0.0006
Breasts	0.005	0.0006
Gallbladder wall	0.008	0.0008
Stomach wall	0.007	0.0007
Heart wall	0.006	0.0006
Kidneys	0.472	0.1019
Intestine, lower large: wall	0.006	0.0007
Intestine, upper large: wall	0.007	0.0007
Intestine, small	0.008	0.0010
Liver	0.008	0.0008
Lungs	0.006	0.0006
Muscle	0.006	0.0006
Ovaries	0.006	0.0008
Pancreas	0.023	0.0083
Red marrow	0.006	0.0005
Osteogenic cells	0.008	0.0010
Skin	0.005	0.0005
Spleen	0.001	0.0001
Testes	0.002	0.0003
Thymus	0.005	0.0006
Thyroid	0.005	0.0006
Urinary bladder wall	0.005	0.0007
Uterus	0.004	0.0003
Total body	0.008	0.0009
Effective dose (mSv/MBq)	0.007	0.0007

Table 3 Estimated absorbed doses (mGγ/MBq) and effective doses (mSv/MBq) in children acquired using the newborn, 1-year old and 5-year old models in Olinda/EXM 1.1.

	Newborn	1-year old	5-year old
Kidneys	5.430 ± 1.086	2.037 ± 0.408	1.125 ± 0.225
Pancreas	0.530 ± 0.217	0.160 ± 0.062	0.082 ± 0.021
Adrenals	0.129 ± 0.015	0.059 ± 0.007	0.033 ± 0.004
Spleen	0.112 ± 0.017	0.050 ± 0.006	0.028 ± 0.003
Small intestine	0.114 ± 0.017	0.047 ± 0.007	0.047 ± 0.007
Whole body	0.117 ± 0.014	0.046 ± 0.006	0.023 ± 0.003
Effective dose (mSv/MBq)	0.116 ± 0.016	0.038 ± 0.005	0.019 ± 0.003

Data are presented as mean ± SD.

Discussion

Up to now, reported dosimetry of ^{68}Ga-labelled exendin has relied on extrapolation of human SPECT/CT scans using ^{111}In-labelled exendin or data from small animal SPECT with ^{111}In-labelled exendin. In this study, PET/CT based dosimetry of [^{68}Ga]Ga-NODAGA-exendin-4 was, for the first time, assessed by using human PET/CT scans. The mean total body effective dose is very low (0.71 ± 0.07 mSv/100 MBq, which is currently the standard injected dose in adults). The highest mean absorbed dose of 47.2 ± 10.2 mGγ/100 MBq is received by the kidneys. The calculated effective dose received by adults from [^{68}Ga]Ga-NODAGA-exendin-4 is lower than total body effective doses reported in dosimetry studies for the different tracers used for somatostatin receptor imaging, [^{68}Ga]Ga-DOTATOC, [^{68}Ga]Ga-DOTANOC and [^{68}Ga]Ga-DOTATATE, which were between 2.1 and 2.6 mSv/100 MBq (14-17). The dose is also much lower than the dose from a low-dose CT scan, which is 4.5 mSv for a whole body scan and 1.8 mSv for a scan of 1 bed position of the abdomen in adults. This low dose will allow repeated examinations using [^{68}Ga]Ga-NODAGA-exendin-4 in adults. The low total body effective dose allows 2-4 PET/CT examinations per year in adults (depending on the range of the low-dose CT scan) and up to 14 PET/MRI examinations without exceeding the maximum dose of 10 mSv. Even with this number of examinations, the kidney absorbed dose will remain well below 7 Gγ, which is the threshold for the human kidney acute dose (18) . The absorbed dose to the red marrow is only 0.6 ± 0.05 mGγ/100 MBq. Over 400 examinations could be performed while still remaining below 0.25 Gγ per

year, which has shown to have no damaging effects (18). The number of annual examinations will therefore not be limited by the radiation dose to the kidneys or red marrow.

The dosimetry data derived from adult patients were extrapolated to children of various ages. The estimated total effective dose in newborns is 2.3 ± 0.3 mSv/ 20 MBq, which is the dose given to children with a body weight under 12.5 kg. This effective dose is significantly higher than in adults, but still nearly 4-fold lower than the effective dose reported for the standard PET tracer currently used to diagnose congenital hyperinsulinism in newborns, [18F]FDOPA, which is 0.4 ± 0.04 mSv/MBq resulting in a total dose of 8 ± 0.8 mSv/20 MBq (19).

The pancreas is the organ receiving the second highest radiation dose (2.3 ± 0.8 mGγ/100 MBq in adults). The absorbed dose to the pancreas was determined by assuming a homogenous distribution of the radiotracer across the organ. However, since exendin specifically targets the beta cells in the islets of Langerhans in the pancreas, the activity concentration in these small clusters of endocrine cells is much higher than in exocrine pancreatic tissue (20). Therefore, the radiation dose to the islets may be underestimated using organ-based dosimetry, while the dose to the exocrine pancreas may be overestimated. This issue was previously examined using a macro- and small-scale dosimetry model combining animal and human data using 111In-labelled exendin. These data were extrapolated to gallium-68 showing that the absorbed dose to the islets of Langerhans (maximum 66.0 mGγ for 111In and 1.38 mGγ for 68Ga) (21) remains clearly below the dose known to cause diabetes, which was estimated as a relative risk of 1:61 (95% CI 1·21–2·68) with a radiation dose of 1Gγ to the tail of the pancreas (22). The estimated time-integrated activity coefficients for the pancreas and the kidneys in this study were obtained by converting 111In-exendin SPECT/CT scans of 5 humans to gallium-68. When comparing these to the current data, we find approximately 3 times higher time-integrated activity coefficients for the pancreas (0.0034 ± 0.0014 vs. 0.0012 ± 0.0001) and about 2 times lower coefficients for the kidneys (0.29 ± 0.05 vs. 0.5 ± 0.05). Because of the almost equal contribution of both these organs to the islet dose with the use of gallium-68 (21), these differences will not greatly increase the estimated absorbed dose to the islets. So, even though the data in this study show some differences in comparison to 111In-exendin, it remains clear that use of [68Ga]Ga-NODAGA-exendin-4 will not result in islet toxicity. Especially since the estimated absorbed doses to the pancreas in this study (10.6 ± 4.5 mGγ/20 MBq in newborns, 3.2 ± 1.2 mGγ/ 20MBq in 1-year olds, 2.5 ± 0.4 mGγ/30 MBq in 5-year old and 2.3 ± 0.8 mGγ/ 100 MBq in adults) are by far lower than 1 Gγ.

Previous studies on dosimetry for 68Ga-labelled exendin have relied on animal data extrapolated to humans. Extrapolation of organ and whole-body dosimetry data to other species might be unreliable due to variations in tracer biodistribution

between species, resulting for instance from differences in receptor expression, like for example the strikingly higher GLP-1R expression found in the lungs and thyroid gland of rodents as compared to humans (23). Reported total effective doses vary considerably between the different animal models that have previously been used. Reported effective doses range from 0.012 to 0.032 mSv/MBq depending on the studied species (Spraque-Dawley rats, Lewis rats, pigs, cynomolgus monkeys and one human) (24-26). Also estimated organ absorbed doses are not consistent. Based on a Rip1Tag2 mouse model of pancreatic beta cell tumors, an extrapolated human kidney absorbed dose of 1.85 mGγ/MBq was reported (25). In other studies, based on various different species, lower kidney doses were found better corresponding to the kidney doses found in this study. In Spraque-Dawley rats, a kidney dose of 0.52 mGγ/MBq was described (26) and in a dosimetry study comparing several species (Lewis rats, pigs, cynomolgus monkeys and one human), similar kidney doses (0.25-0.65 mGγ/MBq) were reported.

Conclusion

Our dosimetric calculations demonstrate low effective radiation doses from [^{68}Ga] Ga-NODAGA-exendin-4 to adults as well as to children. These doses are several fold lower than those reported for current tracers used for imaging of insulinomas/ neuroendocrine tumors and congenital hyperinsulinism and are much lower than doses from a low-dose CT scan. This is beneficial for the application of [^{68}Ga] Ga-NODAGA-exendin-4 as a diagnostic or research tool in children, patients with benign diseases and healthy volunteers, allowing repeated examinations in case of prospective follow-up studies, for example to examine beta cell mass in different phases of progression of diabetes mellitus or to assess transplantation success and monitor the survival of transplanted islets.

References

1. Tornehave D, Kristensen P, Romer J, Knudsen LB, Heller RS. Expression of the GLP-1 receptor in mouse, rat, and human pancreas. The journal of histochemistry and cytochemistry : official journal of the Histochemistry Society. 2008;56(9):841-51.
2. Chatziioannou A, Kehagias D, Mourikis D, Antoniou A, Limouris G, Kaponis A, et al. Imaging and localization of pancreatic insulinomas. Clinical imaging. 2001;25(4):275-83.
3. Ramage JK, Davies AH, Ardill J, Bax N, Caplin M, Grossman A, et al. Guidelines for the management of gastroenteropancreatic neuroendocrine (including carcinoid) tumours. Gut. 2005;54 Suppl 4:iv1-16.
4. Reubi JC. Peptide receptors as molecular targets for cancer diagnosis and therapy. Endocrine reviews. 2003;24(4):389-427.
5. Christ E, Wild D, Ederer S, Behe M, Nicolas G, Caplin ME, et al. Glucagon-like peptide-1 receptor imaging for the localisation of insulinomas: a prospective multicentre imaging study. The lancet Diabetes & endocrinology. 2013;1(2):115-22.
6. Wild D, Macke H, Christ E, Gloor B, Reubi JC. Glucagon-like peptide 1-receptor scans to localize occult insulinomas. The New England journal of medicine. 2008;359(7):766-8.
7. Christ E, Wild D, Forrer F, Brandle M, Sahli R, Clerici T, et al. Glucagon-like peptide-1 receptor imaging for localization of insulinomas. The Journal of clinical endocrinology and metabolism. 2009;94(11):4398-405.
8. Antwi K, Fani M, Nicolas G, Rottenburger C, Heye T, Reubi JC, et al. Localization of Hidden Insulinomas with (6)(8)Ga-DOTA-Exendin-4 PET/CT: A Pilot Study. Journal of nuclear medicine : official publication, Society of Nuclear Medicine. 2015;56(7):1075-8.
9. Antwi K, Fani M, Heye T, Nicolas G, Rottenburger C, Kaul F, et al. Comparison of glucagon-like peptide-1 receptor (GLP-1R) PET/CT, SPECT/CT and 3T MRI for the localisation of occult insulinomas: evaluation of diagnostic accuracy in a prospective crossover imaging study. European journal of nuclear medicine and molecular imaging. 2018;45(13):2318-27.
10. Laje P, States LJ, Zhuang H, Becker SA, Palladino AA, Stanley CA, et al. Accuracy of PET/CT Scan in the diagnosis of the focal form of congenital hyperinsulinism. Journal of pediatric surgery. 2013;48(2):388-93.
11. Lord K, Dzata E, Snider KE, Gallagher PR, De Leon DD. Clinical presentation and management of children with diffuse and focal hyperinsulinism: a review of 223 cases. The Journal of clinical endocrinology and metabolism. 2013;98(11):E1786-9.
12. Lohr M, Kloppel G. Residual insulin positivity and pancreatic atrophy in relation to duration of chronic type 1 (insulin-dependent) diabetes mellitus and microangiopathy. Diabetologia. 1987;30(10):757-62.
13. Matveyenko AV, Butler PC. Relationship between beta-cell mass and diabetes onset. Diabetes, obesity & metabolism. 2008;10 Suppl 4:23-31.
14. Hartmann H, Zophel K, Freudenberg R, Oehme L, Andreeff M, Wunderlich G, et al. [Radiation exposure of patients during 68Ga-DOTATOC PET/CT examinations]. Nuklearmedizin Nuclear medicine. 2009;48(5):201-7.
15. Pettinato C, Sarnelli A, Di Donna M, Civollani S, Nanni C, Montini G, et al. 68Ga-DOTANOC: biodistribution and dosimetry in patients affected by neuroendocrine tumors. European journal of nuclear medicine and molecular imaging. 2008;35(1):72-9.
16. Walker RC, Smith GT, Liu E, Moore B, Clanton J, Stabin M. Measured human dosimetry of 68Ga-DOTATATE. Journal of nuclear medicine : official publication, Society of Nuclear Medicine. 2013;54(6):855-60.
17. Sandstrom M, Velikyan I, Garske-Roman U, Sorensen J, Eriksson B, Granberg D, et al. Comparative biodistribution and radiation dosimetry of 68Ga-DOTATOC and 68Ga-DOTATATE in patients with neuroendocrine tumors. Journal of nuclear medicine : official publication, Society of Nuclear Medicine. 2013;54(10):1755-9.
18. Stewart FA, Akleyev AV, Hauer-Jensen M, Hendry JH, Kleiman NJ, Macvittie TJ, et al. ICRP publication 118: ICRP statement on tissue reactions and early and late effects of radiation in normal tissues and organs--threshold doses for tissue reactions in a radiation protection context. Annals of the ICRP. 2012;41(1-2):1-322.

19. Garg PK, Lokitz SJ, Truong L, Putegnat B, Reynolds C, Rodriguez L, et al. Pancreatic uptake and radiation dosimetry of 6-[18F]fluoro-L-DOPA from PET imaging studies in infants with congenital hyperinsulinism. PloS one. 2017;12(11):e0186340.
20. Brom M, Woliner-van der Weg W, Joosten L, Frielink C, Bouckenooghe T, Rijken P, et al. Non-invasive quantification of the beta cell mass by SPECT with (1)(1)(1)In-labelled exendin. Diabetologia. 2014;57(5):950-9.
21. van der Kroon I, Woliner-van der Weg W, Brom M, Joosten L, Frielink C, Konijnenberg MW, et al. Whole organ and islet of Langerhans dosimetry for calculation of absorbed doses resulting from imaging with radiolabeled exendin. Scientific reports. 2017;7:39800.
22. de Vathaire F, El-Fayech C, Ben Ayed FF, Haddy N, Guibout C, Winter D, et al. Radiation dose to the pancreas and risk of diabetes mellitus in childhood cancer survivors: a retrospective cohort study. The Lancet Oncology. 2012;13(10):1002-10.
23. Korner M, Stockli M, Waser B, Reubi JC. GLP-1 receptor expression in human tumors and human normal tissues: potential for in vivo targeting. Journal of nuclear medicine : official publication, Society of Nuclear Medicine. 2007;48(5):736-43.
24. Selvaraju RK, Bulenga TN, Espes D, Lubberink M, Sorensen J, Eriksson B, et al. Dosimetry of [(68)Ga]Ga-DO3A-VS-Cys(40)-Exendin-4 in rodents, pigs, non-human primates and human - repeated scanning in human is possible. American journal of nuclear medicine and molecular imaging. 2015;5(3):259-69.
25. Wild D, Wicki A, Mansi R, Behe M, Keil B, Bernhardt P, et al. Exendin-4-based radiopharmaceuticals for glucagonlike peptide-1 receptor PET/CT and SPECT/CT. Journal of nuclear medicine : official publication, Society of Nuclear Medicine. 2010;51(7):1059-67.
26. Mikkola K, Yim CB, Fagerholm V, Ishizu T, Elomaa VV, Rajander J, et al. 64Cu- and 68Ga-labelled [Nle(14),Lys(40)(Ahx-NODAGA)NH2]-exendin-4 for pancreatic beta cell imaging in rats. Molecular imaging and biology : MIB : the official publication of the Academy of Molecular Imaging. 2014;16(2):255-63.

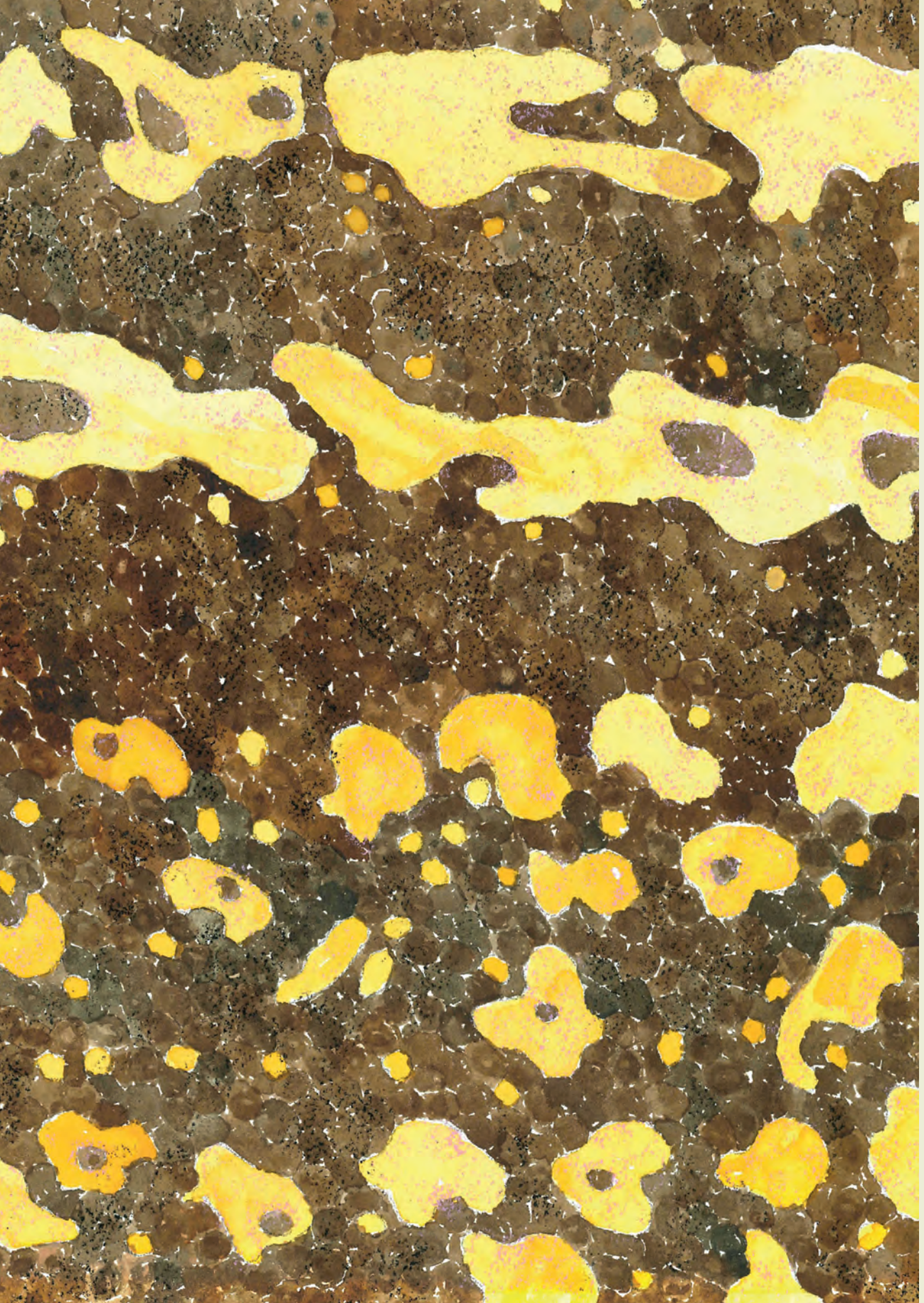

PART 2

Treatment

Targeted optical imaging and photodynamic therapy of insulin-producing lesions

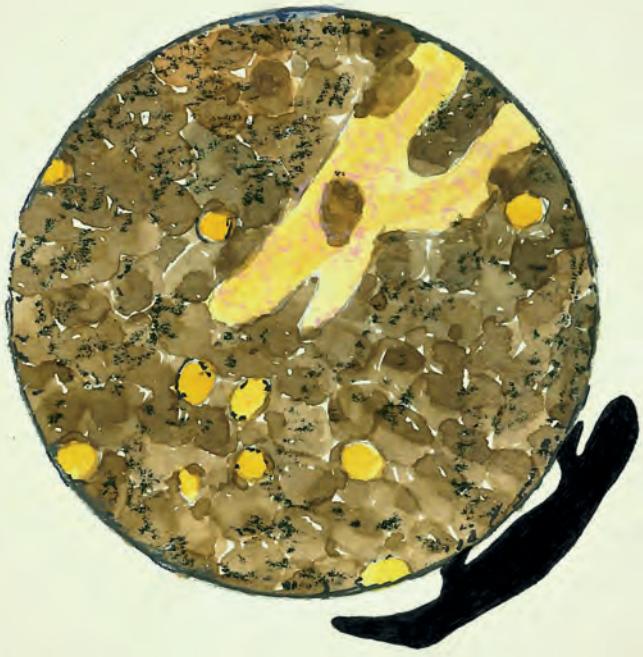

CHAPTER 5

Targeted optical imaging of the glucagon-like peptide 1 receptor using exendin-4-IRDye800CW

Marti Boss[1], Desiree Bos[1], Cathelijne Frielink[1], Gerwin Sandker[1], Selen Ekim[1], Camille Marciniak[2], Francois Pattou[2], Go van Dam[3], Sanne van Lith[1], Maarten Brom[1], Martin Gotthardt[1], Mijke Buitinga[1]

Journal of Nuclear Medicine, 2020 Jan10. doi: 10.2967/jnumed.119.234542

1 Department of Medical Imaging, Radboud University Medical Center, Nijmegen, The Netherlands
2 Department of General and Endocrine Surgery, University Hospital 2 Lille, Lille, France
3 Department of surgery, University Medical Center Groningen, Groningen, The Netherlands

Abstract

The treatment of choice for insulinomas and focal lesions in congenital hyperinsulinism (CHI) is surgery. However, intra-operative detection can be challenging. This could be overcome with intra-operative fluorescence imaging, which provides real-time lesion detection with a high spatial resolution. Here, a novel method for targeted near-infrared (NIR) fluorescence imaging of glucagon-like peptide 1 receptor (GLP-1R) positive lesions, using the GLP-1 agonist exendin-4, labeled with IRDye800CW, was examined *in vitro* and *in vivo*.

Methods

A competitive binding assay was performed using Chinese hamster lung (CHL) cells transfected with the GLP-1R. Tracer biodistribution was determined in BALB/c nude mice bearing subcutaneous CHL-GLP-1R xenografts. *In vivo* NIR fluorescence imaging of CHL-GLP-1R xenografts was performed. Localization of the tracer in the pancreatic islets of BALB/c nude mice was examined using fluorescence microscopy. Laparoscopic imaging was performed to detect the fluorescent signal of the tracer in the pancreas of mini pigs.

Results

Exendin-4-IRDye800CW binds the GLP-1R with an IC_{50} value of 3.96 nM. The tracer accumulates in CHL-GLP-1R xenografts. Subcutaneous CHL-GLP-1R xenografts were visualized using *in vivo* NIR fluorescence imaging. The tracer accumulates specifically in the pancreatic islets of mice and a clear fluorescent signal was detected in the pancreas of mini pigs.

Conclusion

These date provide the first *in vivo* evidence of the feasibility of targeted fluorescence imaging of GLP-1R positive lesions. Intra-operative lesion delineation using exendin-4-IRDye800CW could benefit open as well as laparoscopic surgical procedures for removal of insulinomas and focal lesions in CHI.

Introduction

While pre-operative imaging is essential for tumor detection before surgical cancer treatment, translating this information into the operating room is often challenging. Intra-operative optical imaging can provide real-time detection of tumor lesions and thereby contribute to optimal surgical procedures (1).

Insulinomas; insulin-producing neuroendocrine tumors arising from stem cells or pancreatic beta cells, are the most common cause of endogenous adult hyperinsulinemic hypoglycemia (2). Persistent hypoglycemia also occurs in neonates and is in most cases caused by CHI. There are two subforms of this disease: focal CHI, caused by focal adenomatous islet cell hyperplasia, and diffuse CHI, resulting from diffuse involvement of pancreatic beta cells (3). Symptoms of insulinomas and CHI, caused by episodic hypoglycemia, are severe and include confusion, diplopia and dizziness and, in cases of prolonged hypoglycemia, even seizure, loss of consciousness or death (4).

Insulinomas and focal CHI can be completely cured by surgical removal of the lesion. However, these procedures are complicated by the usually small size of the lesions and their proximity to the pancreatic duct and major vessels (5). Precise localization of the lesion is of great importance and starts with sensitive pre-operative detection. For insulinomas, this is performed using various imaging modalities; Contrast enhanced CT and MRI with sensitivities around 70% and 90% respectively (6), somatostatin receptor PET, for which sensitivities from 33% to 85% are reported (7, 8) and the more invasive endoscopic ultrasound, with a sensitivity of 75% for detection of insulinomas (9). Currently, there is increasing evidence for the superior performance of the novel imaging method GLP-1R SPECT/CT or PET/CT, using radiolabeled exendin-4, a stable analogue of the hormone GLP-1, which specifically binds the GLP-1R on pancreatic beta cells with high affinity (10). With this technique, insulinomas are detected with a sensitivity of up to 97.7% (7, 11, 12). Focal CHI is pre-operatively localized using ^{18}F-DOPA PET/CT with a sensitivity of 85% (13). GLP-1R PET is also being investigated as a potentially more sensitive imaging technique for focal CHI (NCT03768518).

However, even after pre-operative visualization of the lesion, intra-operative detection can be challenging, especially in patients with multiple insulinomas, where very small lesions (< 1 cm) are even more common. Intra-operative ultrasound is routinely used for intraoperative localization of insulinomas. In combination with palpation, success rates ranging from 91% to 100% have been reported (9, 14, 15). However, a laparoscopic procedure, which is preferred when enucleation of the lesion is possible, excludes palpation. Radioguided detection of insulinomas has been proven successful only in a limited number of patients to date (16). Another interesting option for intra-operative detection of GLP-1R positive lesions

is fluorescence imaging, which has a better spatial resolution and could be used for precise delineation of the lesion and fluorescence-guided surgery (1, 17).

Currently, there is much attention for the development of tracers for intra-operative fluorescence imaging, mostly using NIR fluorophores, which have the benefit of a high penetration depth (5-10 mm) through tissue (18). Coupling of the fluorophore to a tumor-targeting moiety is crucial to ensure specific and efficient delivery of a fluorophore to the lesion of interest.

For targeting of insulinomas and focal CHI, the peptide exendin-4 is an attractive targeting agent for optical imaging.

We have developed exendin-4 coupled to the NIR fluorophore IRDye800CW as a specific tracer for fluorescence imaging of insulinomas and focal CHI. We assessed the potential of targeting GLP-1R positive cells *in vitro* and *in vivo* and the feasibility of performing *in vivo* fluorescence imaging with this compound.

Materials and methods

Reagents

Exendin-4-IRDye800CW was supplied by piCHEM (Graz, Austria). IRDye800CW NHS ester was obtained from LI-COR Biosciences (Lincoln, Nebraska, U.S.A.). The N-epsilon amino group of lysine at position 40 was site specifically modified during solid phase peptide synthesis with a mercapto-propionic acid, releasing an unprotected exendin-4 with a free thiol function after triisopropylsilane cleavage. IRDye800CW was modified with a maleimide and coupling to exendin-4 was performed using a thiol reactive crosslinking approach. The purity was >90%. Stock solutions of exendin-4-IRDye800CW were prepared in phosphate-buffered saline (PBS).

Cell Culture

CHL cells stably transfected with the human GLP-1R (19) were cultured (at 37°C and 5% CO_2) in Dulbecco's modified Eagle's medium (DMEM) (Thermo Fisher Scientific, Waltham, MA, USA) with 4.5g/L D-glucose and Glutamax, supplemented with 10% fetal calf serum (FCS) (Life technologies, Carlsbad, CA, USA), 100 IU/mL penicillin G, 10 mg/mL streptomycine, 1 mM sodium pyruvate, 0.1 mM non-essential amino acids and 0.5 mg/ml G418 geneticin.

Competitive Binding Assay

The half-maximal inhibitory concentration (IC_{50}) of exendin-4-IRDye800CW, and unlabeled exendin, as a reference, was determined using CHL-GLP-1R cells in a competitive binding assay as described previously (10, 20). Cells were grown

overnight in six well plates (approximately 10^6 cells/well). Exendin-3-DTPA, labeled with ^{111}In as described earlier (21), was used as tracer. The cells were washed twice with PBS and incubated for 4 hours on ice with 50,000 cpm ^{111}In-DTPA-exendin-3 in the presence of increasing concentrations of exendin-4-IRDye-800CW or exendin-4 (0.1 – 300 nM). After incubation, cells were washed with PBS, solubilized with 2 mL sodium hydroxide (NaOH), collected and the cell-associated activity was measured in a gamma-counter (Wizard 2480, PerkinElmer, Groningen, The Netherlands).

Binding Assay

Receptor specificity of the binding of the exendin-4-IRDye800CW to CHL-GLP-1R cells was determined in a fluorescent binding assay. CHL-GLP-1R cells were grown overnight in 24 well plates to approximately 95% confluency. Cells were washed twice with binding buffer (DMEM supplemented with 0.5% bovine serum albumin (BSA)) and incubated with 300nM exendin-4-IRDye800CW in triplicate with and without a 50x excess of unlabeled exendin-4 (four hours at 37°C). After incubation, cells were washed twice with PBS, lysed using 200 μl sodium hydroxide per well, collected and transferred to a black flat-bottom 96-well plate. Fluorescence was measured using a TECAN infinite M200 Pro plate reader (Infinite Pro 200, Tecan Austria GmbH, Groedig, Austria) (excitation: 750 nm, emission 795 nm). Standard curves were created and binding percentages to the cells were calculated using Microsoft Office Excel 2007.

Animal Tumor Model

Female BALB/c nude mice (Janvier, Le Genest Saint Isle, France) (age: 6-8 weeks) were housed in individually ventilated cages (6 mice per cage) under non-sterile conditions with ad libitum access to chlorophyll-free animal chow and water. CHL-GLP-1R cells were injected subcutaneously on the right shoulder ($5*10^6$ cells/mouse) in 200 μL DMEM with 4.5 g/L D-glucose and Glutamax. All animal experiments were approved by the institutional Animal Welfare Committee of the Radboud University Medical Centre and were conducted in accordance to the guidelines of the Revised Dutch Act on Animal Experimentation.

In Vivo Biodistribution

Female BALB/c nude mice bearing subcutaneous CHL-GLP-1R xenografts were injected intravenously with various concentrations of exendin-4-IRDye800CW in 200 μL PBS with 0.5% BSA (N=6 mice per group, 3, 10, 30 and 100 μg exendin-4-IRDye800CW). Control mice (N=4) were injected with PBS with 0.5% BSA only. After 4 hours, the mice were sacrificed by CO_2 asphyxiation and blood and organs of the mice were removed and collected in Roche MagNA Lyser tubes

(F Hoffmann- La Roche Ltd., Basel, Switzerland), which were weighed before and after organ collection. The circulation time of 4 hours was chosen based on our previous experience with radiolabeled exendin tracers (10). Radioimmunoprecipitation assay (RIPA) lysis buffer (500 μL; 50mM (hydroxymethyl)aminomethane-hydrochloride (TRIS-HCl), pH 7.4 with 150 mM sodiumchloride (NaCl), 1 mM ethylenediaminetatraacetic acid (EDTA), 1% Triton-X-100 and 1% sodium dodecyl sulphate (SDS)) was added to each tube. Organs were then homogenized using a Roche MagNA Lyser (F Hoffmann-La Roche Ltd., Basel, Switzerland) with repeated cycles of 6000 rpm for 25 seconds with cooling on ice for 1 minute after each cycle. Organ homogenates of control mice were used to create standard curves for each organ. Organ homogenates (100 μl) and the standards were transferred in triplicate to a black flat-bottom 96-well plate. Fluorescence was measured using a TECAN infinite M200 Pro plate reader (Infinite Pro 200, Tecan Austria GmbH, Groedig, Austria) (excitation 750 nm, emission 795 nm). Standard curves were created and tracer uptake in the various organs were calculated using Microsoft Office Excel 2007. Tracer uptake in each organ type was corrected for the weight of the dissected organ. To determine the specificity of the tumor uptake, an additional biodistribution experiment was performed with two groups of mice (n=6 per group), which were injected with 3 μg exendin-4-IRDye800CW with co-injection of 150 μg unlabeled exendin-4 in one of the groups).

We validated the biodistribution of the fluorescent tracer using a dual labeled version of the exendin-tracer DTPA-exendin-4 (piCHEM, Graz, Austria), labeled with both ^{111}In and Cy5.5, as previously described (21). With this tracer, we performed biodistribution studies and we compared the tracer uptake in the different organs based on the fluorescent signal with that of the radioactive signal (Figure 1).

In Vivo Fluorescence Imaging of GLP-1R Positive Tumors

To show the feasibility of visualizing GLP-1R positive tumors using *in vivo* fluorescence imaging, BALB/c nude mice bearing subcutaneous CHL-GLP-1R xenografts were injected intravenously with 3 μg exendin-4-IRDye800CW (N=3 per group). One group of mice was co-injected with an excess (150 μg) of unlabeled exendin-4. After 4 hours, fluorescence imaging was performed using the IVIS Lumina closed-cabinet fluorescence scanner (Caliper LifeSciences, Hopkinton, MA) (excitation 745 nm, autofluorescence correction excitation 640 nm, both measured with the ICG filter). After resection of the tumor lesions, mice were imaged again. Subsequently, the mice were dissected to remove the pancreas. Pancreata were fixed overnight in 4% formalin and embedded in paraffin for fluorescence microscopy and immunohistochemistry as described in the following paragraph.

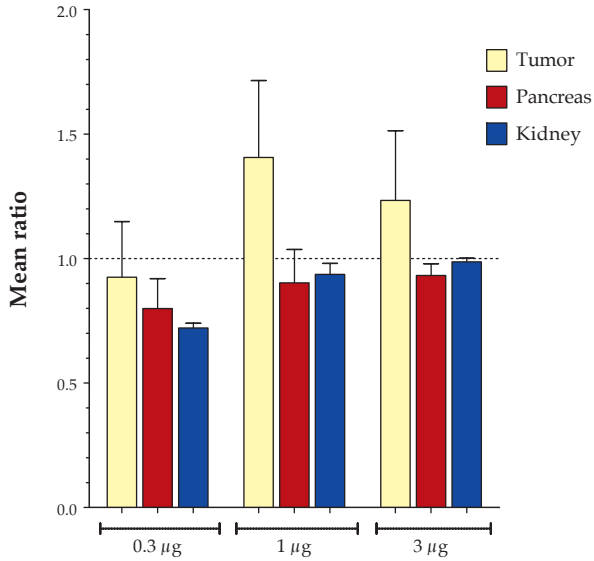

Figure 1 Biodistribution of ^{111}In-DTPA-exendin-4-Cy5.5 (0.3 µg, 1 µg and 3 µg, N=6 mice per group) in tumor, pancreas and kidney. Uptake in organs were determined with radiochemical and fluorescent analysis. Given are the ratios of uptake values determined by the different methods showing a good correlation between the methods.

Fluorescence Microscopy and Immunohistochemistry

Sections of 4 µm were cut at 2 levels, 100 µm apart. One section of each level was deparaffinated in xylene for 2 minutes, after which fluorescence imaging was performed using an Odyssey CLx flatbed fluorescence scanner (800 nm channel, recording time 1-5 minutes, focus 1.0 mm) (LI-COR biosciences, Lincoln, NE, USA). Subsequently, these sections were stained for insulin as previously described (22). Consecutive sections were used for fluorescence microscopy. After deparaffination in xylene (2 times five minutes), cell nuclei were stained with Hoechst (33258, Invitrogen, Waltham, MA, USA). Sections were mounted under a glass cover in modified Kaiser's glycerine. Fluorescence imaging was performed using an inverted microscope (DMI6000B, Leica Biosystems, GmbH, Wetzlar, Germany) equipped with a NIR light source ranging up to 900 nm (X-Cite 200DC, Excelas Excelitas Technologies, Waltham, MA, USA), an NIR filter set (microscope two band- pass filters 850–890 m–2p and a long-pass emission filter HQ800795LP; Chroma Technology Corp, Bellows Falls, VT, USA), a monochrome DFC365 FX fluorescence camera (1·4M Pixel CCD, Leica Biosystems GmbH), and LAS-X software (Leica Biosystems GmbH).

Laparoscopic Imaging of Pancreatic Tracer Uptake in Mini Pigs

The possibility of visualizing tracer uptake in the pancreatic beta cells *in vivo* using a laparoscopic laser device was assessed in mini pigs. This was performed in the Department of Experimental Research of the Lille 2 University Facilities, Lille, France. Surgical interventions were approved by the local ethics committee (IACUC). Three healthy adult Göttingen-like mini pigs (*Sus scrofa,* Denis's breeding, Templeuve, France) were anesthetized using 4% isoflurane (Aerrane, Baxter, France) after receiving premedication (intramuscular injection of ketamine (Ketamine1000, Virbac, Carros, France, 10 mg/kg of body weight) and xylazine (Sédaxylan, CEVA Santé Animale, Libourne, France, 2.5 mg/kg of body weight)). The mini pigs were infused with 1.3 μg/kg exendin-4-IRDye800CW in 20 mL PBS over 30 minutes through an intravenous catheter in the external jugular vein. Four hours after tracer injection, laparoscopic surgery was performed to access the pancreas upon which fluorescence imaging of the pancreatic head and tail was performed using a laser device emitting light at 800 nm and a fluorescence camera (SurgVision BV, The Netherlands).

Statistical Analyses

Statistical calculations were performed using GraphPad Prism (GraphPad Software, La Jolla, CA, USA). IC_{50} values were calculated by fitting the data with non-linear regression using least squares fit with GraphPad Prism.

Results

Exendin-4-IRDye800CW Specifically Binds the GLP-1R with High Affinity

The IC_{50} values of unlabeled exendin-4 and exendin-4-IRDye800CW were 2.5 nM (95% CI; 1.32 - 4.90) and 4.0 nM (95% CI; 2.9 – 5.5) respectively (Figure 2). While the binding affinity of the labeled peptide is significantly lower compared to the unlabeled peptide ($p < 0.01$), the binding affinity is in the same nanomolar range. Addition of an excess of unlabeled exendin-4 decreased binding of exendin-4-IRDye800CW to CHL-GLP-1R cells from 4.1 ± 0.4% to 0.3 ± 0.2% ($p < 0.01$) (Figure 3A).

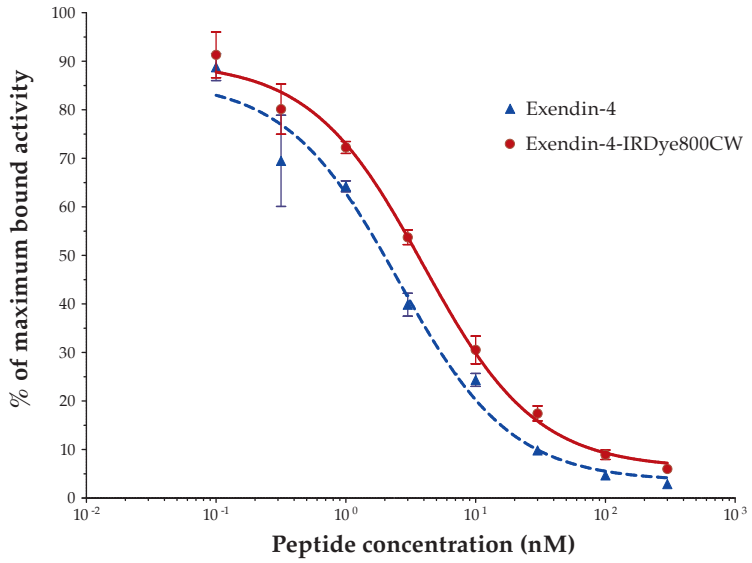

Figure 2 Competition binding assay (IC_{50}) of unlabeled exendin-4 and exendin-4-IRDye800CW on CHL-GLP-1R cells.

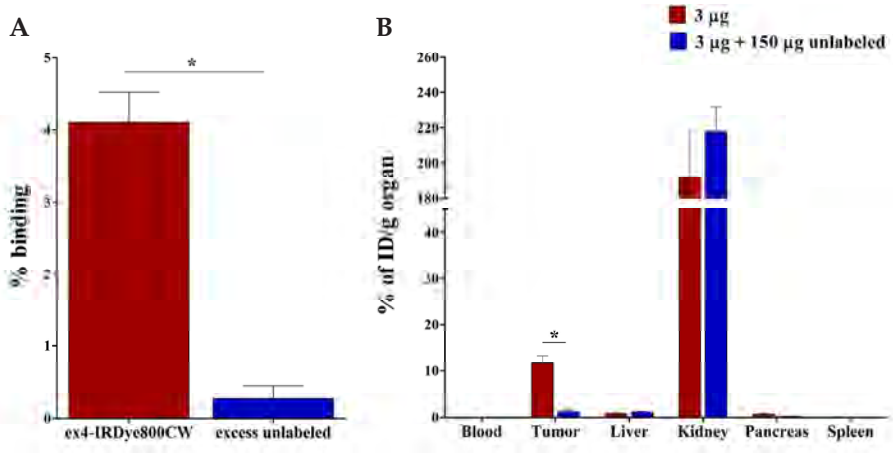

Figure 3 Binding of exendin-4-IRDye800CW (300nM) to CHL-GLP-1R cells with and without an excess of unlabeled exendin-4 (N=3) (A). Biodistribution of exendin-IRDye800CW with and without an excess of unlabeled exendin-4 in blood and various tissues of female BALB/c nude mice carrying subcutaneous CHL-GLP-1R tumors (N=6/group) at 4 hours after tracer injection (B).

Exendin-4-IRDye800CW Accumulates in CHL-GLP-1R Tumors

Absolute tumor uptake of exendin-4-IRDye800CW was 9.6 ± 4.2 μg tracer/g organ with an injected dose of 3 μg and increased dose-dependently to 25.5 ± 2.1 μg/g, 43.2 ± 3.6 μg/g and 62.4 ± 31.8 μg/g with injected doses of 10 , 30 and 100 μg, respectively. Highest uptake of exendin-4-IRDye800CW was observed in the kidneys, due to renal clearance of the tracer (Figure 4).

Co-injection of an excess of unlabeled exendin-4 decreased the tumor uptake of exendin-4-IRDye800CW from 11.6 ± 1.6% ID/g to 1.3 ± 0.4% ID/g ($p < 0.001$) (Figure 3B).

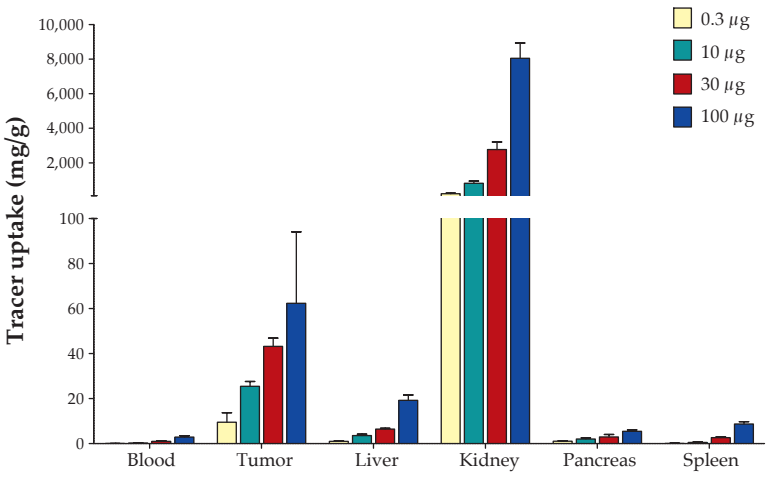

Figure 4 Biodistribution of exendin-IRDye800CW in blood and various tissues of female BALB/c nude mice carrying subcutaneous CHL-GLP-1R tumors (N=6/group) at 4 hours after tracer injection.

In Vivo Fluorescent Tumor Detection is Feasible

Tumors were clearly visualized by fluorescence imaging (Figure 5A and Figure 6). After resection of the tumors, no residual fluorescent signal was detected (Figure 5B). Next to the signal in the tumors, a fluorescent signal was observed in the kidneys. In the mice receiving an excess of the unlabeled peptide, no fluorescent signal was seen in the tumor while the signal in the kidneys persists, demonstrating the receptor specificity of the uptake of exendin-4-IRDye800CW (Figure 5C).

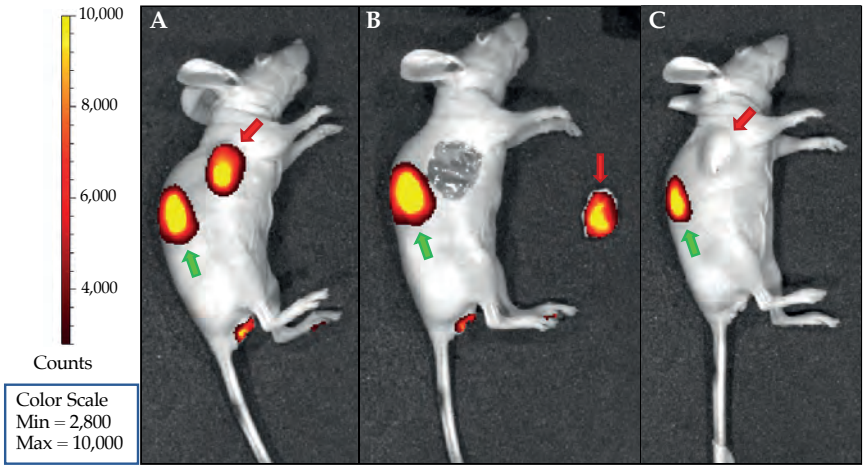

Figure 5 NIR fluorescence images of BALB/c nude mice bearing subcutaneous CHL GLP1-R tumors. Tumors are indicated with red arrows and kidneys with green arrows. (A) Image of an intact mouse. (B) Image of a mouse after resection of the tumor. (C) Image of a mouse injected with the exendin-4-IRDye800CW and an excess of unlabeled peptide.

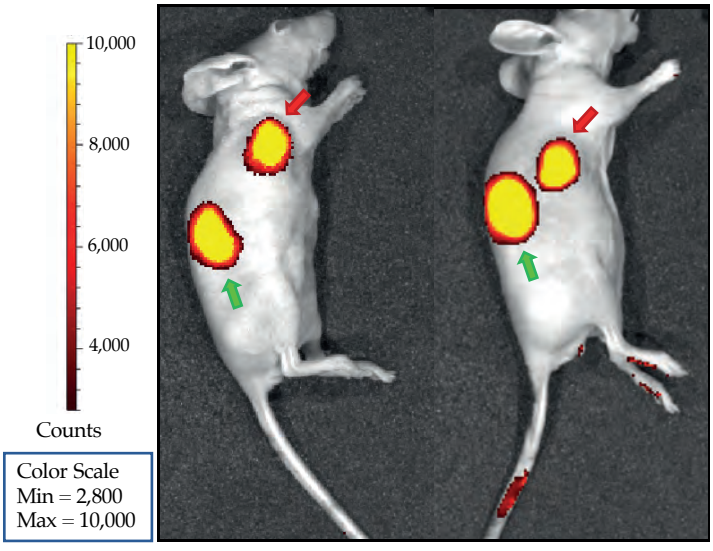

Figure 6 NIR fluorescent images of the additional two BALB/c nude mice bearing subcutaneous CHL GLP-1R tumors. Tumors are indicated with red arrows and kidneys with green arrows.

Exendin-4-IRDye800CW Accumulates Specifically in Murine Pancreatic Islets of Langerhans

Representative images of the islets of one of the mice are shown in Figure 7. The presence of pancreatic islets is clearly indicated by the positive insulin staining. A clear NIR fluorescent signal is observed at the site of the pancreatic islets.

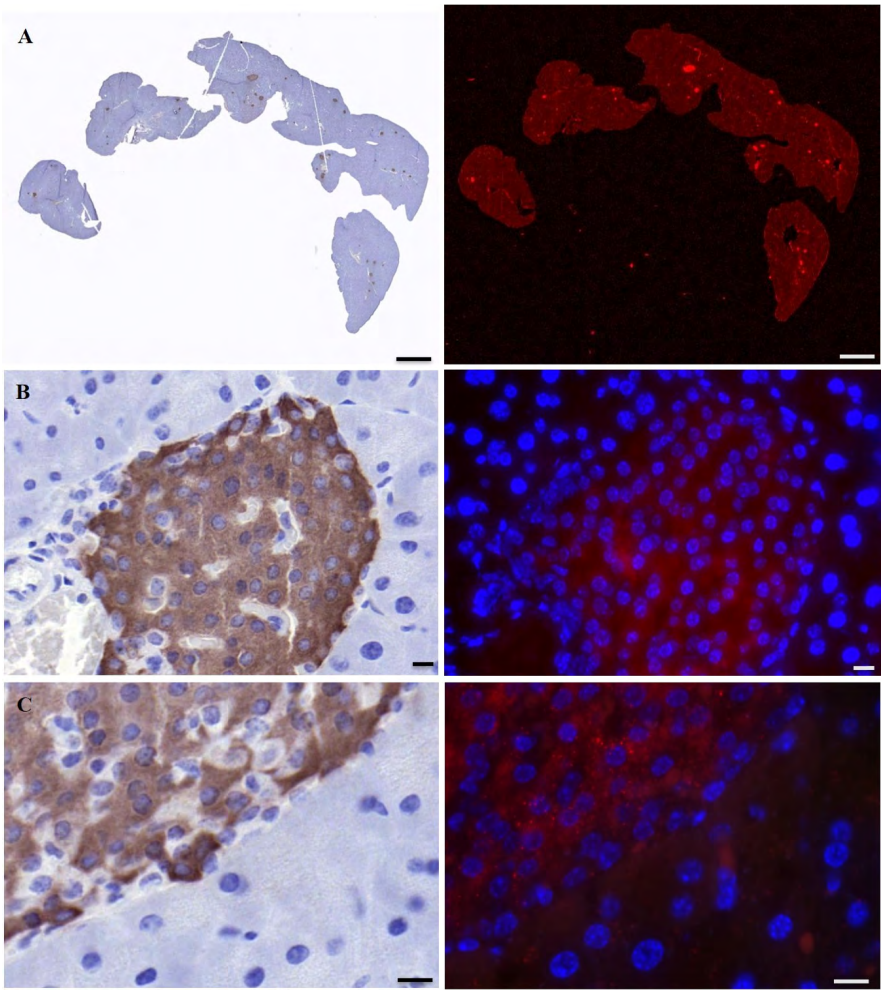

Figure 7 Immunohistochemistry, flat bed fluorescence (A) and fluorescence microscopy (B,C) images of pancreatic tissue of a mouse injected with exendin-4-IRDye800CW. Insulin staining shown in brown (left), 800 nm fluorescent signal in red and nuclei in blue (right). Microscopy images at 40x (B) and 63x (C) magnification. Scale bars indicate 1000 μm (A) or 10 μm (B,C).

The signal appears to be mostly intracellular, which corresponds with the fast internalization of exendin-4 based tracers. A much lower signal is observed in the exocrine pancreatic tissue. The higher fluorescent signal in the pancreatic islets points to receptor specificity of the uptake of exendin-4-IRDye800CW.

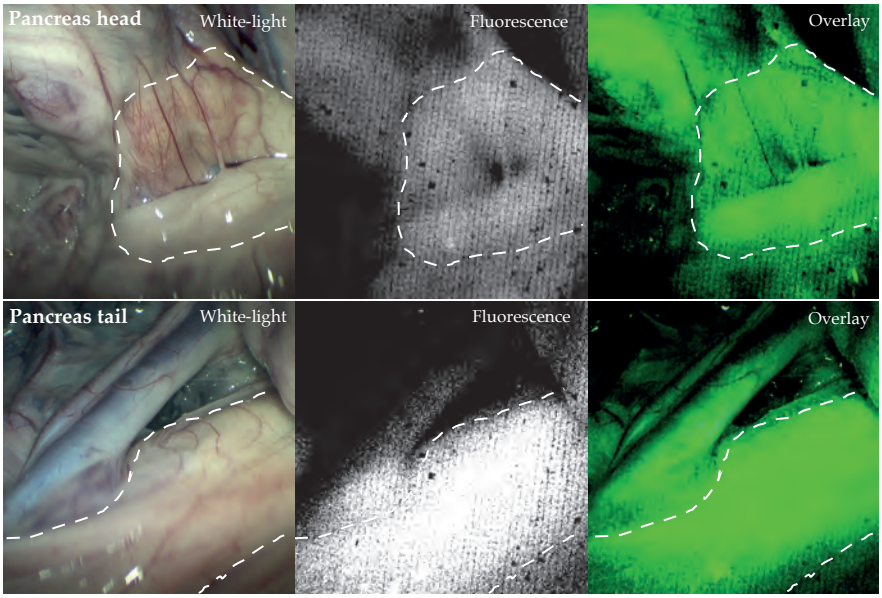

Figure 8 Laparoscopic images of the pancreatic head and tail of a healthy mini pig. On the left white light images, in the middle NIR fluorescent imaging and on the right layover images where the fluorescent signal is depicted in green.

Pancreatic Uptake of Exendin-4-IRDye800CW is Detected by In Vivo Laparoscopic Imaging in Mini Pigs

Laparoscopic NIR fluorescence imaging of the pancreas in healthy mini pigs revealed a clear fluorescent signal in the pancreatic head and tail with which it is possible to discriminate between pancreatic tissue and surrounding tissues (Figure 8).

Discussion

Surgery to remove insulinomas or lesions in focal CHI is challenging and carries substantial risks of morbidity (4, 5). Precise detection of the lesion is essential for an optimal surgical procedure. Real-time intra-operative detection with a high sensitivity and spatial resolution for precise lesion delineation can be provided by targeted fluorescence imaging. An agent for targeted NIR fluorescence imaging of the GLP-1R was developed and examined *in vitro* and *in vivo* in this study.

Exendin-4-IRDye800CW was shown to have a high affinity for the GLP-1R. Because of the high target affinity of the tracer combined with fast clearance from non-target tissues, a signal with high target-to-background values can be achieved.

Exendin-4-IRDye800CW was shown to accumulate dose-dependently in subcutaneous GLP-1R positive tumors in mice. We demonstrate the reliability of the method used to assess the biodistribution of the fluorescent tracer by showing comparable results of fluorescent and radioactive quantification of the uptake of the dual-labeled tracer ^{111}In-DTPA-exendin-4-Cy5.5 in GLP-1R positive tumors, pancreas and kidneys of mice. We furthermore show that with exendin-4-IRDye-800CW, subcutaneous GLP-1R positive tumors could be visualized using NIR fluorescence imaging. Co-injection of an excess of unlabeled exendin-4 completely abolished the fluorescent signal in the tumors, demonstrating the receptor-specificity of the tumor uptake. Furthermore, fluorescence microscopy shows uptake of the tracer specifically in the pancreatic islets of these mice.

The first report on intra-operative imaging of insulinomas involved a non-targeted approach based on the NIR dye methylene blue, which showed higher uptake in insulinomas than normal pancreatic tissue in the proper dilution (23). A targeted approach, as described in this study, has the benefit of creating signals with higher contrast between the target and surrounding tissue and therefore more precise delineation of the lesion. Exendin-4 has already been shown to be very effective for targeting of GLP-1R positive tumors in pre-clinical as well as clinical studies using radiolabeled exendin (7, 10, 11). Reiner *et al*. have previously developed NIR imaging agents, based on exendin-4, for the purpose of *in vivo* quantification of beta cell mass. These tracers were shown to bind the GLP-1R with high affinities (IC_{50}: 0.3 – 3 nM) and a fluorescent signal was observed in the pancreatic islets. However, uptake of these tracers in GLP-1R positive tumors leading to a possible application for fluorescent-guided surgery was not assessed (24, 25). Exendin-4 was used by Brand *et al.* to develop a dual-labeled tracer (^{64}Cu-exendin-4-Cy5) for combined PET and fluorescence imaging of GLP-1R positive tumors. While the affinity of this tracer for the GLP-1R (IC_{50}: 50 nM) was lower than exendin-4-IRDye800CW, specific accumulation in GLP-1R tumors was shown and GLP-1R positive xenografts were visualized using *in vivo* PET imaging.

However, while a fluorescent signal in the xenografts was detected using fluorescence microscopy, *in vivo* fluorescent imaging was not performed (26). We therefore here provide the first evidence of the feasibility of targeted *in vivo* fluorescence imaging of GLP-1R positive lesions.

Using a laparoscopic NIR fluorescence imaging device, a fluorescent signal of exendin-4-IRDye800CW in the pancreas of mini pigs could be detected. Since the exocrine pancreas in pigs is known to have a relatively high GLP-1R density resulting in a low endocrine-exocrine ratio of GLP-1R expression (27), the detected signal is most probably not only originating from the pancreatic islets. In mice, where fluorescence microscopy showed specific uptake of the tracer in the pancreatic islets, the endocrine-exocrine ratio of GLP-1R expression is known to be much higher (27). However, even if the NIR fluorescent signal detected with the laparoscope originates from both the endocrine and exocrine pancreas of the mini pigs, the feasibility of using this laparoscopic procedure to detect the NIR fluorescent signal clearly demonstrates the potential for clinical translation of this approach. Despite the background fluorescence signal in the pancreas resulting from uptake of the tracer in healthy pancreatic beta cells, visualization and delineation of insulinomas in humans using this approach is most likely possible, since insulinomas have a very high GLP-1R density in almost 100% of cases (higher than healthy pancreatic islets) (28) and visualization with high tumor-to-background ratios has been achieved with radiolabeled exendin (7).

Contributing to the potential for clinical translation of this tracer is the use of the NIR fluorophore IRDye800CW. This dye is widely used in the development of targeted fluorescence imaging approaches and several studies already show the first successful clinical applications using this fluorophore. Detection of primary breast cancer lesions as well as peritoneal metastases of colorectal cancer was shown to be feasible using IRDye800CW coupled to the monoclonal antibody (mAb) bevacizumab (29, 30). Also, IRDye800CW coupled to the mAb cetuximab was successfully used for detection of glioblastomas (31). While the first successful clinical results with targeted NIR intra-operative imaging are obtained with mAb based approaches, various peptide-based NIR imaging approaches have been developed and demonstrated to be successful in preclinical settings for a wide range of cancer types. Also, several clinical trials are ongoing (32).

Conclusion

We here show the feasibility of *in vivo* fluorescence imaging of GLP-1R positive lesions using the novel tracer exendin-4-IRDye800CW. While applicable in open as well as laparoscopic procedures, this approach could be especially beneficial for laparoscopic procedures, in which surgeons currently rely solely on intra-operative ultrasound. In the future, fluorescence imaging using exendin-4-IRDye800CW could benefit surgical removal of insulinomas as well as focal lesions in CHI by providing sensitive and specific real-time intra-operative optical lesion delineation.

References

1. de Boer E, Harlaar NJ, Taruttis A, Nagengast WB, Rosenthal EL, Ntziachristos V, et al. Optical innovations in surgery. The British journal of surgery. 2015;102(2):e56-72.
2. Kinova MK. Diagnostics and treatment of insulinoma. Neoplasma. 2015;62(5):692-704.
3. Lord K, Dzata E, Snider KE, Gallagher PR, De Leon DD. Clinical presentation and management of children with diffuse and focal hyperinsulinism: a review of 223 cases. The Journal of clinical endocrinology and metabolism. 2013;98(11):E1786-9.
4. Senniappan S, Shanti B, James C, Hussain K. Hyperinsulinaemic hypoglycaemia: genetic mechanisms, diagnosis and management. Journal of inherited metabolic disease. 2012;35(4):589-601.
5. Richards ML, Gauger PG, Thompson NW, Kloos RG, Giordano TJ. Pitfalls in the surgical treatment of insulinoma. Surgery. 2002;132(6):1040-9; discussion 9.
6. Zhu L, Xue H, Sun Z, Li P, Qian T, Xing X, et al. Prospective comparison of biphasic contrast-enhanced CT, volume perfusion CT, and 3 Tesla MRI with diffusion-weighted imaging for insulinoma detection. Journal of magnetic resonance imaging : JMRI. 2017;46(6):1648-55.
7. Antwi K, Fani M, Heye T, Nicolas G, Rottenburger C, Kaul F, et al. Comparison of glucagon-like peptide-1 receptor (GLP-1R) PET/CT, SPECT/CT and 3T MRI for the localisation of occult insulinomas: evaluation of diagnostic accuracy in a prospective crossover imaging study. European journal of nuclear medicine and molecular imaging. 2018;45(13):2318-27.
8. Prasad V, Sainz-Esteban A, Arsenic R, Plockinger U, Denecke T, Pape UF, et al. Role of (68)Ga somatostatin receptor PET/CT in the detection of endogenous hyperinsulinaemic focus: an explorative study. European journal of nuclear medicine and molecular imaging. 2016;43(9):1593-600.
9. Mehrabi A, Fischer L, Hafezi M, Dirlewanger A, Grenacher L, Diener MK, et al. A systematic review of localization, surgical treatment options, and outcome of insulinoma. Pancreas. 2014;43(5):675-86.
10. Brom M, Joosten L, Oyen WJ, Gotthardt M, Boerman OC. Radiolabelled GLP-1 analogues for in vivo targeting of insulinomas. Contrast media & molecular imaging. 2012;7(2):160-6.
11. Christ E, Wild D, Ederer S, Behe M, Nicolas G, Caplin ME, et al. Glucagon-like peptide-1 receptor imaging for the localisation of insulinomas: a prospective multicentre imaging study. The lancet Diabetes & endocrinology. 2013;1(2):115-22.
12. Luo Y, Pan Q, Yao S, Yu M, Wu W, Xue H, et al. Glucagon-Like Peptide-1 Receptor PET/CT with 68Ga-NOTA-Exendin-4 for Detecting Localized Insulinoma: A Prospective Cohort Study. Journal of nuclear medicine : official publication, Society of Nuclear Medicine. 2016;57(5):715-20.
13. Laje P, States LJ, Zhuang H, Becker SA, Palladino AA, Stanley CA, et al. Accuracy of PET/CT Scan in the diagnosis of the focal form of congenital hyperinsulinism. Journal of pediatric surgery. 2013;48(2):388-93.
14. Fendrich V, Bartsch DK, Langer P, Zielke A, Rothmund M. [Diagnosis and surgical treatment of insulinoma--experiences in 40 cases]. Deutsche medizinische Wochenschrift (1946). 2004;129(17):941-6.
15. Kisker O, Bastian D, Frank M, Rothmund M. [Diagnostic localization of insulinoma. Experiences with 25 patients with solitary tumors]. Medizinische Klinik (Munich, Germany : 1983). 1996;91(6):349-54.
16. Christ E, Wild D, Forrer F, Brandle M, Sahli R, Clerici T, et al. Glucagon-like peptide-1 receptor imaging for localization of insulinomas. The Journal of clinical endocrinology and metabolism. 2009;94(11):4398-405.
17. DeLong JC, Hoffman RM, Bouvet M. Current status and future perspectives of fluorescence-guided surgery for cancer. Expert review of anticancer therapy. 2016;16(1):71-81.
18. Ash C, Dubec M, Donne K, Bashford T. Effect of wavelength and beam width on penetration in light-tissue interaction using computational methods. Lasers in medical science. 2017;32(8):1909-18.
19. van Eyll B, Lankat-Buttgereit B, Bode HP, Goke R, Goke B. Signal transduction of the GLP-1-receptor cloned from a human insulinoma. FEBS letters. 1994;348(1):7-13.
20. Jodal A, Lankat-Buttgereit B, Brom M, Schibli R, Behe M. A comparison of three (67/68)Ga-labelled exendin-4 derivatives for beta-cell imaging on the GLP-1 receptor: the influence of the conjugation site of NODAGA as chelator. EJNMMI research. 2014;4:31.

21. Brom M, Oyen WJ, Joosten L, Gotthardt M, Boerman OC. 68Ga-labelled exendin-3, a new agent for the detection of insulinomas with PET. European journal of nuclear medicine and molecular imaging. 2010;37(7):1345-55.
22. Brom M, Woliner-van der Weg W, Joosten L, Frielink C, Bouckenooghe T, Rijken P, et al. Non-invasive quantification of the beta cell mass by SPECT with (1)(1)(1)In-labelled exendin. Diabetologia. 2014; 57(5):950-9.
23. Winer JH, Choi HS, Gibbs-Strauss SL, Ashitate Y, Colson YL, Frangioni JV. Intraoperative localization of insulinoma and normal pancreas using invisible near-infrared fluorescent light. Annals of surgical oncology. 2010;17(4):1094-100.
24. Reiner T, Kohler RH, Liew CW, Hill JA, Gaglia J, Kulkarni RN, et al. Near-infrared fluorescent probe for imaging of pancreatic beta cells. Bioconjugate chemistry. 2010;21(7):1362-8.
25. Reiner T, Thurber G, Gaglia J, Vinegoni C, Liew CW, Upadhyay R, et al. Accurate measurement of pancreatic islet beta-cell mass using a second-generation fluorescent exendin-4 analog. Proceedings of the National Academy of Sciences of the United States of America. 2011;108(31):12815-20.
26. Brand C, Abdel-Atti D, Zhang Y, Carlin S, Clardy SM, Keliher EJ, et al. In vivo imaging of GLP-1R with a targeted bimodal PET/fluorescence imaging agent. Bioconjugate chemistry. 2014;25(7):1323-30.
27. Eriksson O, Rosenstrom U, Selvaraju RK, Eriksson B, Velikyan I. Species differences in pancreatic binding of DO3A-VS-Cys(40)-Exendin4. Acta diabetologica. 2017;54(11):1039-45.
28. Reubi JC, Waser B. Concomitant expression of several peptide receptors in neuroendocrine tumours: molecular basis for in vivo multireceptor tumour targeting. European journal of nuclear medicine and molecular imaging. 2003;30(5):781-93.
29. Harlaar NJ, Koller M, de Jongh SJ, van Leeuwen BL, Hemmer PH, Kruijff S, et al. Molecular fluorescence-guided surgery of peritoneal carcinomatosis of colorectal origin: a single-centre feasibility study. The lancet Gastroenterology & hepatology. 2016;1(4):283-90.
30. Lamberts LE, Koch M, de Jong JS, Adams ALL, Glatz J, Kranendonk MEG, et al. Tumor-Specific Uptake of Fluorescent Bevacizumab-IRDye800CW Microdosing in Patients with Primary Breast Cancer: A Phase I Feasibility Study. Clinical cancer research : an official journal of the American Association for Cancer Research. 2017;23(11):2730-41.
31. Miller SE, Tummers WS, Teraphongphom N, van den Berg NS, Hasan A, Ertsey RD, et al. First-in-human intraoperative near-infrared fluorescence imaging of glioblastoma using cetuximab-IRDye800. Journal of neuro-oncology. 2018;139(1):135-43.
32. Joshi BP, Wang TD. Targeted Optical Imaging Agents in Cancer: Focus on Clinical Applications. Contrast media & molecular imaging. 2018;2018:2015237.

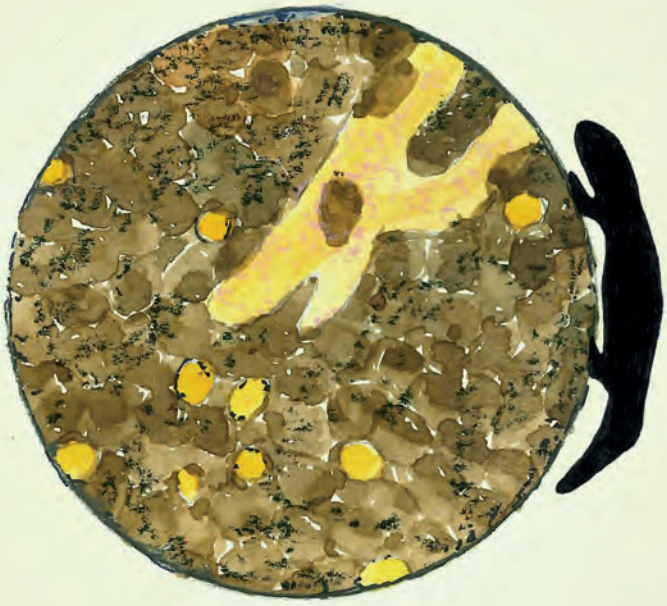

CHAPTER 6

Receptor-targeted photodynamic therapy of glucagon-like peptide 1 receptor positive lesions

Marti Boss, Desiree Bos, Cathelijne Frielink, Gerwin Sandker, Patricia Bronkhorst, Sanne A.M. van Lith, Maarten Brom, Mijke Buitinga, Martin Gotthardt

Journal of Nuclear Medicine, 2020 May8. doi: 10.2967/jnumed.119.238998

Department of Medical Imaging, Radboud University Medical Center, Nijmegen, The Netherlands

Abstract

Treatment of hyperinsulinemic hypoglycemia is challenging. Surgical treatment of insulinomas and focal lesions in congenital hyperinsulinism (CHI) is invasive and carries major risks of morbidity. Medication to treat nesidioblastosis and diffuse CHI has varying efficacy and causes significant side effects. Here, we describe a novel method for therapy of hyperinsulinemic hyperglycemia, highly selectively killing beta cells by receptor-targeted photodynamic therapy (rtPDT) with exendin-4-IRDye700DX, targeting the glucagon-like peptide 1 receptor (GLP-1R).

Methods

A competitive binding assay was performed using Chinese hamster lung (CHL) cells transfected with the GLP-1R. The efficacy and specificity of rtPDT with exendin-4-IRDye700DX was examined *in vitro* in cells with different levels of GLP-1R expression. Tracer biodistribution was determined in BALB/c nude mice bearing subcutaneous CHL-GLP-1R xenografts. Induction of cellular damage and the effect on tumor growth were analyzed to determine treatment efficacy.

Results

Exendin-4-IRDye700DX has a high affinity for the GLP-1R with an IC_{50} value of 6.3 nM. rtPDT caused significant specific phototoxicity in GLP-1R positive cells (2.3 ± 0.8 % and 2.7 ± 0.3 % remaining cell viability in CHL-GLP-1R and INS-1 cells resp.). The tracer accumulates dose-dependently in GLP-1R positive tumors. *In vivo* rtPDT induces cellular damage in tumors, shown by strong expression of cleaved-caspase-3 and leads to a prolonged median survival of the mice (36.5 vs. 22.5 days resp. $p<0.05$).

Conclusion

These data show *in vitro* as well as *in vivo* evidence for the potency of rtPDT using exendin-4-IRDye700DX. This could in the future provide a new, minimally invasive and highly specific treatment method for hyperinsulinemic hypoglycemia.

Introduction

Insulin production by pancreatic beta cells is usually a well-regulated process. However, uncontrolled overproduction of insulin can arise, in most cases as a result of insulin-producing lesions. Such lesions cause major clinical symptoms and treatment can be challenging. In adults, these lesions manifest in endogenous adult hyperinsulinemic hypoglycemia, most often caused by an insulinoma; an insulin-producing neuroendocrine tumor arising from pancreatic beta cells (1). In 0.5% to 5% of cases, adult hyperinsulinemic hypoglycemia is caused by nesidioblastosis, characterized by proliferation of abnormal beta cells throughout the pancreas (2). In neonates, the most common cause of persistent hyperinsulinism is CHI (3). In diffuse CHI, there is diffuse involvement of the pancreatic beta cells, while in focal CHI the disease is caused by focal adenomatous islet cell hyperplasia (4). Episodic hypoglycemia due to endogenous hyperinsulinism causes neuroglycopenic and autonomic symptoms. Prolonged hypoglycemia may lead to seizures, loss of consciousness, permanent brain damage or brain death (5).

Insulinomas and focal CHI can be cured by surgical removal of the lesion (3, 6). Enucleation is possible in case of superficially localized lesions with sufficient distance to the pancreatic duct (2-3 mm). Otherwise, a more extensive surgical procedure like partial or distal pancreatectomy may be required. While such procedures can often be performed laparoscopically (7, 8), they remain challenging and may carry major risks of morbidity (9, 10). The only surgical treatment option for patients with nesidioblastosis and diffuse CHI not responding to medication is partial pancreatectomy. Even after such an invasive procedure, hypoglycemic episodes often persist, requiring continued treatment with medication and, in certain cases of CHI, total pancreatectomy (2, 4).

Because of these challenges, a novel, preferably minimally invasive treatment option for hyperinsulinemic hypoglycemia in adults as well as in children is warranted. In this study, we assess the feasibility of specific ablation of insulin-producing cells with PDT. PDT is based on inducing cell death by irradiation of a light-sensitive molecule, or photosensitizer (PS). The PS absorbs photons and is transferred to a higher energy state. By transfer of energy from the activated PS to the oxygen in the surrounding tissue, reactive oxygen species (ROS) are produced, which can cause cellular damage (11). To ensure efficient and specific delivery of the PS to the target tissue, the PS is coupled to a tumor-specific targeting moiety (12).

An attractive targeting moiety for rtPDT of insulin-producing cells is exendin-4. This peptide is a stable analogue of the hormone GLP-1. It specifically binds to the GLP-1R, which is expressed on pancreatic beta cells and in high levels in nearly 100% of benign insulinomas (13). GLP-1R imaging using ^{111}In- and ^{68}Ga-labelled exendin-4 has been shown to be a successful pre-operative imaging technique for

insulinomas (14-16) and is also under investigation in CHI (clinicaltrials.gov; NCT03768518).

We have developed an approach for rtPDT of insulin producing lesions using the peptide exendin-4 coupled to the photosensitizer IRDye700DX. We hypothesize that this novel method will allow specific cell killing of GLP-1R positive cells.

Materials and methods

Reagents

Exendin-4-IRDye700DX was supplied by piCHEM (Graz, Austria). IRDye700DX NHS ester was obtained from LI-COR Biosciences (Lincoln, Nebraska, U.S.A.). IRDye700DX absorbs and emits light in the NIR range and has a higher extinction coefficient ($2.1x10^5$ $M^{-1}cm^{-1}$ at 689 nm) than non-NIR PSs (12, 17). The N-epsilon amino group of lysine at position 40 was site specifically modified during solid phase peptide synthesis with a mercapto-propionic acid, releasing an unprotected exendin-4 with a free thiol function after triisopropylsilane cleavage. IRDye700DX was modified with a maleimide and coupling to exendin-4 was performed using a thiol reactive crosslinking approach. The purity was >90%. Stock solutions of exendin-4-IRDye700DX were prepared in phosphate-buffered saline (PBS). The structure and amino acid sequence of the tracer are shown in figure 1. Absorbance and emission spectra of exendin-4-IRDye700DX are shown in figure 2.

Cell culture

CHL cells stably transfected with the GLP-1R (18) were cultured in Dulbecco's modified Eagle's medium (DMEM) with 4.5g/L D-glucose and Glutamax, supplemented with 10% fetal calf serum (FCS), 100 IU/mL penicillin G, 10mg/mL streptomycine, 1 mM sodium pyruvate, 0.1 mM non-essential amino acids and 0.3 mg/mL G418 geneticin. The rat insulinoma cell line INS-1 was cultured in RPMI 1640 medium, supplemented with 10% FCS, 100 IU/mL penicillin G, 10mg/mL streptomycine, 2 mmol/L L-glutamine, 1 mmol/L pyruvate, 10 mmol/L 4-(2-hydroxyethyl)-1-piperazineethanesulfonic acid (HEPES) and 50 μmol/L 2-mercaptoethanol. The human pancreatic tumor cell line PANC-1 was cultured in RPMI 1640 medium supplemented with 10% FCS, 100 IU/mL penicillin G, 10 mg/mL streptomycine and 2 mmol/L L-glutamine.

Competitive binding assay

The half-maximal inhibitory concentration (IC_{50}) of exendin-4-IRDye700DX and unlabeled exendin, as a reference, was determined using CHL-GLP-1R cells as described previously (19, 20). 10^6 cells/well were grown overnight in six well plates.

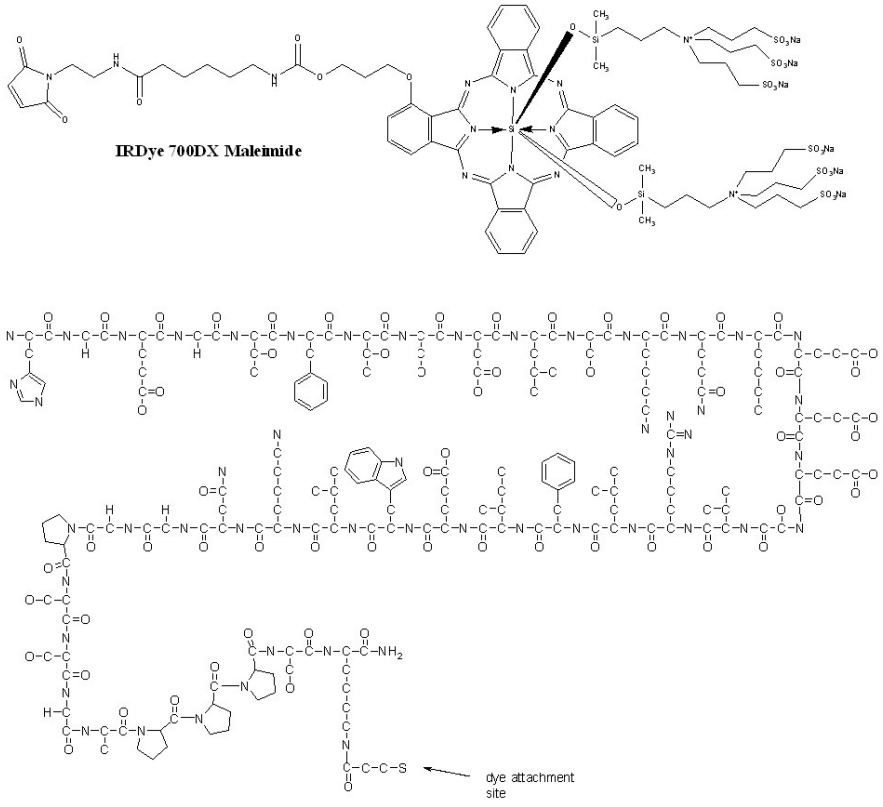

Figure 1 Structure and amino acid sequence of exendin-4-IRDye700DX

Cells were washed twice with PBS and incubated for 4 hours on ice with 50,000 cpm ^{111}In-labelled exendin in the presence of increasing concentrations of exendin-4-IRDye700DX (0.1–300 nM). Cells were then washed with PBS, solubilized with 2 mL sodium hydroxide (NaOH), collected and the cell-associated activity was measured in a gamma-counter (Wizard 2480, PerkinElmer, Groningen, The Netherlands).

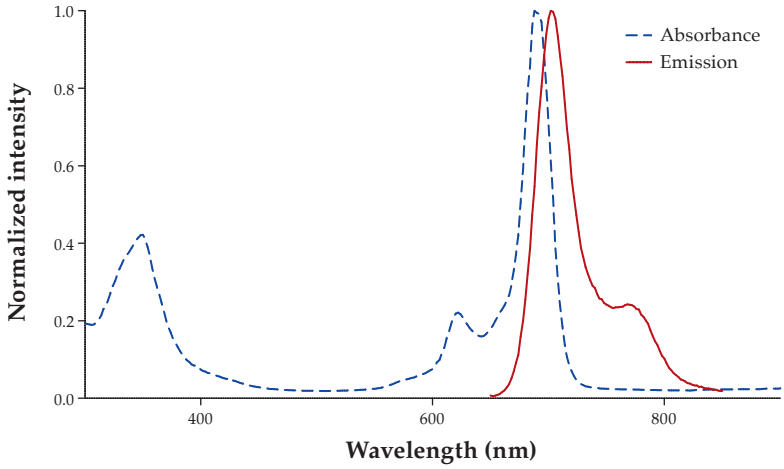

Figure 2 Absorbance and emission spectra of exendin-4-IRDye700DX.

In vitro receptor-targeted photodynamic therapy

CHL-GLP-1R cells, INS-1 cells and PANC-1 cells were seeded into 24-well plates (Thermo Scientific) (150,000 cells/well) and grown overnight. Medium was replaced by binding buffer (medium with 0.1% bovine serum albumin (w/v) (BSA)) with exendin-4-IRDye700DX (300nM for CHL-GLP-1R cells and 400nM for INS-1 and PANC-1 cells (concentrations based on optimization experiments). As a control, cells incubated with binding buffer only were used. Separate wells were incubated with an excess (15 μM for CHL-GLP-1R cells and 20 μM for INS-1 and PANC-1 cells) of unlabeled exendin-4 together with exendin-4-IRDye700DX. After incubation at 37°C (CHL-GLP-1R cells 4 hours, INS-1 and PANC-1 cells 24 hours), cells were washed with binding buffer. Subsequently, cells were irradiated with a NIR light-emitting diode (LED) (21) (emission wavelength 670-710 nm, forward voltage: 2.6 V, power output: 490 mW) using 126 individual LED bulbs ensuring homogenous illumination (21). CHL-GLP-1R cells were irradiated at 90 J/cm^2 (over 6 min). INS-1 and PANC-1 cells were irradiated at 150 J/cm^2 (over 10 min). Cells incubated with exendin-4-IRDye700DX that were not irradiated were included as a control. All experiments were carried out in triplicate.

Four hours after irradiation, during which the cells were kept at 37°C and 5% CO_2, the ATP content as a measure of cell viability was determined using a CellTiter-Glo® luminescent assay (Promega Benelux, Leiden, The Netherlands) according to the instructions of the manufacturer. Luminescence was measured using a TECAN infinite M200 Pro plate reader (PerkinElmer, Groningen, The Netherlands). The ATP content as a measure of cell viability was expressed as a percentage,

determined by comparing the luminescent signal with the signal from untreated cells, which were considered 100% viable.

Additionally, a co-culture of INS-1 and PANC-1 cells was plated in 24-well plates (70,000 and 40,000 cells/well, respectively). Before seeding, INS-1 cells were labeled with the fluorescent dye DiO and PANC-1 cells with DiD dye according to the manufacturer's protocol (Life Technologies, Thermo Fisher Scientific, Waltam, MA, USA). Cells were grown overnight and then incubated with 400 nM exendin-4-IRDye700DX in binding buffer or binding buffer alone for 24 hours at 37°C and 5% CO_2. Subsequently, cells were irradiated with 150 J/cm^2 of NIR light. After 4 hours, cells were incubated with 1 μg/mL propidium iodide (Thermo Fisher Scientific, Waltham, MA, USA) in PBS for 15 minutes at room temperature. Cells were visualized using an EVOS microscope (Thermo Fisher Scientific, Waltam, MA, USA).

Animal tumor model

Female BALB/c nude mice (Janvier, Le Genest Saint Isle, France), 6-8 weeks old, were housed in individually ventilated cages (6 mice per cage) under non sterile conditions with ad libitum access to chlorophyll-free animal chow and water. CHL-GLP-1R cells (5*10^6 cells/ mouse in 200 μl DMEM with 4.5g/L D-glucose and Glutamax) were injected subcutaneously on the right flank of the mice.

In vivo biodistribution

Female BALB/c nude mice with CHL-GLP-1R xenografts were injected intravenously with exendin-4-IRDye700DX in 200 μl PBS with 0.5% BSA (N=5 per group, 1, 3 and 10 μg exendin-4-IRDye-700DX). Four mice were injected with only PBS with 0.5% BSA. After 4 hours, mice were sacrificed by CO_2 asphyxiation and the tumor and organs were removed and collected in Roche MagNA Lyser tubes (F Hoffmann-La Roche Ltd., Basel, Switzerland). Radioimmunoprecipitation assay (RIPA) lysis buffer (500 μL; 50mM (hydroxymethyl)aminomethane-hydrochloride (TRIS-HCl), pH7.4 with 150 mM sodiumchloride (NaCl), 1 mM ethylenediaminetetraacetic acid (EDTA), 1% Triton-X-100 and 1% sodium dodecyl sulfate (SDS)) was added to each tube. Organs were homogenized using a Roche MagNA Lyser (F Hoffmann-La Roche Ltd., Basel, Switzerland) with repeated cycles of 6000 rpm for 25 sec with cooling on ice for 1 minute between cycles. Organ homogenates of the control mice (injected only with PBS with 0.5% BSA) were used to create standard curves of exendin-4-IRDye700DX for each organ. 100 μl of homogenates were transferred in triplicate to a black flat-bottom 96-well plate and fluorescence intensity was measured using a TECAN infinite M200 Pro plate reader (PerkinElmer, Groningen, The Netherlands) (excitation wavelength: 620 nm, emission wavelength: 700 nm). Standard curves and tracer uptake were calculated using Microsoft Office Excel 2007.

Receptor-targeted photodynamic therapy in vivo; immunohistochemistry

Female BALB/c nude mice with subcutaneous GLP-1R positive xenografts (N=8 per group) were injected intravenously with 30 μg exendin-4-IRDye700DX in 200 μl PBS with 0.5% BSA or 200 μl PBS with 0.5% BSA only, and after 4 hours exposed to 100 J/cm^2 NIR LED light. One group was treated only with exendin-4-IRDye700DX without NIR light exposure. Two or 24 hours after NIR light exposure, mice were sacrificed by CO_2 asphyxiation. Tumors were harvested, fixated in 4% buffered formalin, embedded in paraffin and sectioned at 4 μm thickness. Slices were deparaffinized with xylene and rehydrated in ethanol. Antigen retrieval was performed with 10 mM citrate pH 6.0 in a PT-Module (Thermo Fisher Scientific, Waltam, MA, USA) (10 min, 96ºC). Endogenous peroxidase activity was quenched with 3% H_2O_2 for 10 min. Slices were incubated with 20% normal goat serum for 30 min and subsequently with rabbit-anti-cleaved-caspase-3 (1:4000 in PBS + 1% BSA, ASP175, Cell Signaling Technology, Leiden, The Netherlands) in a humidified chamber at 4ºC overnight in the dark. Slides were then washed 3 times with 10 mM PBS and incubated with goat-anti-rabbit-biotin (1:200 in PBS + 1% BSA, Vector Laboratories, Peterborough, UK) for 30 min at room temperature. After washing with PBS, slides were incubated with Vectastain Elite ABC kit (Vector Laboratories, Peterborough, UK) for 30 min at room temperature. The bound antibodies were visualized using diaminobenzine (DAB, Bright DAB, BS04 Immunologic, VWR, Dublin, Ireland). Slides were counterstained with 3 times diluted hematoxylin (Klinipath, Olen, Belgium) for 5 seconds and mounted with a cover slip (permount, Fisher Scientific, Waltam, MA, USA).

The immunohistochemical staining was independently analyzed by two blinded observers. Scores were allocated to each slide following an ordinal 6-point scale ranging from 0 (no staining), 1 (very weak staining), 2 (weak staining), 3 (intermediate staining), 4 (intense staining) to 5 (very intense staining). The scores of the two observers were averaged.

Receptor-targeted photodynamic therapy in vivo; survival

Female BALB/c nude mice with CHL-GLP-1R xenografts were randomized into 2 groups of 8 animals based on tumor size. When tumors were at least 30 mm^3, mice were injected intravenously with 30 μg exendin-4-IRDye700DX in 200 μl PBS with 0.5% BSA or PBS with 0.5% BSA only. After 4 hours, mice were exposed to 150 J/cm^2 of NIR LED light under inhalation anesthesia (2,5% isoflurane mixed with 100% O_2 (1 L/min)). Kidneys were protected from exposure by covering them with gauze and aluminum foil. Tumor diameters were measured by a blinded observer three times per week in three dimensions using a caliper. Mice were euthanized by CO_2 asphyxiation when tumor volume reached more than 1000 mm^3

(tumor volume was calculated by 1.25*π* (((length + width + height) / 6) ^3). Overall survival was defined as the day that tumors reached a size of 1000 mm^3.

Statistics

Statistical calculations were performed using GraphPad Prism (GraphPad Software, La Jolla, CA, USA). IC_{50} values were calculated by fitting the data with non-linear regression using least squares fit with GraphPad Prism. *In vitro* cell viability after various treatments, assessed by a CellTiter-Glo® assay, were compared by two-way ANOVA with post-hoc Bonferroni tests. Tracer uptake in various tumors was compared between the different injected doses by one-way ANOVA.

Survival curves were compared with the log-rank (Mantel-Cox) test using GraphPad Prism (version 5.03).

Study approval

All animal experiments have been approved by the institutional Animal Welfare Committee of the Radboud University Medical Centre and were conducted in accordance to the guidelines of the Revised Dutch Act on Animal Experimentation.

Results

Exendin-4-IRDye700DX binds the GLP-1R with high affinity

The IC_{50} values of exendin-4 and exendin-4-IRDye700DX, were 2.54 nM (95% CI; 1.32–4.90) and 6.25 nM (95% CI; 3.07–12.74), respectively (Fig. 3). While the binding affinity of the labeled peptide is significantly lower compared to the unlabeled peptide ($p < 0.0001$), it binds with a high affinity to the GLP-1R in the nanomolar range.

In vitro receptor-targeted PDT with exendin-4-IRDye700DX and NIR light causes specific GLP-1R positive cell death.

rtPDT with exendin-4-IRDye700DX caused significant phototoxicity in cells with high GLP-1R expression (CHL-GLP-1R cells) and the rat insulinoma cell line INS-1, with GLP-1R expression comparable to human insulinomas. Remaining cell viabilities were 2.3±0.8 % and 2.7±0.3 % respectively (Fig. 4). In PANC-1 cells no cellular phototoxicity was observed under these conditions (96.1±1.2 % viable cells). Co-incubation with an excess of unlabeled exendin-4 abolished the phototoxic effect in CHL-GLP-1R cells as well as in INS-1 cells (99.3±1.3 and 98.4±2.1 % cell viability respectively). NIR light irradiation alone did not cause cellular phototoxicity in any of the cell types (106.6±1.2 %, 102.5±5.9 % and 102.0±1.8 %

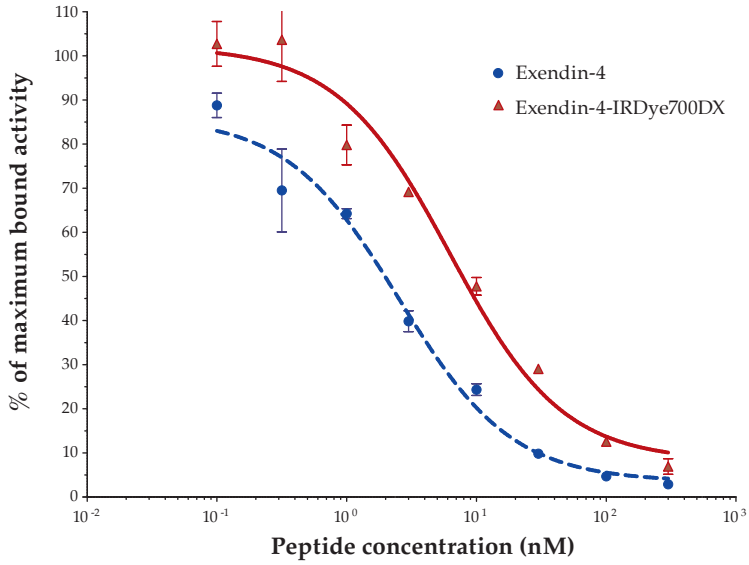

Figure 3 Competition binding assay (IC_{50}) using CHL-GLP-1 cells of unlabeled exendin-4 and exendin-4-IRDye700DX. ^{111}In-DTPA-exendin-4 was used as a tracer.

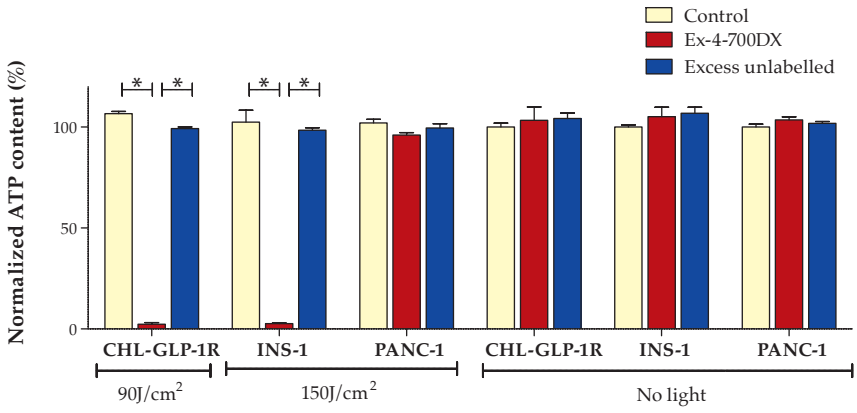

Figure 4 ATP content as a measure of cell viability of CHL-GLP-1R cells, INS-1 cells and PANC-1 cells following incubation with binding buffer (control), exendin-4-IRDye700DX or exendin-4-IRDye-700DX combined with an excess of unlabeled exendin-4 and with or without NIR light irradiation. Experiments were performed in triplicate. Data are presented as mean ± SD. * indicates $p<0.001$.

viable cells in CHL-GLP-1R, INS-1 and PANC-1 cells, respectively). No dark toxicity of the tracer was observed (103.3±6.7 %, 105.2±4.7 % and 103.6±1.4 % cell viability without irradiation in CHL-GLP-1R, INS-1 and PANC-1 cells, respectively). Incubation of a co-culture of INS-1 and PANC-1 cells with exendin-4-IRDye700DX followed by irradiation specifically caused cell death in INS-1 cells, as shown by co-localization of the red and green nuclei (Fig. 5). Absence of p.i. signal upon rtPDT indicated that exendin-4-IRDye700DX alone or NIR light alone did not cause cell death in either cell type.

Exendin-4-IRDye700DX accumulates in GLP-1R positive tumors.

Relative uptake of exendin-4-IRDye700DX in subcutaneous GLP-1R tumors in mice was 3.9±1.9 % injected dose (ID)/g for 1 μg tracer dose and diminishes slightly to 3.3±0.6 %ID/g for 3 μg tracer dose and 2.5±0.8 %ID/g for 10 μg tracer dose ($p = 0.25$) (Fig. 6). As a result, the absolute tumor uptake increases with increasing injected tracer doses to 25.0 μg/g with 10 μg tracer injection. Highest uptake of exendin-4-IRDye700 was observed in the kidneys, due to renal clearance.

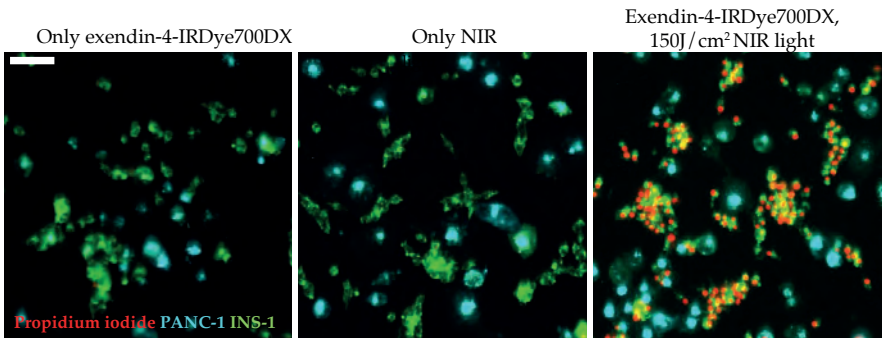

Figure 5 Fluorescence microscopy of INS-1 cells labeled with the fluorescent dye DiO (green) and PANC-1 cells labeled with the fluorescent dye DiD (cyan), co-cultured and incubated with propidium iodide (red), after incubation of exendin-4-IRDye700DX or only binding buffer and with and without NIR irradiation with a radiant exposure of 150 J/cm². The scale bar denotes 100 μm.

In vivo receptor-targeted PDT causes cell death in GLP-1R positive tumors and improves survival

Analysis of the immunohistochemical staining revealed a low expression of cleaved-caspase-3 in the control groups. In both treatment groups the expression of cleaved-caspase-3 was higher than in the control groups. While the intensity of cleaved-caspase-3 staining was variable at 2 hours after treatment, the intensity of

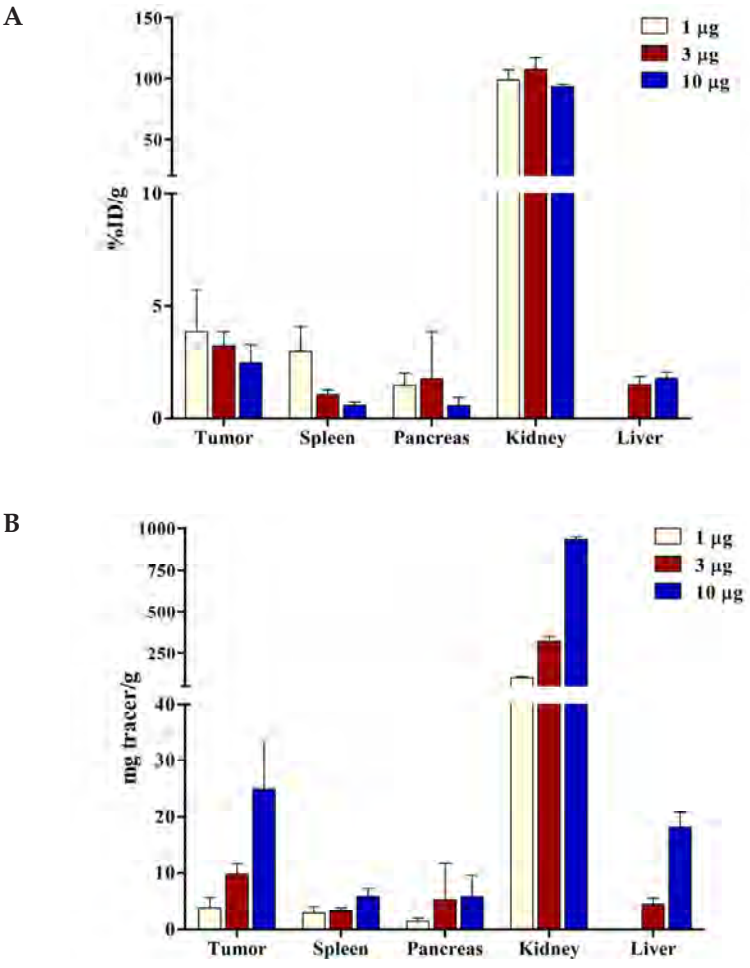

Figure 6 Biodistribution of exendin-4-IRDye700DX (1 μg, 3 μg and 10 μg, N=5 mice per group) in tumors, spleen, pancreas, kidneys and liver of female BALB/c nude mice 4 hours after tracer injection. (A) Relative uptake expressed as % of the injected dose per gram of tissue. (B) Absolute uptake expressed as μg of exendin-4-IRDye700DX per gram of tissue.

the staining was high and uniform in the tumors 24 hours after treatment, showing a significant induction of apoptosis in the tumors. The expression of cleaved-caspase-3 was slightly increased in control group receiving only NIR light irradiation, showing that the light itself induces some cell death, most likely due to the heat produced by the LED light source (Fig. 7).

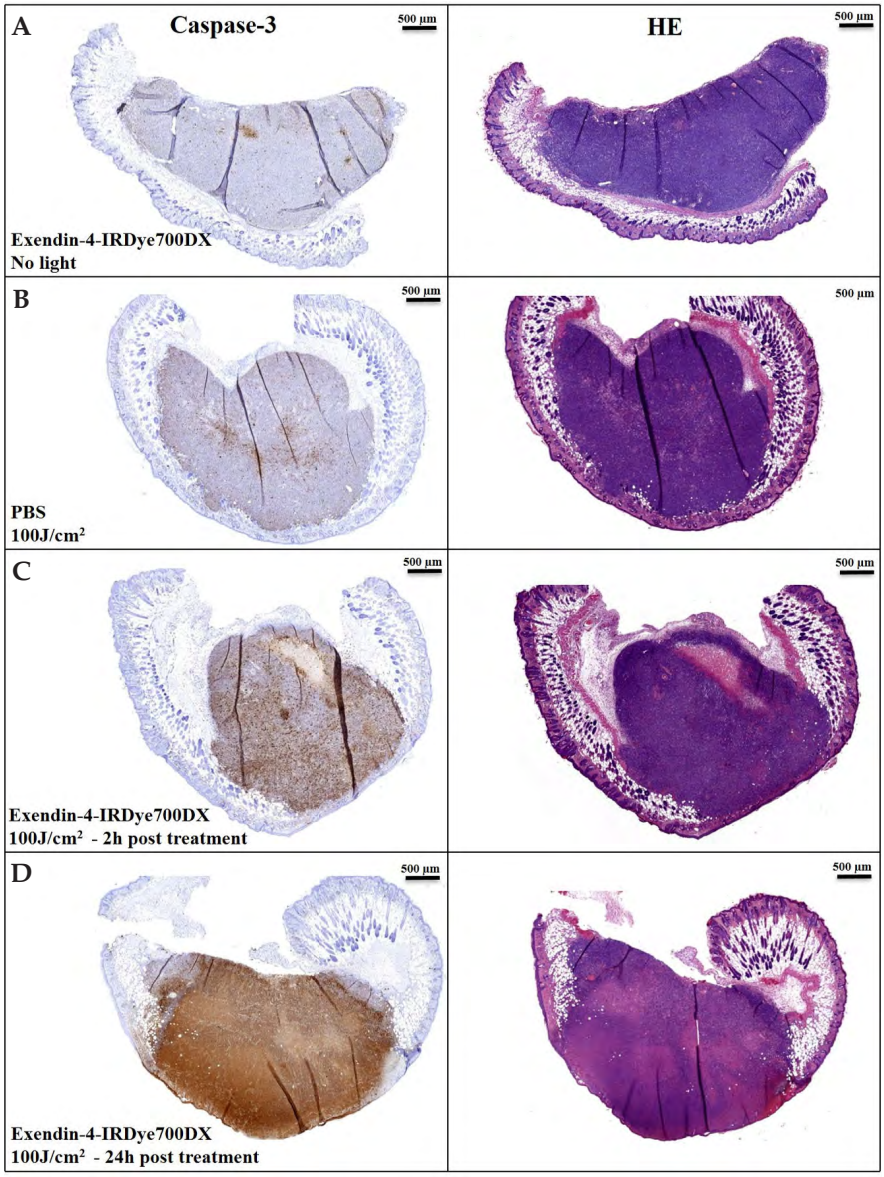

Figure 7 Representative examples of cleaved-caspase-3 and HE staining of CHL-GLP-1R tumors. A) Control tumors after i.v. administration of exendin-4-IRDye700DX. B) Control tumors after only illumination. C) Tumors after i.v. administration of exendin-4-IRDye700DX and illumination, dissected after 2 hours. D) Tumors after i.v. administration of exendin-4-IRDye700DX and illumination dissected after 24 hours. E) Intensity scores of capase-3 staining for tumor sections of all mice.

E

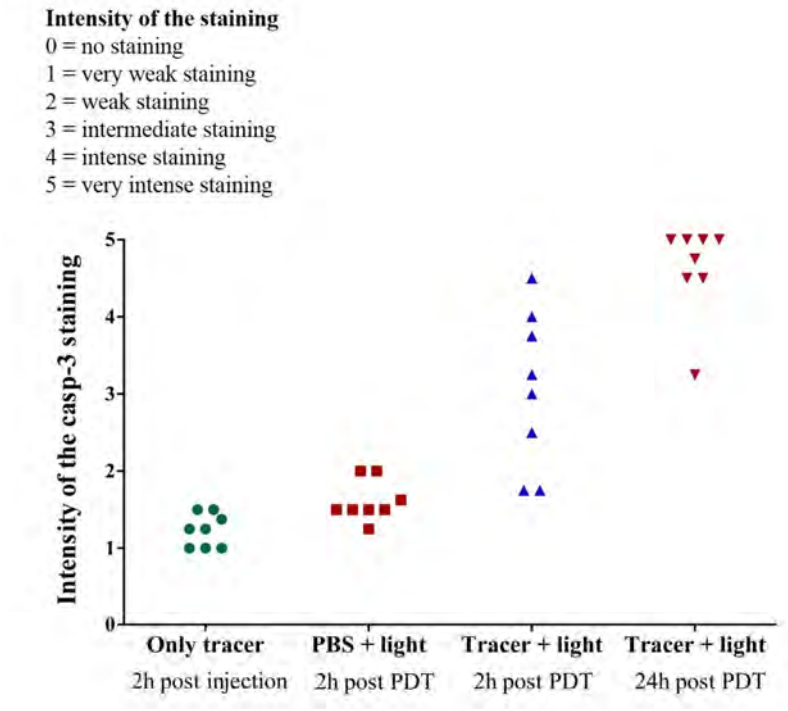

Figure 7 Continued.

At the start of the survival experiment, sizes of the subcutaneous GLP-1R were very variable, although mean tumor sizes were similar between the groups (161±205 mm^3 (35-657 mm^3) in the exendin-4-IRDye700DX group and 171±144 mm^3 (36-480 mm^3) in the control group. Upon light exposure, tumor growth was slower in the group which received exendin-4-IRDye700DX leading to a significantly longer median survival in this group compared to the control group (36.5 vs. 22.5 days resp. $p<0.05$) (Fig. 8).

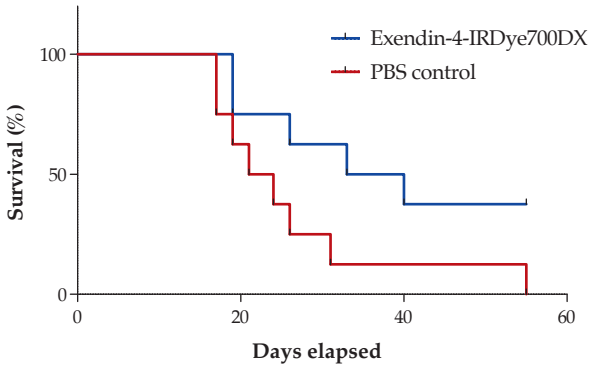

Figure 8 Kaplan-Meier plot of survival of BALB/c nude mice with GLP-1R positive tumors after injection of 30 μg exendin-4-IRDye700DX or PBS (control), followed by illuminaton with a radiant exposure of 150 J/cm^2.

Discussion

Treatment of hyperinsulinemic hypoglycemia is challenging. To address this issue, a treatment strategy which specifically destroys GLP-1R positive cells with rtPDT was developed as an alternative treatment option for all forms of hyperinsulinemic hypoglycemia.

We show effectivity of rtPDT with exendin-4-IRDye700DX *in vitro* and *in vivo*. The specific cytotoxic effect demonstrates that rtPDT with exendin-4-IRDye700DX could enable destruction of GLP-1R positive lesions without causing damage to the surrounding pancreatic tissue.

This is the first evidence of the effectiveness of a peptide-based agent for rtPDT *in vivo* to date. In the current development of tracers for rtPDT, the most widely used carrier molecules are mAbs and nanoparticles, because of their slow clearance from the circulation and high uptake in target organs. A single previous study examining rtPDT using various targeting peptides was limited to *in vitro* studies and showed no efficient cytotoxic effect (22).

We believe that rtPDT with exendin-4-IRDye700DX has the potential to be used as a minimally invasive technique to destroy insulin-producing cells with minimal morbidity. Upon delivery of the tracer, NIR light can be administered interstitially using diffuser fibers which are placed into the target tissue. Using this method of so-called interstitial PDT (iPDT), it is feasible to deliver light to deeply seeded lesions/tissues. Successful results of iPDT have been obtained in for example prostate cancer (23), head and neck cancer (24) and importantly pancreatic

tumors (25). An optimal treatment result depends on optimization of the number of light sources as well as their specific placement and power output (26-28). With percutaneous delivery, areas up to 23 cm^2 can be treated (29), making it suitable for treatment of CHI and nesidioblastosis. Alternatively, the less invasive endoscopic delivery of a fiber can be applied for treatment of small lesions, since a single fiber can be applied using this technique (30, 31).

The data in this paper do not show 100% cell killing. Since these experiments were performed in an immunocompromised mouse model, they did not take into account the possible added effect on cell killing of the immune response elicited by PDT, as has been shown for other tumor types (32). Additionally, because of the minimal invasiveness of PDT, treatment can easily be repeated if hypoglycemia persist. Of interest, in a clinical situation, killing of enough cells to prevent over-production of insulin will be sufficient, eliminating the need for 100% cell killing.

The receptor-targeted approach of PDT with exendin-4-IRDye700DX enables specific killing of GLP-1R expressing cells without damaging the surrounding tissue, and the focused irradiation of the tissue of interest avoids a risk of damaging the kidneys. Since treatment of nesidioblastosis and diffuse CHI will involve irradiation of a larger part of the pancreas, this risks development of impaired glucose tolerance. However, rtPDT has advantages over near-total pancreatectomy, since it avoids the risk of exocrine pancreatic insufficiency and is much less invasive. Also, localization and quantification of the insulin-overproducing cells based on pre-operative PET images using radiolabeled exendin-4 could be used for planning of the rtPDT to optimize the treatment and minimize side effects.

We believe that the data presented here, together with the advances in the technology of interstitial PDT, can provide a basis towards clinical translation of rtPDT using exendin-4-IRDye700DX. For this, verification of efficient targeting to human tissues as well as the potential treatment efficacy by ex-vivo analysis of human tissues will be necessary before initiation of a first clinical trial.

Conclusion

Here, we show the feasibility of rtPDT with exendin-4-IRDye700DX, which is also the first demonstration of efficient PDT using small molecules *in vivo*. In the future, ablating insulin-producing cells using rtPDT with exendin-4-IRDye700DX could provide a new, minimally invasive treatment method for patients with hyperinsulinemic hypoglycemia. Since this treatment could be applied to a specific site of the pancreas in the case of insulinomas or focal CHI or to a larger pancreatic area in the case of nesidioblastosis or diffuse CHI, it clearly has the potential to be effective to normalize blood glucose regulation in all forms of hyperinsulinemic hypoglycemia.

References

1. Kinova MK. Diagnostics and treatment of insulinoma. Neoplasma. 2015;62(5):692-704.
2. Witteles RM, Straus IF, Sugg SL, Koka MR, Costa EA, Kaplan EL. Adult-onset nesidioblastosis causing hypoglycemia: an important clinical entity and continuing treatment dilemma. Archives of surgery (Chicago, Ill : 1960). 2001;136(6):656-63.
3. Senniappan S, Shanti B, James C, Hussain K. Hyperinsulinaemic hypoglycaemia: genetic mechanisms, diagnosis and management. Journal of inherited metabolic disease. 2012;35(4):589-601.
4. Lord K, Dzata E, Snider KE, Gallagher PR, De Leon DD. Clinical presentation and management of children with diffuse and focal hyperinsulinism: a review of 223 cases. The Journal of clinical endocrinology and metabolism. 2013;98(11):E1786-9.
5. Iglesias P, Diez JJ. Management of endocrine disease: a clinical update on tumor-induced hypoglycemia. European journal of endocrinology / European Federation of Endocrine Societies. 2014;170(4):R147-57.
6. Okabayashi T, Shima Y, Sumiyoshi T, Kozuki A, Ito S, Ogawa Y, et al. Diagnosis and management of insulinoma. World journal of gastroenterology. 2013;19(6):829-37.
7. Drymousis P, Raptis DA, Spalding D, Fernandez-Cruz L, Menon D, Breitenstein S, et al. Laparoscopic versus open pancreas resection for pancreatic neuroendocrine tumours: a systematic review and meta-analysis. HPB : the official journal of the International Hepato Pancreato Biliary Association. 2014;16(5):397-406.
8. Fernandez-Cruz L, Blanco L, Cosa R, Rendon H. Is laparoscopic resection adequate in patients with neuroendocrine pancreatic tumors? World journal of surgery. 2008;32(5):904-17.
9. Kowalewski AM, Szylberg L, Kasperska A, Marszalek A. The diagnosis and management of congenital and adult-onset hyperinsulinism (nesidioblastosis) - literature review. Polish journal of pathology : official journal of the Polish Society of Pathologists. 2017;68(2):97-101.
10. Richards ML, Gauger PG, Thompson NW, Kloos RG, Giordano TJ. Pitfalls in the surgical treatment of insulinoma. Surgery. 2002;132(6):1040-9; discussion 9.
11. Dolmans DE, Fukumura D, Jain RK. Photodynamic therapy for cancer. Nature reviews Cancer. 2003;3(5):380-7.
12. Mitsunaga M, Ogawa M, Kosaka N, Rosenblum LT, Choyke PL, Kobayashi H. Cancer cell-selective in vivo near infrared photoimmunotherapy targeting specific membrane molecules. Nature medicine. 2011;17(12):1685-91.
13. Reubi JC, Waser B. Concomitant expression of several peptide receptors in neuroendocrine tumours: molecular basis for in vivo multireceptor tumour targeting. European journal of nuclear medicine and molecular imaging. 2003;30(5):781-93.
14. Christ E, Wild D, Ederer S, Behe M, Nicolas G, Caplin ME, et al. Glucagon-like peptide-1 receptor imaging for the localisation of insulinomas: a prospective multicentre imaging study. The lancet Diabetes & endocrinology. 2013;1(2):115-22.
15. Christ E, Wild D, Forrer F, Brandle M, Sahli R, Clerici T, et al. Glucagon-like peptide-1 receptor imaging for localization of insulinomas. The Journal of clinical endocrinology and metabolism. 2009;94(11):4398-405.
16. Wild D, Macke H, Christ E, Gloor B, Reubi JC. Glucagon-like peptide 1-receptor scans to localize occult insulinomas. N Engl J Med. 2008;359(7):766-8.
17. Detty MR, Gibson SL, Wagner SJ. Current clinical and preclinical photosensitizers for use in photodynamic therapy. Journal of medicinal chemistry. 2004;47(16):3897-915.
18. van Eyll B, Lankat-Buttgereit B, Bode HP, Goke R, Goke B. Signal transduction of the GLP-1-receptor cloned from a human insulinoma. FEBS letters. 1994;348(1):7-13.
19. Brom M, Joosten L, Oyen WJ, Gotthardt M, Boerman OC. Radiolabelled GLP-1 analogues for in vivo targeting of insulinomas. Contrast media & molecular imaging. 2012;7(2):160-6.
20. Jodal A, Lankat-Buttgereit B, Brom M, Schibli R, Behe M. A comparison of three (67/68)Ga-labelled exendin-4 derivatives for beta-cell imaging on the GLP-1 receptor: the influence of the conjugation site of NODAGA as chelator. EJNMMI research. 2014;4:31.

21. de Boer E, Warram JM, Hartmans E, Bremer PJ, Bijl B, Crane LM, et al. A standardized light-emitting diode device for photoimmunotherapy. Journal of nuclear medicine : official publication, Society of Nuclear Medicine. 2014;55(11):1893-8.
22. You H, Yoon HE, Jeong PH, Ko H, Yoon JH, Kim YC. Pheophorbide-a conjugates with cancer-targeting moieties for targeted photodynamic cancer therapy. Bioorganic & medicinal chemistry. 2015;23(7):1453-62.
23. Trachtenberg J, Weersink RA, Davidson SR, Haider MA, Bogaards A, Gertner MR, et al. Vascular-targeted photodynamic therapy (padoporfin, WST09) for recurrent prostate cancer after failure of external beam radiotherapy: a study of escalating light doses. BJU international. 2008;102(5):556-62.
24. Lou PJ, Jager HR, Jones L, Theodossy T, Bown SG, Hopper C. Interstitial photodynamic therapy as salvage treatment for recurrent head and neck cancer. Br J Cancer. 2004;91(3):441-6.
25. Bown SG, Rogowska AZ, Whitelaw DE, Lees WR, Lovat LB, Ripley P, et al. Photodynamic therapy for cancer of the pancreas. Gut. 2002;50(4):549-57.
26. Kim MM, Darafsheh A. Light Sources and Dosimetry Techniques for Photodynamic Therapy. Photochemistry and photobiology. 2020.
27. van Doeveren TEM, Bouwmans R, Wassenaar NPM, Schreuder WH, van Alphen MJA, van der Heijden F, et al. On the Development of a Light Dosimetry Planning Tool for Photodynamic Therapy in Arbitrary Shaped Cavities: Initial Results. Photochemistry and photobiology. 2020.
28. Dupont C, Baert G, Mordon S, Vermandel M. Parallelized Monte-Carlo dosimetry using graphics processing units to model cylindrical diffusers used in photodynamic therapy: From implementation to validation. Photodiagnosis Photodyn Ther. 2019;26:351-60.
29. Huggett MT, Jermyn M, Gillams A, Illing R, Mosse S, Novelli M, et al. Phase I/II study of verteporfin photodynamic therapy in locally advanced pancreatic cancer. Br J Cancer. 2014;110(7):1698-704.
30. DeWitt JM, Sandrasegaran K, O'Neil B, House MG, Zyromski NJ, Sehdev A, et al. Phase 1 study of EUS-guided photodynamic therapy for locally advanced pancreatic cancer. Gastrointest Endosc. 2019;89(2):390-8.
31. Choi JH, Oh D, Lee JH, Park JH, Kim KP, Lee SS, et al. Initial human experience of endoscopic ultrasound-guided photodynamic therapy with a novel photosensitizer and a flexible laser-light catheter. Endoscopy. 2015;47(11):1035-8.
32. Beltran Hernandez I, Yu Y, Ossendorp F, Korbelik M, Oliveira S. Preclinical and Clinical Evidence of Immune Responses Triggered in Oncologic Photodynamic Therapy: Clinical Recommendations. J Clin Med. 2020;9(2).

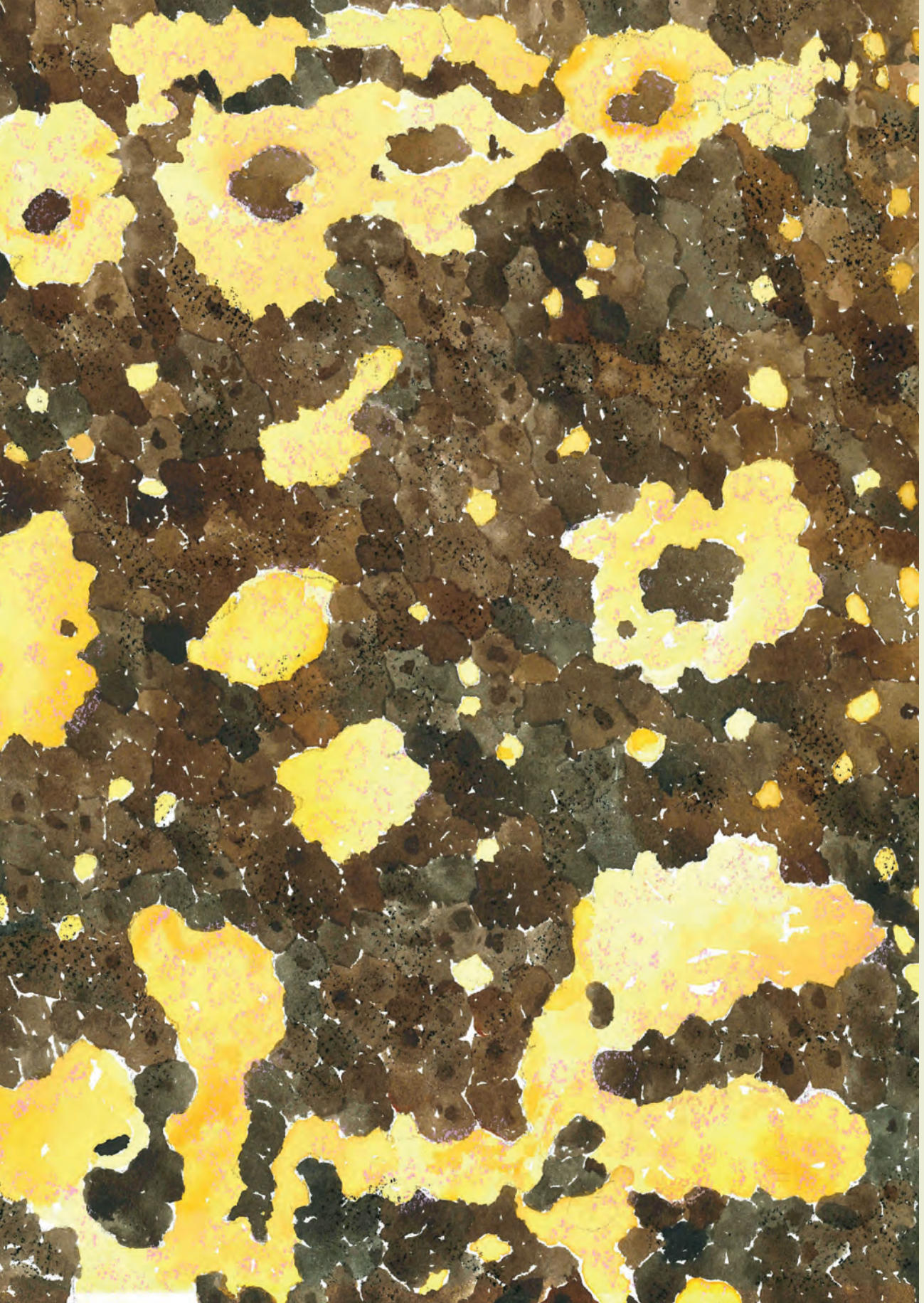

PART 3

Discussion and summary

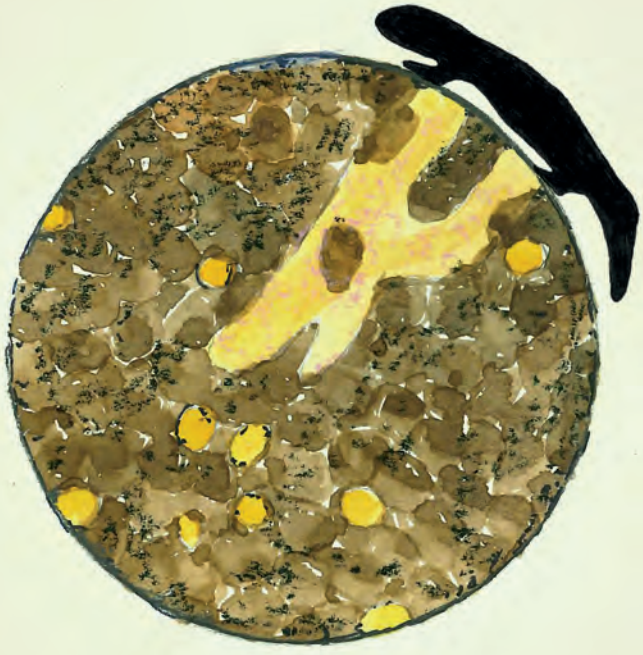

CHAPTER 7

General discussion and future perspectives

Diagnostic benefits

AHH

For patients with AHH, a fast and accurate diagnosis is of high importance, as AHH has a large impact on the quality of life of the patients. For example, episodic hypoglycemia can lead to fear of engaging in certain activities like sports, driving a car or even going for walk alone. Patients can also be afraid to go to sleep, because of fear of having a hypoglycemic episode during the night. Recurrent hypoglycemic episodes prevent some patients from working and many patients gain weight because of frequent eating. Untreated AHH can even be dangerous, since hypoglycemia unawareness can prevent patients from taking action to raise their blood glucose levels. This could result in seizures, loss of consciousness and even brain damage or brain death. Since symptoms of hypoglycemia can be misattributed to psychiatric, neurological or cardiac disorders, the diagnosis of patients can be delayed if lesions are not readily discovered using imaging (1). Currently, multiple different imaging procedures, and in some cases more invasive diagnostic procedures, are performed in most of the patients before a definite diagnosis is reached, and procedures are sometimes repeated over time if an insulinoma is not detected. Accelerating this process by introducing a more sensitive non-invasive imaging technique would thus be of great interest.

Because of the improved sensitivity and image quality of [^{68}Ga]Ga-NODA-GA-exendin-4 PET/CT compared to other imaging techniques, its implementation as the primary diagnostic procedure for insulinomas could significantly reduce the burden of the diagnostic process for the patients. In many patients, performance of GLP-1R PET as a primary diagnostic procedure could eliminate the need for additional diagnostics. A combination with triple phase CT would also provide the anatomical information for surgical planning. Such a one-stop shop for insulinoma detection, besides being beneficial for the patients, could also improve the cost-effectiveness of the diagnostic process for AHH. To precisely determine the potential cost benefit, cost effectiveness modeling based on the results of our prospective clinical trial would be of interest.

Malignant insulinomas

In less than 10% of cases, malignant insulinomas occur. When presenting with liver metastases, these malignant insulinomas have a poor patient prognosis (2). While overexpressed in almost all benign insulinomas, the receptor density of the GLP-1R in malignant insulinomas has been described to be lower (3). In contrast, malignant insulinomas express the SSTR more often than benign insulinomas, leading to a higher detection rate of malignant insulinomas by SSTR PET compared to GLP-1R PET (4). While GLP-1R PET has the potential of becoming the primary

diagnostic modality for benign insulinomas, SSTR PET is more suitable as primary diagnostic modality for detection of the rarer malignant insulinomas. Because of the difference in receptor expression between benign and malignant insulinomas, the combination of GLP-1R and SSTR imaging could impact patient care, since a negative GLP-1R imaging result combined with a positive SSTR imaging result in a patient with AHH could indicate towards a malignant insulinoma in cases without metastases.

CHI

In patients with CHI, replacement of [^{18}F]F-DOPA PET by [^{68}Ga]Ga-NODAGA-exendin-4 PET as the primary diagnostic imaging modality could lead to the detection focal lesions which would otherwise have been missed. This would have a major impact on the lives of these patients. It could provide the possibility for a cure and prevent continuing medicinal treatment with its associated side effects (5). It could also prevent the execution of unnecessary near-total pancreatectomies and thereby the occurrence of associated morbidities like pancreatic exocrine insufficiency and diabetes (6). GLP-1R PET could thus significantly improve the future quality of life of these patients.

A challenge: kidney uptake

A challenge in diagnostic imaging of insulinomas and focal CHI with [^{68}Ga]Ga-NODAGA-exendin-4 PET is the high uptake of the tracer in the kidneys due to renal clearance and tubular re-absorption (7). Tracer uptake in the left kidney in some cases hinders detection of lesions in the pancreatic tail. There are certain methods to reduce kidney uptake of peptide-based tracers. Co-infusion of positively charged amino acids, trypsinized albumin or the plasma expander gelofusine can be used for competitive inhibition of tubular re-absorption. In pre-clinical models, co-infusion of poly-glutamic acid and gelofusine was reported to reduce renal uptake of ^{111}In-labeled exendin-4 by 48% (8). Gelofusine alone was shown to reduce renal uptake of ^{111}In-labeled exendin-4 by 18% in healthy volunteers, without affecting tracer uptake in the pancreas (9). An effect of gelofusine on renal uptake of ^{68}Ga-labeled exendin-4 is still to be established. There are several other strategies that have been developed to reduce renal uptake of radiolabeled exendin, such as introduction of a cleavable linker to allow renal excretion of the radionuclides (10) and incorporation of highly lipophilic groups (11), but these have not yet been tested in humans. Further research into effective methods to reduce the renal uptake of radiolabeled exendin is of interest, since it would be beneficial for the diagnostic accuracy of [^{68}Ga]Ga-NODAGA-exendin-4.

Treatment benefits

Fluorescence-guided surgery

Since it can be difficult to detect insulinomas and focal lesions in CHI intra-operatively, even after pre-operative detection, fluorescence-guided surgery would be beneficial. Surgery of the pancreas is challenging and associated with risks of complications like pancreatic fistulas and bleeding (12). By giving the surgeon very specific real-time information on the location of the lesion by fluorescence imaging, surgeons will not have to rely on palpation and intra-operative ultrasound. This could lead to more optimal and faster surgical procedures (13-15) and possibly a lower risk of morbidity. A great benefit of fluorescence-guided surgery is that it can be performed in an open setting as well as laparoscopically (16), so it can benefit enucleations as well as partial pancreatectomies, depending on the location of the lesion.

Combining fluorescence-guiding with radio-guiding

A disadvantage of fluorescence imaging is the limited penetration depth, as a result of tissue absorption and scattering of the photons. A fluorescent signal will therefore only be detected in close proximity to the lesion. This will probably not be a problem in most cases of insulinomas and focal CHI, since the surgeon can be initially guided to the location of the lesion by the pre-operative scan. However, in particular for occult lesions located deep in the pancreatic tissue, combining fluorescence-guiding with radio-guiding could be of interest. Radio-guided detection of insulinomas using radiolabeled exendin-4 has already been proven successful in a limited number of patients with insulinomas (17). Radio-guided tumor detection is limited to an acoustic signal derived from a probe with a certain detection angle, leading to limited spatial resolution (18). Combining fluorescence imaging with radio-guiding could exploit the benefits of both these techniques and enable detection of deep-seated lesions followed by precise lesion delineation. Combined radio-guiding and fluorescence-guiding could be achieved by development of a multimodal tracer by labeling exendin-4-IRDye800CW with a radionuclide. There is currently much attention for the development of such dual-labeled tracers (19). For example, the monoclonal antibody girentuximab labeled with ^{111}In and IRDye800CW for radiodetection followed by fluorescence-guided resection of renal cell carcinoma is already being assessed clinically (NCT02497599). Development of a dual-labeled exendin-based tracer could be of interest if, upon clinical assessment, fluorescence-guided surgery of insulinomas and focal CHI using exendin-4-IRDye800CW proves to be hindered by the penetration depth of the fluorescent signal. However, radio-guiding has the disadvantage of causing a radiation burden for the surgeons. Therefore, if the

fluorescent signal of exendin-4-IRDye800CW is readily detected in the lesions, combination with radio-guiding will not be preferable.

Optimization of imaging systems

Important for the clinical translation of this fluorescence-guided surgery technique is the optimization of the imaging systems used by the surgeons to detect the fluorescent signal. Most clinical fluorescence imaging systems which are currently available have been developed for the detection of high concentrations of indocyanine green in the blood. With a targeted approach like exendin-4-IRDye-800CW, the concentration of the fluorescent dye that can be reached within the tumor is much lower. So, while the current clinical fluorescent imaging systems are suitable for the detection of photons with wavelengths in the NIR range, their sensitivity needs improvement. Since there is currently much attention for targeted NIR fluorescence-guided surgery, steps are also being taken to improve the imaging systems by ameliorating software systems, emission filters, background correction and charge-coupled device cameras (20).

Photodynamic therapy

rtPDT with exendin-4-IRDye700DX has the potential to provide a minimally invasive treatment alternative for AHH and CHI. Even with sensitive and precise pre-operative localization of insulinomas and focal CHI and the possibility for fluorescence-guided surgery, the surgical treatment is still invasive. Ablating the lesion by specific irradiation with NIR light using diffuser fibers placed into the target tissue could provide a less invasive treatment method. Since rtPDT with exendin-4-IRDye700DX could specifically destroy GLP-1R positive cells, it could have a lower risk of side effects related to damage to adjacent tissues than surgical removal of the lesion. This could lead to a faster recovery and better quality of life for the patients after treatment.

In the future, rtPDT could also greatly improve the treatment of patients with nesidioblastosis and diffuse CHI, because it could be a minimally invasive way to cure these patients. Today, the only cure for nesidioblastosis and diffuse CHI is extensive pancreatic resection, which is associated with high morbidity levels. In patients unresponsive to medication this is currently the only treatment option. Treatment with rtPDT could destroy the diseased beta cells without causing damage to exocrine pancreatic tissue, eliminating the risk of pancreatic exocrine insufficiency which is associated with near-total pancreatectomy. Even for patients that do respond to medication, the current treatment is far from optimal, since the available medication often causes severe side effects. rtPDT could therefore also be a valuable alternative treatment option for these patients.

Clinical translation

Before rtPDT with exendin-4-IRDye700DX can be translated into the clinic, it is important to assess the safety of the treatment. In the past, problems with PDT approaches have occurred because of the development of side effects, such as photo-allergic reactions damaging healthy tissues (21, 22). Because of the targeted approach, the uptake of exendin-4-IRDye700DX in target tissues is high with low background values. The kidneys and the duodenum are the only abdominal organs, besides the pancreatic beta cells, in which high tracer uptake is found. We therefore expect that specific irradiation of the target site using a fiber bundle, while avoiding irradiation of the kidneys and duodenum, will avoid damage of healthy tissue leading to side effects. In addition to this, the PS IRDye-700DX is only activated by NIR light and not by visible light. Even if some accumulation of the tracer in superficial organs like the skin would occur, this will therefore not result in photo-allergy.

In addition to evaluation of the safety of the approach, the first step towards clinical translation is the validation of efficient targeting of the tracer to the target tissue in humans as well as the potential treatment efficacy by *ex vivo* analysis of human specimens.

Besides this, clinical translation will depend on an effective way of delivering the light to the target tissue. While the first PDT approaches focused on superficial lesions, which are easily accessible with light, advances in the field now enable the use of PDT in deeply seated lesions using interstitial PDT. This entails delivery of NIR light either via percutaneous needles or endoscopically using diffuser fibers which are places into the target tissue. This approach has already demonstrated successful results in clinical studies in for example prostate cancer (23), head and neck cancer (24) and importantly pancreatic tumors (25). For successful clinical translation, optimization of the treatment regarding the dose of the tracer as well as the number of light sources, their specific placement and power output (26-28) are crucial.

Individualized treatment

Delivery of light using interstitial PDT can be tailored to the desired effect, like illumination of a small area with a high light intensity for insulinomas and focal CHI and illumination of a larger area with a lower light intensity for the treatment of nesidioblastosis and diffuse CHI. In patients with nesidioblastosis and diffuse CHI, the optimal rtPDT treatment would destroy a sufficient number of beta cells to prevent overproduction of insulin, while preserving enough beta cells to maintain glucose homeostasis. A possible way to achieve this is by quantification of [^{68}Ga]Ga-NODAGA-exendin-4 PET scans performed for pre-operative diagnostics. A benefit of PET imaging is the possibility for reliable quantification (29). The

possibility of using radiolabeled exendin to quantify beta cell mass has already been demonstrated in rats, where pancreatic uptake of ^{111}In-labeled exendin correlated linearly with beta cell mass (30). Furthermore, in humans, quantification of SPECT images showed a significantly lower uptake of ^{111}In-labeled exendin in the pancreas of patients with type 1 diabetes as compared to healthy individuals (31). By correlating tracer uptake of ^{68}Ga-labeled exendin in the pancreas with the amount of NIR irradiation needed to cure patients without developing pancreatic endocrine insufficiency, the treatment could be tailored to the individual patient.

The future in diagnostics and treatment of hyperinsulinemic hypoglycemia

In this thesis we show the potential benefit of exendin-based tracers for diagnosis as well as treatment of hyperinsulinemic hypoglycemia.

[^{68}Ga]Ga-exendin-4 PET/CT outperforms all current standard non-invasive imaging modalities used for the detection of insulinomas as well as focal lesions in CHI (chapter 2 & 3). By using the chelator NODAGA we can label exendin-4 with ^{68}Ga with a high specific activity enabling imaging with low pharmacological peptide doses. This has resulted in minimal side effects in adult patients as well as children. Furthermore, because of the low radiation dose to the patients, the tracer is safe for use in patients of all ages (chapter 4). We therefore believe [^{68}Ga]Ga-NODAGA-exendin-4 has the potential to become the primary diagnostic imaging modality for adult endogenous AHH as well as CHI.

After patients are diagnosed with a specific subform of AHH or CHI and potential lesions are localized using radiolabeled exendin-4, treatment of the patients can be optimized using the NIR fluorescent tracers exendin-4-IRDye-800CW and exendin-4-IRDye700DX. Intra-operative fluorescence imaging using exendin-IRDye800CW can aid surgical removal of insulinomas and focal lesions in CHI by providing sensitive real-time visual information for lesion localization and delineation (chapter 5). In cases where removal of the tumor is hindered by the vicinity of vital structures or in patients with nesidioblastosis or diffuse CHI, surgery or medicinal treatment could be replaced by or complemented with rtPDT. By performing rtPDT with exendin-4-IRDye700DX, GLP-1R positive cells can be specifically destroyed without causing damage to other cells (chapter 6).

By optimizing the diagnostic process as well as the treatment of patients with any form of hyperinsulinemic hypoglycemia, the use of exendin-based tracers potentially has a major impact on the quality of life of these patients in the future.

References

1. Suzuki K, Miyamoto M, Miyamoto T, Hirata K. Insulinoma with early-morning abnormal behavior. Internal medicine (Tokyo, Japan). 2007;46(7):405-8.
2. Vanderveen K, Grant C. Insulinoma. Cancer Treat Res. 2010;153:235-52.
3. Korner M, Stockli M, Waser B, Reubi JC. GLP-1 receptor expression in human tumors and human normal tissues: potential for in vivo targeting. Journal of nuclear medicine : official publication, Society of Nuclear Medicine. 2007;48(5):736-43.
4. Wild D, Christ E, Caplin ME, Kurzawinski TR, Forrer F, Brandle M, et al. Glucagon-like peptide-1 versus somatostatin receptor targeting reveals 2 distinct forms of malignant insulinomas. Journal of nuclear medicine : official publication, Society of Nuclear Medicine. 2011;52(7):1073-8.
5. Senniappan S, Shanti B, James C, Hussain K. Hyperinsulinaemic hypoglycaemia: genetic mechanisms, diagnosis and management. Journal of inherited metabolic disease. 2012;35(4):589-601.
6. Arya VB, Senniappan S, Demirbilek H, Alam S, Flanagan SE, Ellard S, et al. Pancreatic endocrine and exocrine function in children following near-total pancreatectomy for diffuse congenital hyperinsulinism. PloS one. 2014;9(5):e98054.
7. Vegt E, Melis M, Eek A, de Visser M, Brom M, Oyen WJ, et al. Renal uptake of different radiolabelled peptides is mediated by megalin: SPECT and biodistribution studies in megalin-deficient mice. European journal of nuclear medicine and molecular imaging. 2011;38(4):623-32.
8. Gotthardt M, van Eerd-Vismale J, Oyen WJG, de Jong M, Zhang H, Rolleman E, et al. Indication for Different Mechanisms of Kidney Uptake of Radiolabeled Peptides. Journal of Nuclear Medicine. 2007;48(4):596-601.
9. Buitinga M, Jansen TJP, van der Kroon I, Woliner-van der Weg W, Boss M, Janssen M, et al. Succinylated gelatin improves the theranostic potential of radiolabeled exendin-4 in insulinoma patients. Journal of nuclear medicine : official publication, Society of Nuclear Medicine. 2018.
10. Jodal A, Pape F, Becker-Pauly C, Maas O, Schibli R, Behe M. Evaluation of (1)(1)(1)in-labelled exendin-4 derivatives containing different meprin beta-specific cleavable linkers. PLoS One. 2015;10(4):e0123443.
11. Dialer LO, Jodal A, Schibli R, Ametamey SM, Behe M. Radiosynthesis and evaluation of an (18) F-labeled silicon containing exendin-4 peptide as a PET probe for imaging insulinoma. EJNMMI Radiopharm Chem. 2018;3(1):1.
12. Richards ML, Gauger PG, Thompson NW, Kloos RG, Giordano TJ. Pitfalls in the surgical treatment of insulinoma. Surgery. 2002;132(6):1040-9; discussion 9.
13. de Boer E, Harlaar NJ, Taruttis A, Nagengast WB, Rosenthal EL, Ntziachristos V, et al. Optical innovations in surgery. The British journal of surgery. 2015;102(2):e56-72.
14. DeLong JC, Hoffman RM, Bouvet M. Current status and future perspectives of fluorescence-guided surgery for cancer. Expert review of anticancer therapy. 2016;16(1):71-81.
15. Landau MJ, Gould DJ, Patel KM. Advances in fluorescent-image guided surgery. Annals of translational medicine. 2016;4(20):392.
16. Takahashi H, Zaidi N, Berber E. An initial report on the intraoperative use of indocyanine green fluorescence imaging in the surgical management of liver tumorss. Journal of surgical oncology. 2016;114(5):625-9.
17. Christ E, Wild D, Forrer F, Brandle M, Sahli R, Clerici T, et al. Glucagon-like peptide-1 receptor imaging for localization of insulinomas. The Journal of clinical endocrinology and metabolism. 2009;94(11):4398-405.
18. Tsuchimochi M, Hayama K. Intraoperative gamma cameras for radioguided surgery: technical characteristics, performance parameters, and clinical applications. Physica medica : PM : an international journal devoted to the applications of physics to medicine and biology : official journal of the Italian Association of Biomedical Physics (AIFB). 2013;29(2):126-38.
19. Hernandez Vargas S, Ghosh SC, Azhdarinia A. New Developments in Dual-labeled Molecular Imaging Agents. Journal of nuclear medicine : official publication, Society of Nuclear Medicine. 2019.
20. AV DS, Lin H, Henderson ER, Samkoe KS, Pogue BW. Review of fluorescence guided surgery systems: identification of key performance capabilities beyond indocyanine green imaging. Journal of biomedical optics. 2016;21(8):80901.

21. van Straten D, Mashayekhi V, de Bruijn HS, Oliveira S, Robinson DJ. Oncologic Photodynamic Therapy: Basic Principles, Current Clinical Status and Future Directions. Cancers. 2017;9(2).
22. Bugaj AM. Targeted photodynamic therapy--a promising strategy of tumor treatment. Photochemical & photobiological sciences : Official journal of the European Photochemistry Association and the European Society for Photobiology. 2011;10(7):1097-109.
23. Trachtenberg J, Weersink RA, Davidson SR, Haider MA, Bogaards A, Gertner MR, et al. Vascular-targeted photodynamic therapy (padoporfin, WST09) for recurrent prostate cancer after failure of external beam radiotherapy: a study of escalating light doses. BJU international. 2008;102(5):556-62.
24. Lou PJ, Jager HR, Jones L, Theodossy T, Bown SG, Hopper C. Interstitial photodynamic therapy as salvage treatment for recurrent head and neck cancer. Br J Cancer. 2004;91(3):441-6.
25. Bown SG, Rogowska AZ, Whitelaw DE, Lees WR, Lovat LB, Ripley P, et al. Photodynamic therapy for cancer of the pancreas. Gut. 2002;50(4):549-57.
26. Kim MM, Darafsheh A. Light Sources and Dosimetry Techniques for Photodynamic Therapy. Photochemistry and photobiology. 2020.
27. van Doeveren TEM, Bouwmans R, Wassenaar NPM, Schreuder WH, van Alphen MJA, van der Heijden F, et al. On the Development of a Light Dosimetry Planning Tool for Photodynamic Therapy in Arbitrary Shaped Cavities: Initial Results. Photochemistry and photobiology. 2020.
28. Dupont C, Baert G, Mordon S, Vermandel M. Parallelized Monte-Carlo dosimetry using graphics processing units to model cylindrical diffusers used in photodynamic therapy: From implementation to validation. Photodiagnosis Photodyn Ther. 2019;26:351-60.
29. Kherlopian AR, Song T, Duan Q, Neimark MA, Po MJ, Gohagan JK, et al. A review of imaging techniques for systems biology. BMC systems biology. 2008;2:74.
30. Brom M, Joosten L, Frielink C, Boerman O, Gotthardt M. (111)In-exendin uptake in the pancreas correlates with the beta-cell mass and not with the alpha-cell mass. Diabetes. 2015;64(4):1324-8.
31. Brom M, Woliner-van der Weg W, Joosten L, Frielink C, Bouckenooghe T, Rijken P, et al. Non-invasive quantification of the beta cell mass by SPECT with (1)(1)(1)In-labelled exendin. Diabetologia. 2014; 57(5):950-9.

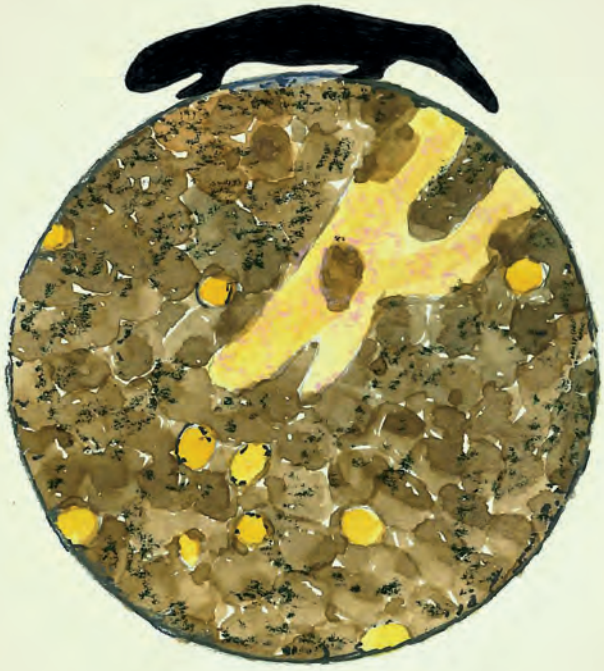

CHAPTER 8

Summary

Summary

In the rare disorder hyperinsulinemic hypoglycemia, uncontrolled overproduction of insulin by the pancreatic beta cells results in dangerously low blood glucose levels. Adult hyperinsulinemic hypoglycemia (AHH) is most commonly caused by insulinomas. Congenital hyperinsulinism (CHI), occurring in a focal or diffuse subform, is the most common cause of hyperinsulinemic hypoglycemia in children, often neonates.

Because of the severe symptoms, AHH and CHI have a large impact on patient lives. Therefore, quick and accurate diagnosis is essential. For AHH, this entails sensitive and accurate detection and localization of insulinomas. For CHI, the distinction between the focal and the diffuse subform is key, as well as accurate localization of the focus in case of focal CHI. Diagnosis of AHH and CHI is currently challenged by the limited sensitivity of available imaging techniques. Treatment of AHH and CHI is also challenging. Medication leads to significant side effects and surgery, which is the only curative option, carries risks of complications.

Exendin is a peptide which specifically binds the glucagon-like peptide 1 receptor (GLP-1R) on pancreatic beta cells. This thesis describes the use of exendin-based tracers for diagnostic imaging, intra-operative fluorescence imaging and receptor-targeted photodynamic therapy (rtPDT) of hyperinsulinemic hypoglycemia, as tools to overcome the challenges in diagnostics and treatment.

Non-invasive imaging of hyperinsulinemic hypoglycaemia.

The current standard non-invasive imaging techniques used for detection of insulinomas; CT, MRI and somatostatin receptor PET, have limited sensitivity. In **chapter two** we describe a prospective, multicenter study in which we compare the effectiveness of [^{68}Ga]Ga-NODAGA-exendin-4 PET/CT with all these standard imaging techniques for detection of insulinomas in 42 patients with AHH. [^{68}Ga]Ga-NODAGA-exendin-4 PET/CT performed better than all other imaging techniques with a higher accuracy and sensitivity. Furthermore, image quality of [^{68}Ga]Ga-NODAGA-exendin-4 PET was better than somatostatin receptor PET.

In **chapter three** we examine the effectiveness of [^{68}Ga]Ga-NODAGA-exendin-4 PET for detection of focal CHI. In 19 CHI patients, we compared [^{68}Ga]Ga-NODAGA-exendin-4 PET with the standard imaging method [^{18}F]F-DOPA PET. We show that the image quality of [^{68}Ga]Ga-NODAGA-exendin-4 PET is superior, which leads to a better diagnostic accuracy and certainty which aids planning of the surgical treatment.

The use of [^{68}Ga]Ga-NODAGA-exendin-4 PET for diagnosis of AHH and CHI results in a radiation dose to the patients. In **chapter four** we show a dosimetry

study, based on human [^{68}Ga]Ga-NODAGA-exendin-4 PET images, in which we find that the effective radiation doses are very low for adults as well as children, enabling safe use of this technique.
These chapters show the potential of [^{68}Ga]Ga-NODAGA-exendin-4 PET to become the primary diagnostic imaging modality for AHH as well as CHI in the future.

Targeted optical imaging and photodynamic therapy of insulin-producing lesions

Even after successful pre-operative detection of insulinomas and focal CHI, surgery can be complicated by challenging intra-operative detection of the lesions. In **chapter five**, we describe near-infrared fluorescence imaging of GLP-1R positive cells using exendin-4-IRDye800CW. We show that this tracer successfully targets GLP-1R positive cells and enables *in vivo* fluorescence imaging of GLP-1R expressing tumors in mice. Furthermore, we show laparoscopic detection of the fluorescent signal of exendin-4-IRDye800CW in the pancreas of mini pigs. By allowing real-time intraoperative lesion detection, this technique could benefit surgical removal of insulinomas and focal lesions in CHI.

Surgery of insulinomas and CHI carries major risks of morbidity. In **chapter six** we examine selective killing of GLP-1R positive cells using rtPDT with exendin-4-IRDye700DX as an alternative treatment strategy. We show that rtPDT causes effective and selective phototoxicity in GLP-1R positive cells *in vitro* and that rtPDT is able to induce cellular damage in GLP-1R expressing tumors *in vivo* in mice, thereby prolonging their survival. This shows the future potential of rtPDT with exendin-4-IRDye700DX as a minimally invasive treatment method for AHH and CHI.

Samenvatting

Bij de zeldzame ziekte hyperinsulinemische hypoglykemie, leidt ongecontroleerde overproductie van insuline door de beta cellen in het pancreas tot gevaarlijk lage bloedsuikerniveaus. Hyperinsulinemische hypoglykemie in volwassenen (AHH) wordt in de meeste gevallen veroorzaakt door een insulinoom. Congenitaal hyperinsulinisme (CHI), voorkomend in een focale of diffuse vorm, is de meest voorkomende oorzaak van hyperinsulinemische hypoglykemie bij kinderen, vaak pasgeboren kinderen.

Vanwege de ernstige symptomen hebben AHH en CHI een grote invloed op het leven van patiënten. Snelle en accurate diagnose is daarom essentieel. In het geval van AHH betekent dit gevoelige en accurate detectie en lokalisatie van insulinomen. In het geval van CHI is het maken van onderscheid tussen de focale en diffuse vorm belangrijk. Bij de focale vorm is ook de precieze lokalisatie van de focus essentieel. De diagnose van AHH en CHI worden momenteel bemoeilijkt door de beperkte sensitiviteit van de beschikbare beeldvormingstechnieken. Ook de behandeling van AHH en CHI is een uitdaging. Medicatie leidt tot ernstige bijwerkingen en operaties, de enige behandeling die tot genezing kan leiden, brengen een risico op complicaties met zich mee.

Exendin is een peptide dat specifiek bindt aan de glucagon-like peptide 1 receptor (GLP-1R) op de beta cellen in het pancreas. Dit proefschrift beschrijft het gebruik van op exendin gebaseerde signaalmoleculen voor diagnostische beeldvorming, intra-operatieve fluorescentie beeldvorming en receptor-gerichte fotodynamische therapie (rtPDT) voor hyperinsulinemische hypoglykemie, als een middel om de uitdagingen bij de diagnostiek en therapie te overwinnen.

Niet-invasieve beeldvorming van hyperinsulinemische hypoglykemie

De huidige standaard niet-invasieve beeldvormingstechnieken gebruikt voor de detectie van insulinomen; CT, MRI en somatostatine-receptor PET, hebben beperkte sensitiviteit. In **hoofdstuk 2** beschrijven we een prospectieve, multicenterstudie waarin we de effectiviteit van [^{68}Ga]Ga-NODAGA-exendin-4 PET/CT voor de detectie van insulinomen vergelijken met al deze standaard beeldvormingstechnieken in 42 patiënten met AHH. [^{68}Ga]Ga-NODAGA-exendin-4 PET/CT presteerde beter dan alle andere beeldvormingstechnieken met een hogere accuraatheid en gevoeligheid. Verder was de beeldkwaliteit van [^{68}Ga]Ga-NODAGA-exendin-4 PET beter dan van somatostatine-receptor PET. In **hoofdstuk 3** onderzoeken we de effectiviteit van [^{68}Ga]Ga-NODAGA-exendin-4 PET/CT voor de detectie van de focale vorm van CHI. We vergeleken [^{68}Ga]Ga-NODAGA-exendin-4 PET/CT met de standaard beeldvormingstechniek [^{18}F]F-DOPA PET in 19

CHI patiënten. We laten een betere beeldkwaliteit van [^{68}Ga]Ga-NODAGA-exendin-4 PET zien, leidend tot een betere diagnostische accuraatheid en zekerheid, wat helpt bij de planning van de chirurgische behandeling.

Het gebruik van [^{68}Ga]Ga-NODAGA-exendin-4 PET voor de diagnose van AHH en CHI brengt een stralingsdosis voor de patiënt met zich mee. In **hoofdstuk 4** laten we een dosimetrie studie zien, gebaseerd op humane [^{68}Ga]Ga-NODAGA-exendin-4 PET/CT beelden. Hierin vinden we dat de effectieve stralingsdosis voor zowel volwassenen als kinderen heel laag is, waardoor deze techniek veilig gebruikt kan worden.

Deze hoofdstukken laten de potentie zien van [^{68}Ga]Ga-NODAGA-exendin-4 PET om in de toekomst de primaire beeldvormingstechniek te worden voor zowel AHH als CHI.

Gerichte optische beeldvorming en fotodynamische therapie van insuline-producerende lesies.

Zelfs na succesvolle pre-operatieve detectie van insulinomen en de focale vorm van CHI kan de chirurgische behandeling bemoeilijkt worden door moeizame intra-operatieve detectie van de lesies. In **hoofdstuk 5** beschrijven we nabij-infrarode fluorescentie beeldvorming van GLP-1R positieve cellen met behulp van exendin-4-IRDye800CW. We laten zien dat dit signaalmolecuul succesvol gericht is naar GLP-1R positieve cellen en dat dit *in vivo* fluorescentie beeldvorming van tumoren die de GLP-1R tot expressie brengen mogelijk maakt in muizen. Verder laten we laparoscopische detectie van het fluorescente signaal van exendin-4-IRDye800CW in het pancreas van mini varkens zien. Door real-time intra-operatieve detectie van lesies mogelijk te maken, kan deze techniek de chirurgische verwijdering van insulinomen en focale lesies bij CHI ten goede komen.

Chirurgische behandeling van insulinomen en CHI brengt grote morbiditeitsrisico's met zich mee. In **hoofdstuk 6** onderzoeken we het selectief doden van GLP-1R positieve cellen met behulp van rtPDT met exendin-4-IRDye700DX als alternatieve behandelingsstrategie. We laten zien dat rtPDT effectieve en selectieve lichtschade veroorzaakt bij GLP-1R positieve cellen *in vitro.* Verder laten we zien dat rtPDT *in vivo* in muizen celschade kan aanrichten in tumoren die de GLP-1R tot expressie brengen, waardoor de levensduur van de muizen verlengd wordt. Dit laat de toekomstige potentie zien van rtPDT met exendin-4-IRDye700DX als minimaal invasieve, alternatieve behandelingsmethode voor AHH en CHI.

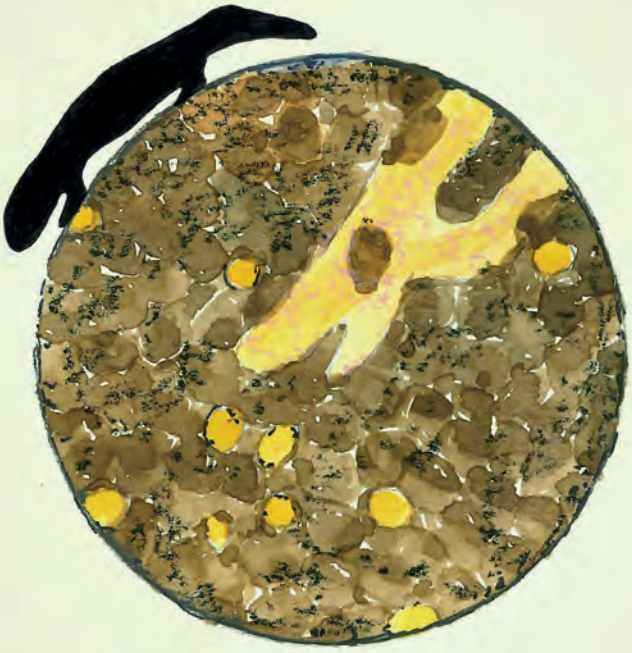

CHAPTER 9

Research data management
List of publications
Curriculum Vitae
Dankwoord

Research data management

Findable

Preclinical data

All raw and processed data obtained during my PhD and described in this thesis have been stored on the hard drive of the department of Medical Imaging at the Radboud university medical center. This hard drive is password protected and automatic back-ups are made several times a day. Most of the data is captured in notebooks and a digital copy of these notebooks is stored on the hard drive as well. Raw data from equipment (*e.g.* SPECT/CT, gamma counter) are backed-up on university servers belonging to the department. Large data, for example SPECT/CT images and immunohistochemical images are stored on external hard-drives and are located at the department of Medical Imaging.

All mouse studies were performed according to the Institute of Laboratory Animal Research Guidelines. Animal experiments were approved by the Animal Ethical Committee of the Radboud University, Nijmegen, The Netherlands.

Clinical data

For the clinical studies described in this thesis, the European Guidance for Healthcare Professionals on Confidentiality and Privacy in Healthcare was respected, all documents and data were handled with strict confidentiality. In the documentation and data analysis phase, the patient-related data were recorded pseudonymously and were identifiable only by randomization number, initials and birth date. Data collected, being sensitive personal data (directive 95/46/EC), were kept treated and transferred in a confidential manner according to regulations.

All clinical data of patients participating in the studies described in this thesis are collected online in InferMed's electronic data capture system MACRO, which is installed on a European server under supervision of Radboudumc ICT department.

The following protection measures are in place:

- Daily full back ups are made.
- Recovery mechanisms are in place for fast system recovery.
- These rooms are placed in a secured space with video surveillance, which is only accessible for authorized personnel.
- These rooms are climate controlled, fire protected and deployed with emergency power.
- Access to the servers is secured by restricted accounts that are password protected.
- Servers are placed in separated and secured LAN zones.
- Servers will have correct OS patch levels, services and protection software.

MACRO is designed to support the requirements of internationally recognized ICH Good Clinical Practice and FDA 21 CRF Part11. SOPs (Standard Operating Procedures) are in place for the data management procedures that will be followed. Biological material are stored as linked anonymised material.

Accessible

All protocols and data are accessible by contacting the corresponding author or one of the researchers involved in these studies.

Interoperable

All protocols and data are documented in English.

Reusable

All data will be saved for at least 15 years after publication of the respective study. All used methods and data analyzed during these studies are available upon request from the corresponding author.

List of publications

- Costes S, Boss M, Thomas AP, Matveyenko AV. Activation of Melatonin Signaling Promotes beta-Cell Survival and Function. Molecular endocrinology (Baltimore, Md). 2015;29(5):682-92.
- Brom M, Eter WA, van der Kroon I, Willekens SMA, Eek A, Boss M, et al. Beta Cell Imaging as Part of "Imaging on Metabolic Diseases". In: Kiessling F, Pichler BJ, Hauff P, editors. Small Animal Imaging: Basics and Practical Guide. Cham: Springer International Publishing; 2017. p. 605-25.
- Gotthardt M, Eizirik DL, Aanstoot HJ, Korsgren O, Mul D, Martin F, Boss M et al. Detection and quantification of beta cells by PET imaging: why clinical implementation has never been closer. Diabetologia. 2018;61(12):2516-9.
- Boss M, Rooijackers HMM, Buitinga M, Janssen MJR, Arens AIJ, de Geus-Oei LF, et al. PET imaging during hypoglycaemia to study adipose tissue metabolism. European journal of clinical investigation. 2019:e13120.
- Jansen TJP, van Lith SAM, Boss M, Brom M, Joosten L, Behe M, et al. Exendin-4 analogs in insulinoma theranostics. Journal of labelled compounds & radiopharmaceuticals. 2019.
- Buitinga M, Jansen T, van der Kroon I, Woliner-van der Weg W, Boss M, Janssen M, et al. Succinylated Gelatin Improves the Theranostic Potential of Radiolabeled Exendin-4 in Insulinoma Patients. *J Nucl Med*. 2019;60:812-816.
- Boss M, Buitinga M, Jansen TJP, Brom M, Visser EP, Gotthardt M. PET-Based Human Dosimetry of (68)Ga-NODAGA-Exendin-4, a Tracer for beta-Cell Imaging. *J Nucl Med*. 2020;61:112-116.
- Boss M, Bos D, Frielink C, et al. Targeted Optical Imaging of the Glucagonlike Peptide 1 Receptor Using Exendin-4-IRDye 800CW. *J Nucl Med*. 2020;61:1066-1071.
- Boss M, Bos DL, Frielink C, et al. Receptor-targeted photodynamic therapy of glucagon-like peptide 1 receptor positive lesions. *J Nucl Med*. 2020.
- Dorst DN, Rijpkema M, Boss M, et al. Targeted photodynamic therapy selectively kills activated fibroblasts in experimental arthritis. *Rheumatology* (Oxford). 2020.

Curriculum vitae

Marti Boss was born in Arnhem, The Netherlands on January 19, 1985. She attended primary school in Hulsberg and high school in Heerlen (VWO) at the Sintermeerten College. In 2003 she started studying Psychology at the University of Maastricht. After her first year she switched to studying Molecular Lifesciences. After obtaining her bachelor's degree in 2008 she started the master Molecular and Cellular Lifesciences at the University of Utrecht. She performed internships in the laboratory of Prof. Jan-Willem Akkerman at the department of Clinical Chemistry and Hematology of the University Medical Center Utrecht and in the laboratory of Prof. Peter Butler at the Larry Hillblom Islet Research Center at the University of California Los Angeles in the United States. In 2010 she received her master's degree. She started her PhD research in the group of Prof. Martin Gotthardt at the department of Medical Imaging, of which the results are described in this thesis, in 2014. Currently she is continuing her work at this department as a post-doctoral researcher.

Dankwoord

Hoi allemaal. Daar is hij dan eindelijk, mijn boekje! Beter laat dan nooit zullen we maar zeggen. Maar zonder de hulp van heel veel mensen had ik het zeker niet laat, maar nooit voor elkaar gekregen. Ik wil dus iedereen die op welke manier dan ook heeft bijgedragen ontzettend bedanken!
Vanaf mijn eerste dag op de nucleaire geneeskunde tot de dag van vandaag is het een fantastische werkomgeving. 'Het warme bad van de nucleaire 😊' Ik denk dat deze combinatie van wetenschappelijke ondersteuning en onmetelijke gezelligheid maar zelden voorkomt. Allemaal bedankt voor deze topjaren waarvan er hopelijk nog veel zullen volgen.

Als eerste wil ik mijn promotieteam bedanken.
Lieve Martin, mijn leraar en partner in crime. Het is geweldig om voor je te werken. Bedankt voor alle vrijheid en het vertrouwen dat je me de aflopen jaren gegeven hebt. En natuurlijk voor alles wat ik van je geleerd heb. Ook al ben je soms druk en chaotisch, je maakt altijd tijd om even te sparren en staat altijd klaar met waardevolle input. Ook bedankt voor alle gezelligheid: kopjes koffie, (soms iets teveel) biertjes en de vele gezellige tripjes. We zijn een goed team en je helpt me altijd weer vooruit in mijn wetenschappelijke carrière. Bedankt voor alles!
Lieve Maarten, wat heb ik veel gehad aan al jouw kennis! Met mijn vragen kon ik altijd bij je terecht en je nam altijd rustig de tijd om te helpen. Ook nadat je weg bent gegaan bleef je altijd bereikbaar en heb je me geholpen met alle papers. Bedankt voor alles en hopelijk kunnen we nog vaak samen een mooi NVDO-feestje vieren!
Lieve Sanne, na een paar cocktails in Wenen konden we het gelijk goed met elkaar vinden en is er nog veel gezelligheid gevolgd! Je bent pas later aangesloten bij mijn promotieteam, maar ik heb ontzettend veel gehad aan je input, vooral het PDT paper was zonder jou niet zo mooi geworden!

Lieve Mijke, samen begonnen we op de nucleaire en het was meteen gezellig. Wat was het leuk om samen onze weg te zoeken in wat toen het ondoordringbare woud van de klinische studies leek. Toen je ervoor koos om naar Leuven te vertrekken heb ik wel even een traantje weg moeten pinken. Gelukkig woon je nu in Maastricht zodat het gemakkelijk is elkaar af en toe nog te zien. En hopelijk kunnen we ook nog veel samenwerken in de toekomst!

Annemarie, zonder jou als projectmanager had het BetaCure project nooit een succes kunnen worden! Samen hebben we alle frustraties kunnen delen, maar ook de successen en natuurlijk de vele gezellige tripjes. In je nieuwe functie werken we helaas niet meer samen, maar hopelijk kunnen we in plaats daarvan nog veel leuke dingen doen samen, zoals skiën! Ik ben super blij dat je mijn paranimf wil zijn!

Lieve analisten, allemaal super bedankt voor alle hulp en geweldige organisatie van het lab! Desirée, na de dramatische eerste *in vivo* PDT experimenten hebben we er toch nog een succes van kunnen maken. Bedankt voor de lange fluorescente biodistributie dagen, ook aan Gerwin! Cathelijne, je werkt maar 3 dagen per week, maar het lijken er wel 7! Bedankt voor al je harde werk!

Alle PhDers, te veel om op te noemen, maar dat heb je als je 7 jaar over je boekje doet 😉. Allemaal super bedankt voor de gezelligheid! Van de koffiekamer, Aesculaaf, een karaokebar in Glasgow, de Choco in Barcelona, de Kuhstall in Düsseldorf, Iba-feestjes, Hollandse avonden en ga zo maar door. Wat een feest, zo'n promotietijd met jullie!
Tom, bedankt voor de fijne samenwerking en super dat je een baan hebt gevonden waarin we elkaar in de toekomst wellicht nog tegenkomen. Ik ga je woordgrappen zeker missen!
Laura, samen zijn we een Rijnstate-Radboud team en dat werkt fantastisch! Ik ben blij dat ik je je allereerste ski-lesje heb mogen geven, je was een natuurtalent 😊. Ik hoop dat we nog lang zo fijn blijven samenwerken.
Daphne D, tijdens de monster reuma-experimenten waarbij we in de weekenden nog samen op PRIME stonden hebben we toch altijd veel gelachen. Bedankt voor de mooie afronding van deze projecten!
Daphne L, jouw technische kennis is een grote bijdrage voor veel projecten. Bedankt voor de samenwerking met dosimetrie! Gelukkig blijf je ook op de afdeling en kan ik dus veel van je blijven leren!
Selen, your hard work was the basis for the exendin-IRDye800CW paper. Thank you for introducing me into the world of fluorescence!

Patricia, bedankt voor alle hulp bij de PDT experimenten, en natuurlijk voor het leuke gezelschap tijdens onze tripjes naar Lille.

Iedereen in hotlab, bedankt voor het opzetten van de exendin labeling en alle volgende labelingen. Na slapeloze nachten over een onverklaarbaar HPLC-piekje is het toch nog allemaal goed gekomen! Peter L, bedankt voor alle coördinatie en al je antwoorden op mijn domme radiochemie vragen. Maichel, Gerben, Danny en Natasha, wat is het toch een k*t peptide he! Maar het heeft toch tot mooie resultaten geleid, dus bedankt voor het doorzettingsvermogen!

Sjoerd, bedankt voor de hulp met anonimiseren van mijn ratjetoe aan scans.

Michel, het opzetten van klinische studies was voor mij zonder enige ervaring een soort doolhof. Had ik mijn weg eindelijk gevonden, kwam ik toch weer een doodlopende straat tegen. Jij was echt de gids! Met al mijn vragen kon ik en kan ik nog steeds bij jou terecht.

Erik Visser, bedankt voor je hulp bij het dosimetrie hoofdstuk. Ik heb enorm veel van je geleerd!

Alle laboranten, en in het bijzonder Jur en Peter. Dank jullie wel voor jullie hulp bij alle patiëntenscans. Zonder jullie onmetelijke flexibiliteit zou het nooit mogelijk zijn om zoveel klinische studies te doen op de afdeling. En als ik even in paniek raakte vanwege veel te lage bloedsuikers, bleven jullie altijd rustig en gaven me vertrouwen. Ik kan nooit genoeg lekkers in jullie snoeppot doen om jullie voldoende te bedanken!

Mijn lieve kamergenoten, Lieke, Sanne en René. Wat een ellende was en is het toch allemaal 😉. Gelukkig zitten we allemaal in hetzelfde schuitje. Met jullie kan ik geweldig sparren en gezellig kletsen. En na de grootste frustraties of teleurstellingen kan ik met jullie altijd heel snel weer lachen!

Iedereen op PRIME en natuurlijk in het bijzonder Bianca. Bedankt voor al jullie hulp bij de dierexperimenten!

All the partners in the BetaCure project, Fritz Andreae, Martin Béhé, Pratik Shah, Damian Wild, Pirjo Nuutila, Oliver Blankenstein, Olof Eriksson, Vikas Prasad, Adrienne Brouwers, Go van Dam, Christof Rottenburger, Winfried Brenner, François Pattou and many others. thank you for the great collaboration! I learned so much from all of you, especially that working together leads to the best results. I will take this with me throughout the rest of my career and hopefully we will keep the collaborations going.

John Hermans, bedankt voor de hulp met het beoordelen van de CT's en MRI's en de prettige samenwerking!

Bedankt aan alle centra zowel nationaal als internationaal die bijgedragen hebben aan de inclusie van patiënten in de studies.
Een heel speciaal bedankje aan alle patiënten en ouders van patiënten die deel hebben genomen aan de studies. Ik waardeer dit ontzettend en hopelijk heeft dit onderzoek jullie kunnen helpen en zal het in de toekomst nog veel meer patiënten kunnen helpen.

Al mijn lieve vrienden heel erg bedankt dat jullie er altijd voor mij zijn!
Lieve Solange, mijn oudste en liefste vriendin, we hebben al zoveel samen meegemaakt, bedankt voor alles. Zodra het weer kan laten we de mannen op de kinderen passen en gaan wij lekker aan de wijn!
Lieve Frauke, na de Jekerstraat, of eigenlijk al na die eerste avond in de café de Wekker, is de liefde niet meer overgegaan. Bedankt voor alle gezelligheid, de avonturen en ontelbare mooie nachten. Ik ben super blij dat je mijn paranimf wil zijn!
Lieve Femke, mijn lova! Je bent zo'n sterk en bijzonder persoon. Bedankt dat ik altijd met je kan praten, maar natuurlijk ook feesten. Ik kan niet wachten om te zien waar het leven je gaat brengen en wat je nog allemaal gaat doen en het samen met je te beleven. Ik ben trots op je!
Lieve Eva, al zien we elkaar nu even niet zo veel, je bent en blijft niet alleen een vriendin, maar een soort zusje. Hopelijk kunnen Pinky en Brain weer snel samen de kroegen onveilig maken.
Lieve Sarah, je was mijn liefste huisgenootje op het Ledig Erf en ik ben nog steeds zo blij met je vriendschap! Hester en Renate, van Leiden tot in Nijmegen zijn jullie me blijven steunen en is de gezellige vriendschap gebleven. Jullie zijn toppers! Judith, Nienke en Annemarie. Mijn ski-vakantie maatjes. Bedankt voor de leuke tripjes en andere gezellige dagen!

All my friends from the master; Tessa, Joao, Marcelo, Caspar, Timo, Ian, Steven and Jan, thank you for the great time we had together in Utrecht! We don't see each other as much anymore, but I appreciate you all so much and hopefully we can all get together again really soon, the last time in Portugal was great!

Lieve Ammie en Frank, zonder jullie was ik nooit zo ver gekomen. Jullie hebben me altijd gestimuleerd en vrij gelaten om mijn eigen weg te gaan, ook al heb ik jullie ook vast wel wat kopzorgen opgeleverd. Bedankt voor alle steun en liefde!
Lieve Rik, van Maastricht naar Utrecht blijven we elkaar volgen. Het is zo fijn dat je dicht in de buurt ben en ik altijd bij je terecht kan!

Lieve schoonfamilie, Ko, Heleen, Martine, Edith, Dennis, Stijn, Anne, Robin, Tom en Evi. Ik heb me vanaf het begin thuis gevoeld bij jullie. Bedankt voor alle lieve berichtjes en kaartjes als de promotietijd me even zwaar viel. Jullie zijn geweldig!

Lieve Arjan, het begon met een dak boven mijn hoofd, maar heeft uiteindelijk geleid tot een geweldige vriendschap en liefde, wie had dat gedacht! Hoe rot de dag ook geweest is, als ik thuiskom bij jou kan ik meteen weer lachen! Bedankt voor het helpen relativeren, je humor, je liefde, maar vooral natuurlijk al het lekker eten 😉.

Marti